Ministry of Higher Education and Scientific Research

وزارة التعليم العالي والبحث العلمي

Badji Mokhtar University of Annaba

جامعة باجي مختار – عنابـــة

Faculty of Technology

كـليـة التكنـولـوجيـا

Electromechanical department

قسـم الإلكتروميكانيك

Thesis

Presented to obtain the diploma of

Doctorate

Field : Electromechanics

Specialty : Electromechanics

By :

FEDDAOUI Anis

Theme :

Artificial intelligence for the control of a renewable energy installation: the case of a wind turbine.

Thesis defended on 17th February, 2026 ahead the jury composed of:

N°	Full name	Degree	Institution	Quality
01	HEROUS Lazhar	Prof.	Badji Mokhtar University - Annaba	President
02	FARAH Lotfi	MCA	Badji Mokhtar University - Annaba	Rapporteur
03	BENRETTEM Abdelouahab	Prof.	Badji Mokhtar University - Annaba	Co-rapporteur
04	BOURAS Hichem	MCA	Badji Mokhtar University - Annaba	Examiner
05	KHELIL Khaled	Prof.	Mohamed Cherif Messaadia University -SouK Ahras	Examiner
06	AMARA KORBA Mohammed Cherif	Prof.	Mohamed Cherif Messaadia University -SouK Ahras	Examiner

Acknowledgement

Praise be to Allah, and there is no power nor strength except through Allah.

I am deeply grateful to my Supervisor, Dr. FARAH Lotfi, and Co-Supervisor, Pr. BENRETTEM Abdelouahab, for their unwavering guidance, insightful feedback, and constant encouragement throughout this journey. Their wisdom and mentorship have been invaluable, and I express my profound respect and heartfelt gratitude to them.

My sincere thanks go to the President of the Jury, Mr. HEROUS Lazhar, professor at the University of Badji Mokhtar, for honoring me by presiding over this jury. His presence is a testament to the significance of this work, and I am genuinely grateful for his time and support.

I would also like to extend my deepest thanks to the jury members, Mr.Bouras Hichem, professor at the University of Badji Mokhtar Annaba, Mr. Khelil Khaled and Mr. AMARA KORBA Mohammed Cherif, professors at the University of Mohamed Cherif Messaadia Souk Ahras, for the honor of reviewing and evaluating my work as an examiner. His constructive insights and feedback have been immensely helpful.

Special recognition goes to Mr. DJEHAF Mohammed Abdeldjallil and Mr.DJERIRI Youcef, Doctors at the University of Sidi Bel Abbes, for his invaluable assistance and thoughtful advice throughout my research.

I am particularly thankful to Dr. BENAMIRA Nadir and Dr. Khalfa Dalila, Adjoints of the Post Graduation, for their invaluable help and assistance, dedication to work, facilitation, and understanding. I am grateful for their encouragement.

I am forever thankful to my family for their unwavering love and support and to my friends and colleagues, KADA BENCHIHA Larbi, CHIBANE Oualid, ABDEMEZIANE Mohammed Raid, BOUHENNECHE Mohammed, and AMARA Seif, for their constant encouragement and belief in me. Their companionship and moral support have been a source of strength and motivation.

Lastly, I extend my gratitude to all the teachers and mentors who, knowingly or unknowingly, have contributed to my growth and this achievement. Though they may not remember me, their lessons have left an indelible mark. I hope they see this as a tribute to their dedication and influence on my journey.

Dedication

With immense pleasure, an open heart, and boundless joy, I dedicate this modest work to:

My dear parents, F. Mastour and Messaoud, who are for me the embodiment of kindness and the source of endless tenderness. No dedication could ever be eloquent enough to express what you truly deserve for all the sacrifices you have made for me since my birth, through my childhood, and up to this day. This work is the fruit of your sacrifices, given selflessly for my education and development. May God grant you good health and a long life.

To my wife, my son Abdullah and my daughter Aicha, who have supported me through these years. May God prolong your life and protect you always.

To my beloved brothers, Nidalo, Haithem, Oussama, and Issam, whom I love deeply. I pray that God brings you happiness and helps you achieve all your dreams.

To my nieces and nephews Chihab, Iyed, Rabiaa, Radjaa, Nibras, Nardjes, Soumia and Aissel.

To my dear cousins Mohammed, Alaa, and Abderrahim.

To all the members of my extended family (Feddaoui and Mastour).

To my friends Abdelilah Aouidat, Dorgli Kheiredinne, Sliman Miloud, Fadili Abdelilah, Rodoine, Belhaimeur Rahim, Djebar Yasser, Zougar Brahim, Merbah Youcef, Tedj Nour, Taleb Riadh, Khamelich Islem, Meziane Imad eddine, Sari Madjid and Bouras Samir.

To my cherished colleagues, Boukhari Yasser Alaa Eddine, Belkraouan Imad, Benallal Abdelhak, and Gacemi Salim.

Abstract

This thesis investigates advanced control and power management strategies for Doubly Fed Induction Generator (DFIG)-based wind turbines, with a focus on leveraging artificial intelligence (AI) techniques to overcome the limitations of traditional controllers. As renewable energy integration grows, maintaining grid stability and optimizing power output amidst variable wind conditions have become paramount. However, conventional control methods like the Proportional-Integral (PI) controller, while reliable, struggle with the nonlinearities and uncertainties inherent in wind turbine systems, especially under fluctuating wind speeds.

To address these challenges, this research introduces AI-enhanced control strategies, including optimized PI controllers, Sliding Mode Control (SMC), Super Twisting SMC, Fuzzy Logic Control, and Artificial Neural Networks (ANN). The thesis begins with a theoretical foundation, providing detailed modeling of the wind turbine's aerodynamic system and DFIG dynamics, which supports a deeper understanding of control requirements. Following this, optimized PI controllers are examined, with Particle Swarm Optimization (PSO) proving particularly effective for reducing steady-state error, though limitations in rotor power stability indicated the need for more advanced methods.

The study advances to explore intelligent control techniques. A hybrid Fuzzy-Super Twisting SMC controller is developed, effectively addressing issues like chattering and demonstrating superior performance in handling nonlinearities compared to classical methods. Additionally, ANN is utilized to enhance the PI controller, eliminating overshoot and achieving smoother responses. These AI-driven controllers collectively demonstrate improved responsiveness, stability, and adaptability in wind turbine control.

Expanding to wind farm power management, the thesis proposes a novel algorithm for balancing power across turbines. This algorithm dynamically redistributes power in response to underperforming turbines, effectively maintaining grid stability. Benchmarking against a traditional PI controller, the new approach exhibits precise, proportional power allocation and immediate responsiveness to changing conditions, thereby optimizing overall power output.

The findings affirm the potential of AI-based strategies to enhance both turbine-level control and wind farm-level power management. By integrating advanced control algorithms with AI techniques, this research contributes to the development of resilient and efficient wind energy systems, laying the groundwork for future innovations in renewable energy control.

Keywords: Wind Energy Conversion System, Doubly Fed Induction Generator, Optimized PI, Super Twisting Sliding Mode Control, Fuzzy Logic Control, Artificial Neural Network, Wind Farm Power Management.

الملخص

تتناول هذه الأطروحة استراتيجيات متقدمة للتحكم وإدارة الطاقة في التوربينات الريحية التي تعتمد على المولد الحثي ذو التغذية المزدوجة, مع التركيز على استغلال تقنيات الذكاء الاصطناعي للتغلب على قيود وحدود أدوات التحكم التقليدية. مع تزايد الاعتماد على الطاقة المتجددة, أصبح الحفاظ على استقرار الشبكة الكهربائية وتحسين إنتاج الطاقة وسط ظروف الرياح المتغيرة أمرًا بالغ الأهمية. ومع ذلك، فإن الأساليب التقليدية للتحكم, مثل المتحكم التناسبي التكاملي, على الرغم من موثوقيتها, تعاني من صعوبة التعامل مع اللاخطية والشكوك المتأصلة في أنظمة التوربينات الريحية، وخاصة في ظل تقلبات سرعة الرياح.

لمعالجة هذه التحديات، تقدم هذه الدراسة استراتيجيات تحكم محسنة بالذكاء الاصطناعي، بما في ذلك متحكمات تناسبية تكاملية المحسنة, التحكم بالإنزلاق, التحكم بالإنزلاق المعزز, التحكم المنطقي الضبابي, و الشبكات العصبية الإصطناعية. تبدأ الأطروحة بتقديم الأساس النظري، حيث يتم تناول النمذجة التفصيلية للنظام الهوائي للتوربينات الريحية وديناميكيات المولد الحثي ذو التغذية المزدوجة، مما يدعم فهماً أعمق لمتطلبات التحكم. بعد ذلك، يتم دراسة المتحكمات التناسبية التكاملية المحسنة, حيث يُظهر تحسينها باستخدام تقنية تحسين السرب الجزيئي فعالية عالية في تقليل الخطأ في حالة الاستقرار, إلا أن محدودية الاستقرار في طاقة الدوار أشارت إلى الحاجة لأساليب أكثر تقدماً.

تتوسع الدراسة لاستكشاف تقنيات التحكم الذكي. تم تطوير متحكم هجين يجمع بين المنطق الضبابي والتحكم بالانزلاق المعزز, والذي يعالج بفعالية مشاكل مثل التذبذب ويظهر أداءً متفوقًا في التعامل مع اللاخطية مقارنة بالأساليب التقليدية. بالإضافة إلى ذلك, يتم استخدام الشبكات العصبية الاصطناعية لتعزيز أداء المتحكم التناسبي التكاملي, مما يلغي تجاوزات الإشارة ويحقق استجابات أكثر سلاسة.

في إدارة الطاقة على مستوى المزرعة الريحية, تقترح الأطروحة خوارزمية جديدة لتوزيع الطاقة بين التوربينات. تقوم هذه الخوارزمية بإعادة توزيع الطاقة ديناميكيًا استجابةً للتوربينات ذات الأداء المنخفض, مما يحافظ بفعالية على استقرار الشبكة. وعند مقارنة هذا النهج مع المتحكم التناسبي التكاملي التقليدي, أظهرت الخوارزمية الجديدة تخصيصًا دقيقًا ومتناسبًا للطاقة واستجابة فورية للتغيرات, مما يُحسّن من إنتاجية الطاقة الكلية.

تؤكد النتائج على إمكانيات استراتيجيات التحكم المستندة إلى الذكاء الاصطناعي في تحسين التحكم في التوربينات وإدارة الطاقة على مستوى المزرعة الريحية. من خلال دمج خوارزميات التحكم المتقدمة مع تقنيات الذكاء الاصطناعي، تسهم هذه الدراسة في تطوير أنظمة طاقة ريحية متجددة ومستدامة، وتضع الأساس لمزيد من الابتكارات في مجال التحكم بالطاقة المتجددة.

الكلمات المفتاحية: نظام تحويل طاقة الرياح, مولد حثي مزدوج التغذية, التحكم التناسبي التكاملي المحسن, الإنزلاق الفائق الإلتواء, التحكم بالمنطق الضبابي, الشبكة العصبية الإصطناعية, إدارة طاقة مزرعة الرياح.

Résumé

Cette thèse aborde des stratégies avancées pour le contrôle et la gestion de la puissance des éoliennes basées sur le générateur asynchrone à double alimentation (GADA), en mettant l'accent sur l'utilisation de techniques d'intelligence artificielle pour surmonter les limites des méthodes de contrôle classiques. Avec l'augmentation de la dépendance aux énergies renouvelables, la stabilité du réseau électrique et l'optimisation de la production énergétique dans des conditions de vent variables deviennent essentielles. Cependant, les méthodes de contrôle traditionnelles, comme le régulateur proportionnel-intégral (PI), bien qu'efficaces, montrent des limites face aux non-linéarités et aux incertitudes inhérentes aux systèmes d'éoliennes, en particulier avec les fluctuations de vitesse du vent.

Pour relever ces défis, cette étude présente des stratégies de contrôle améliorées par intelligence artificielle, y compris des régulateurs PI optimisés, le contrôle par mode glissant (CMG), le contrôle par mode glissant super-torsadé (CMG-ST), la logique floue, et les réseaux de neurones artificiels (RNA). La thèse commence par une présentation des bases théoriques, abordant la modélisation détaillée des systèmes aérodynamiques des éoliennes et de la dynamique des GADA, fournissant ainsi une compréhension approfondie des exigences de contrôle. Ensuite, les régulateurs PI optimisés sont étudiés, et l'amélioration via l'optimisation par essaims particulaires montre une grande efficacité dans la réduction des erreurs en régime permanent. Toutefois, les limites de stabilité en puissance du rotor indiquent la nécessité de méthodes plus avancées.

L'étude se poursuit avec l'exploration des techniques de contrôle intelligent. Un contrôleur hybride combinant logique floue et contrôle par mode glissant super-torsadé (Floue-CMGST) est développé, adressant efficacement les problèmes de chattering et offrant des performances supérieures pour gérer les non-linéarités par rapport aux méthodes classiques. De plus, les réseaux de neurones artificiels sont utilisés pour améliorer les performances du régulateur PI, éliminant les dépassements de signal et produisant des réponses plus harmonieuses.

Pour la gestion de la puissance à l’échelle de la ferme éolienne, la thèse propose un nouvel algorithme de distribution de puissance entre les éoliennes. Cet algorithme redistribue dynamiquement la puissance en réponse aux turbines sous-performantes, maintenant ainsi efficacement la stabilité du réseau. Comparé au régulateur PI classique, ce nouvel algorithme montre une répartition proportionnelle et précise de la puissance avec une réponse immédiate aux variations, améliorant la productivité énergétique globale.

Les résultats soulignent le potentiel des stratégies de contrôle basées sur l'intelligence artificielle pour optimiser le contrôle des éoliennes et la gestion de la puissance au sein des parcs éoliens. En intégrant des algorithmes de contrôle avancés avec des techniques d'intelligence artificielle, cette étude contribue au développement de systèmes éoliens renouvelables et durables, et ouvre la voie à de futures innovations dans le domaine du contrôle des énergies renouvelables.

Mots clés : Système de Conversion d'Énergie Éolienne, Générateur Asynchrone à Double Alimentation, PI Optimisé, Contrôle par Mode Glissant Super Torsadé, Contrôle par Logique Floue, Réseau de Neurones Artificiels, Gestion de Puissance de Parc Éolien.

Table of contents

Table of figures

List of tables

List of abbreviations

COP26	26th Conference of the Parties
GWEC	Global Wind Energy Council
WECS	Wind Energy Conversion System
CAGR	Compound Annual Growth Rate
FOC	Field Oriented Control
DTC	Direct Torque Control
DPC	Direct Power Control
MDP	Model Predictive Control
MAS	Multi Agent Systems
DFIG	Doubly Fed Induction Generator
AC	Alternative Current
DC	Direct Current
BEM	Blade Element Momentum
TSR	Tip Speed Ratio
PI	Proportional Integral
PSO	Paricle Swarm Optimization
GWO	Grey Wolf Optimization
GA	Genetic Algorithm
DSA	Direct Synthesis Approach
GE	General Electric
MPPT	Maximum Power Point Tracking
ITAE	Integral Time Absolute Error
AI	Artificial Intelligence
ML	Machine Learning
SMC	Sliding Mode Control
STSMC	Super Twisting Sliding Mode Control
FLC	Fuzzy Logic Control
ANN	Artificial Neural Network
NL	Negative Large
NM	Negative Medium
NS	Negative Small
ZE	Zero Equal
PS	Positive Small
PM	Positive Medium
PL	Positive Large
HFSTSMC	Hybrid Fuzzy Super Twisting Sliding Mode Control
MSE	Mean Squared Error

List of symbols

E	Kinetik energy
m	Mass of air
v	Wind speed
ρ	Air density
V	Volume of air
Q	Volumetric flow rate
t	time
A	Swept area of the turbine blades
P_w	Power available from the wind
R	Radius of the rotor
P_t	Power extracted by the turbine
C_p	Power coefficient
β	Pitch angle
λ	Tip speed ratio
ω_{mech}	Rotational speed of the turbine blades in radians per second
ω_m	Electrical rotational speed
θ_0	Initial angle by which rotor and stator coils are offset in electrical space
θ_m	Angle between the rotor and stator axis
θ_{da}	Angle between stator and d-axis
θ_{dA}	Angle between rotor and d-axis
ω_d	Synchronous speed of the generator
$v_{a,b,c}$	Three phase voltage
v_{ds}	Stator voltage in the d-axis
v_{qs}	Stator voltage in the q-axis
v_{dr}	Rotor voltage in the d-axis
v_{qr}	Rotor voltage in the q-axis
i_{ds}	Stator current in the d-axis
i_{qs}	Stator current in the q-axis
i_{dr}	Rotor current in the d-axis
i_{qr}	Rotor current in the q-axis
ϕ_{ds}	Stator flux linkage in the d-axis
ϕ_{qs}	Stator flux linkage in the q-axis
ϕ_{dr}	Rotor flux linkage in the d-axis
ϕ_{qr}	Rotor flux linkage in the q-axis
R_r	Rotor resistance
R_s	Stator resistance
L_s	Stator leakage inductance
L_r	Rotor leakage inductance
L_m	Magnetising (mutual) inductance
f_{syn}	Synchronous frequency
T_{turb}	Turbine torque
$T_{em,gen}$	Electromagnetic torque
J_{turb}	Turbine moment of inertia
P_s	Stator active power
Q_s	Stator reactive power
P_r	Rotor active power
Q_r	Rotor reactive power

σ	Sigma (Constant)
S	Parameter of complex frequency
$v_{dr,comp}$	Rotor voltage compenstation part in the d-axis
$v_{qr,comp}$	Rotor voltgae compenstation part in the q-axis
v'_{dr}	Rotor voltage control part in the d-axis
v'_{dr}	Rotor voltage control part in the q-axis
P	Number of poles
$P(\theta)$	Park matrix
C	Clarck Matrix
K_{opt}	Optimal gain
K_p	Proportional gain
K_i	Integral gain
G_{ol}	Open loop transfer function
PM	Phase margin
ω_c	Crossover frequency
j	Imaginary unit
$X_{\alpha,\beta,\delta}$	Position of alpha, beta and delta wolves
X_p	Postion of prey
v_i	Velocity of particle i
x_i	Position of particle i
$Pbest$	Persona; best position of particle i
$Gbest$	Global best position among all particles
$S(x)$	Sliding surface
$Sign(x)$	Signum function
u_{sw}	Switching control
u_{eq}	Equivalent control
$V(x)$	Lyapunov function
$P_{s,cangen}$	Stator active power can generate by each turbine in wind farm
$P_{s,ref}$	Total grid power required
$P_{s,target}$	Target power output per turbine
n	Number of tubines wind farm
$P_{s,i}$	Redistributed power for tubines
$ratio_i$	Power generation ratio
Sum_{under}	Cumulative deficit
Sum_{over}	Surplus generation capacity

Chapter I

Introduction & state of the art

I.1. Background and motivation

The urgent need for transitioning to renewable energy has been underscored by recent environmental, political, and economic challenges. The year 2023 highlighted this imperative as the wind industry expanded significantly, adding over 116.6 GW of new global wind capacity and bringing the total installed capacity to 1021 GW, marking a 11% growth from 2020 (as shown in in Figure I.1 and in Figure I.2) [1]. This growth reflects the increasing recognition of wind energy's crucial role in achieving climate goals, particularly as international negotiations around climate change, such as COP26, emphasize the goal of limiting global warming to 1.5°C [1], [2].

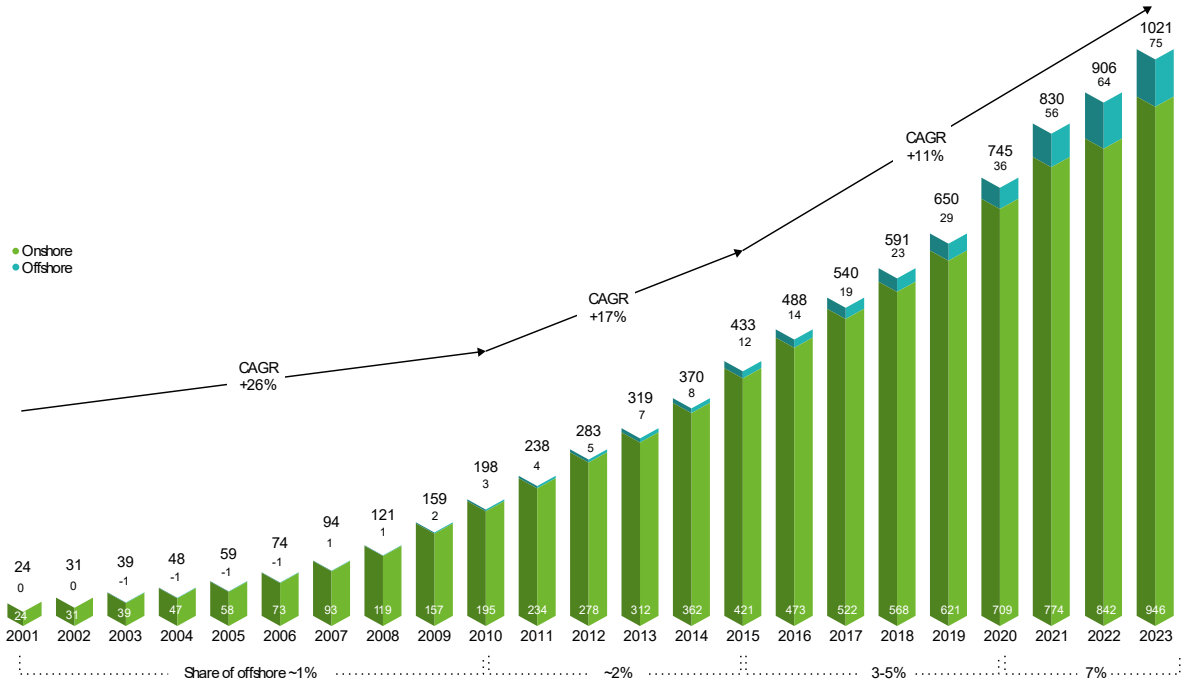

Fig. I.1 Historic development of total installations 2001-2023 (GW) [1].

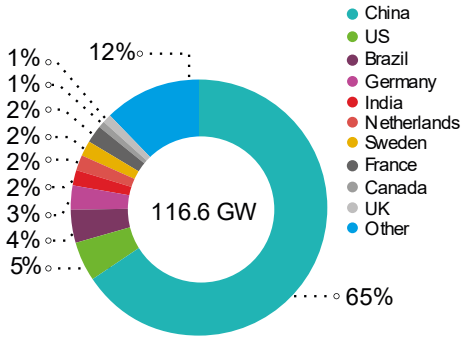

Fig. I.2 New wind power capacity in 2023 [2].

Despite progress, the expansion rate of wind energy installations remains insufficient to meet global climate targets. For instance, according to the Global Wind Energy Council (GWEC), by 2030, we may fall short of the necessary wind energy capacity to maintain a 1.5°C trajectory, achieving only 64% of required installations at current growth rates. As seen in Figure I.3, projections indicate a need for a fourfold increase in annual installations to meet these goals. The impact of this shortfall is not limited to climate change; it also affects energy security, as underscored by events like Russia's invasion of Ukraine in 2022, which exposed the vulnerabilities tied to fossil fuel dependence and the geopolitical risks it entails.

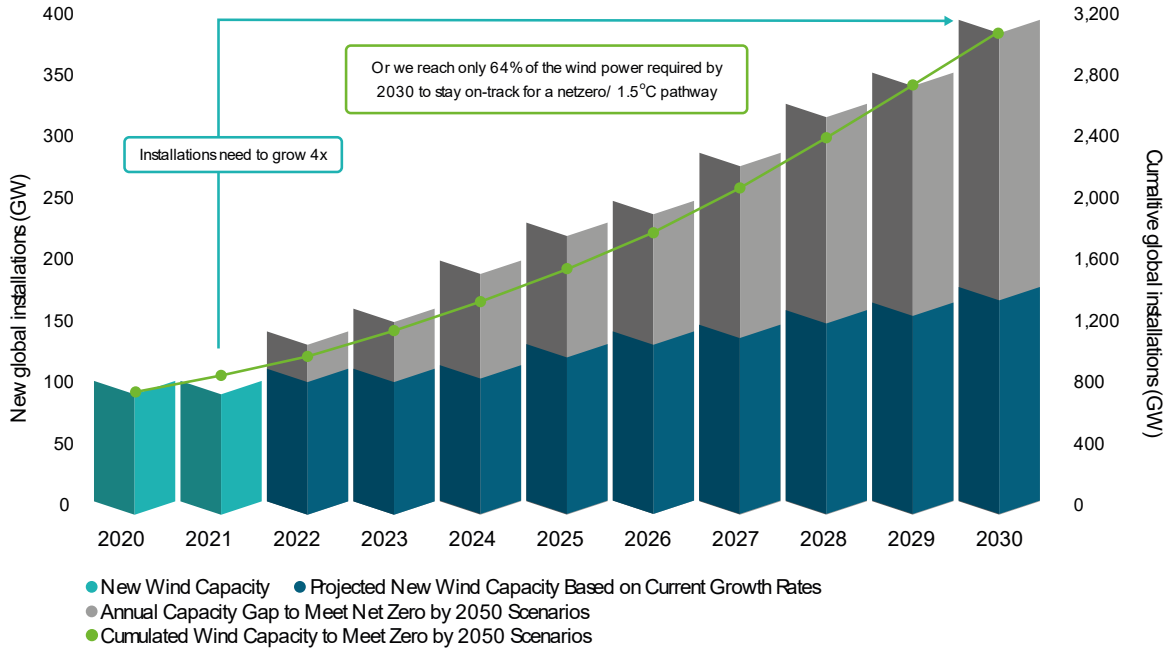

Fig. I.3 Decadal growth slowdown results in projected wind energy deficits by 2030 [2].

With increasing demands for sustainable and resilient energy sources, wind energy has emerged as a leading solution. The reliance on Doubly Fed Induction Generators (DFIGs) in wind turbines has gained traction due to their ability to provide efficient active and reactive power control, which is vital for grid stability. The enhanced control capabilities of DFIGs enable wind farms to contribute more effectively to grid reliability, positioning them as essential components in modern renewable energy systems [3], [4], [5], [6]. This thesis focuses on addressing challenges in power management for wind farms, with the specific aim of leveraging artificial intelligence to improve the control systems governing DFIG-based turbines.

Wind energy, however, faces obstacles such as supply chain limitations, regulatory inconsistencies, and high initial costs, which can hinder its deployment and sustainability. As the wind energy industry scales, overcoming these challenges through innovative approaches, such as AI-driven control strategies, becomes essential. These approaches have the potential to optimize turbine performance, enhance stability, and contribute to the goal of a carbon-neutral energy grid, laying the foundation for future research in intelligent wind farm management.

I.2. Problem statement

The increasing global adoption of wind energy as a renewable energy source brings with it significant challenges, particularly in the control and optimization of wind turbines and wind farms. Traditional control methods, such as the Proportional-Integral (PI) controller, are widely used due to their simplicity and effectiveness in basic scenarios. However, these methods exhibit limitations when faced with the complex dynamics of wind energy systems, particularly the nonlinearities, parameter uncertainties, and highly variable wind conditions inherent in real-world environments. The conventional PI controller, for instance, struggles to adapt dynamically to the fluctuations in wind speed and cannot sufficiently address the needs of grid stability and efficient power output [7], [8].

The existing literature highlights a range of methods that attempt to address these challenges, yet many lack the robustness needed for the real-time control and optimization of wind energy systems. While some studies explore advanced control strategies, such as Sliding Mode Control (SMC) or Fuzzy Logic Control (FLC), there is still a noticeable gap in

comprehensive approaches that leverage Artificial Intelligence (AI) to improve wind turbine and wind farm performance under a broad range of operational conditions. Particularly, the integration of AI techniques—such as Neural Networks, optimized control through metaheuristics, and hybrid control methods—into wind energy systems remains underexplored, despite its potential to enhance adaptability, accuracy, and resilience [6], [9], [10], [11], [12], [13], [14], [15], [16].

Furthermore, one of the most critical challenges lies in maintaining grid stability while optimizing turbine performance. Wind energy systems must align with strict grid requirements, adjusting dynamically to meet demand while minimizing the impact of variable wind speeds on power output. However, conventional control approaches often result in inefficiencies, such as oscillations or steady-state errors, which compromise both grid stability and turbine lifespan. Thus, there is an urgent need for control strategies that not only improve the precision and responsiveness of individual turbines but also coordinate power distribution effectively across wind farms, ensuring a stable and reliable energy supply to the grid.

This thesis addresses these limitations by developing advanced control strategies that integrate AI techniques to manage the complexities of wind turbine systems. The proposed approach aims to enhance the stability and efficiency of DFIG-based wind turbines and support effective wind farm management, contributing to the ongoing transition to renewable energy and a more sustainable power grid.

I.3. Objective of the study

The primary objectives of this study are as follows:

- Optimize the stator power control of a DFIG-based wind turbine to improve energy capture and maintain operational stability.
- Develop and implement AI-based control strategies tailored for wind turbines to enhance their adaptability and efficiency under fluctuating wind conditions.
- Evaluate and compare the performance of these AI-driven control techniques against traditional methods, such as PI controllers, to highlight advancements in precision, responsiveness, and reliability under variable environmental conditions.
- Design and apply a novel algorithm for power management across a wind farm, ensuring stable power output to the grid through effective redistribution of power among turbines.

I.4. Scope and limitations

This thesis primarily focuses on the control and management of Doubly-Fed Induction Generator (DFIG)-based wind turbines, aiming to enhance the efficiency and stability of these systems within wind farms. The study explores the application of Artificial Intelligence (AI) techniques, specifically using methods such as Artificial Neural Networks (ANN), Fuzzy Logic, and hybrid controllers, to improve turbine performance under variable and often challenging wind conditions. Additionally, it addresses wind farm power management, particularly through the redistribution of power among individual turbines to ensure consistent grid supply and optimal utilization of available resources.

However, this research has several limitations. The control strategies and algorithms developed are validated through simulations rather than real-world implementation, as practical testing remains beyond the scope of this study. Additionally, due to the absence of modern hardware, the work is restricted to specific control strategies, focusing on AI-driven and hybrid approaches while excluding other potential control methods. This limitation is driven by the constraints of current laboratory resources and the need to prioritize selected advanced control techniques.

I.5. State of the art in DFIG-based wind turbine control and power management

I.5.1. DFIG-based wind turbines and control techniques

DFIG-based wind turbines are popular in variable-speed wind energy applications because of their ability to decouple active and reactive power, enhancing grid stability and power quality. Conventional control methods, such as Proportional-Integral (PI) controllers, have historically been applied to regulate these power flows. PI control, however, often struggles with non-linearities inherent in wind energy conversion systems (WECS) and fluctuating wind speeds [17]. To overcome these limitations, advanced control strategies have been developed, focusing on robustness, efficiency, and adaptability to changing conditions.

I.5.2. Advanced control strategies

Studies have introduced several non-linear control techniques to improve WECS performance, including Field-Oriented Control (FOC), Direct Torque Control (DTC), and Direct Power Control (DPC) [18], [19], [20], [21]. While FOC offers precision, it requires complex coordinate transformations, making it parameter-dependent and less robust to disturbances. DTC and DPC provide faster responses but can introduce high torque ripples and non-constant switching frequencies, affecting stability and efficiency. As a result, researchers have integrated AI-based controllers, including fuzzy logic and neural networks, to address these limitations.

I.5.3. AI-driven control for enhanced stability and efficiency

AI techniques like fuzzy logic control (FLC) and artificial neural networks (ANN) have shown promise in improving the robustness of DFIG control. FLC is particularly effective in handling parameter variations and uncertainties, providing stable power outputs under fluctuating wind conditions. ANN-based Direct Power Control (DPC) further enhances DFIG performance by learning optimal control actions, improving power decoupling and minimizing parameter dependencies [22], [23], [24].

Hybrid approaches combining traditional and AI-based control have been developed to balance precision and robustness. For example, fuzzy-PI and sliding mode controllers (SMC) are often used for handling rapid wind variations and grid faults [25], [26], [27]. These hybrid controllers offer greater stability and faster convergence than standalone PI or SMC methods, especially under grid disturbances.

I.5.4. Wind farm power management

The management of wind farm power has evolved significantly to address grid stability challenges and optimize energy output. Conventional centralized control methods are increasingly being supplemented by distributed and adaptive control algorithms. These methodologies fall into three main categories: heuristic-based approaches, optimization-driven methods, and advanced AI-based strategies.

- **Heuristic-based control approaches**

  Rule-based and heuristic control methods rely on predefined decision-making frameworks. Traditional decision-tree-based controllers and lookup tables offer simplicity and computational efficiency but struggle to adapt to rapidly changing wind conditions. Fuzzy logic controllers improve flexibility by dynamically adjusting control responses based on turbine performance and environmental conditions. Expert systems further enhance decision-tree controllers by incorporating rule-based inference mechanisms [4], [28]. However, these heuristic methods are limited by their dependence on predefined knowledge bases, making them less effective in nonstationary wind environments.

- **Optimization-based control**

Optimization-based control methods use mathematical models to determine the best power dispatch strategies. These approaches include linear, nonlinear, and mixed-integer programming techniques aimed at minimizing power losses and maintaining grid stability [29]. Constraints such as wake effects, voltage regulation, and turbine lifespan must be considered.

Genetic Algorithms (GA) apply evolutionary principles to optimize turbine coordination and power dispatch. While effective, GA requires significant computational resources due to iterative solution refinement. Particle Swarm Optimization (PSO) offers an alternative inspired by swarm intelligence, adjusting turbine control parameters dynamically. Distributed PSO further enhances scalability by segmenting wind farms for localized optimization [30]. Although PSO is computationally less demanding than GA, its convergence depends on careful parameter tuning and real-time adaptability.

Optimization strategies must also consider regulatory requirements, such as reactive power compensation and frequency response mandates [4], [31]. Studies have demonstrated that optimization-based control enhances power dispatch accuracy, but real-time computational efficiency remains a challenge [32].

- **Advanced AI-based control algorithms**

Model Predictive Control (MPC) and Distributed MPC (DMPC) are key techniques for wind farm power management, allowing real-time forecasting and dynamic power dispatch adjustments. These methods effectively reduce wake losses and improve energy efficiency [33]. MPC's ability to handle constraints within a multi-objective framework enhances its adaptability to fluctuating wind conditions [4], [34].

PI controllers remain essential at the turbine level for managing active and reactive power, providing a simple yet effective solution for stabilizing power fluctuations. Despite their lack of adaptability compared to MPC and AI-based methods, they complement predictive control frameworks by ensuring responsive regulation.

Artificial Neural Networks (ANNs) offer another advanced approach, modeling nonlinear interactions within wind farms to predict turbine behavior under varying wind conditions [35]. Deep Reinforcement Learning (DRL) builds upon ANN-based control by enabling autonomous learning and policy optimization in complex environments. DRL continuously adapts power dispatch to maximize energy output while maintaining grid stability [36].

Multi-Agent Systems (MAS) leverage AI to coordinate turbine responses dynamically, redistributing power based on wind fluctuations and underperforming turbines [37]. These methods enhance operational efficiency by minimizing oscillations and optimizing total power output.

Each control strategy presents trade-offs in computational complexity, adaptability, and regulatory compliance. Heuristic approaches offer low computational costs but lack responsiveness to dynamic conditions. Optimization-based techniques improve grid integration and energy efficiency but require significant computational power. AI-driven methods, such as MPC and DRL, provide superior adaptability and predictive capabilities but demand extensive computing resources.

I.5.5. Identified research gaps

Current literature reveals several gaps:

- Integration of AI with classical control: Although hybrid AI-classical controllers show improved performance, their scalability and adaptability to larger wind farms remain

limited. More research is needed to fully integrate AI models with classical techniques for both local and distributed control

- Stator power optimization: Effective stator power management remains challenging due to the limitations of conventional control in the presence of grid disturbances and variable wind speeds. AI-based control strategies focused on optimizing stator power in DFIG systems are underexplored, leaving room for novel approaches.
- Robust distributed control for wind farms: While centralized control methods are commonly used, distributed AI-based control remains a less investigated area. Research is required to develop scalable, distributed algorithms that can dynamically manage power across multiple turbines to ensure grid stability in real time.

This state of the art review underscores the need for advanced AI-based control solutions in DFIG wind turbines and wind farm power management. The proposed research aims to fill these gaps by developing novel AI-enhanced controllers and power management algorithms that optimize wind turbine output and ensure reliable integration into the grid under varying conditions.

I.6. Structure of the thesis

This thesis is structured to progressively develop and analyze advanced control and management solutions for DFIG-based wind turbines and wind farms, with a focus on AI integration.

Chapter I: provides an introduction to the research problem, objectives, scope, and significance of the study, alongside a summary of relevant literature in renewable energy systems, conventional and AI-enhanced control strategies, and wind farm power management.

Chapter II: investigates into the theoretical foundations of wind turbine modeling and control techniques, covering aerodynamic modeling, the dynamics of Doubly Fed Induction Generators (DFIG), and key control methodologies. This chapter sets the groundwork for the control strategies examined in later sections.

Chapter III: addresses the design, implementation, and optimization of Proportional-Integral (PI) controllers for wind turbine control. It includes an analysis of PI control performance and introduces optimization techniques aimed at improving response accuracy and adaptability in variable wind conditions.

Chapter IV: explores advanced control strategies incorporating AI-based methods such as fuzzy logic, artificial neural networks (ANN), and hybrid control approaches. Each technique is evaluated based on its potential to handle non-linearities and improve system robustness, focusing on stator power control within DFIG systems.

Chapter V: shifts the focus to wind farm power management, detailing the development and implementation of novel algorithms designed to dynamically allocate power across multiple turbines. This chapter includes simulations and comparisons of AI-driven power management with traditional methods to assess grid stability and efficiency under fluctuating wind conditions.

Chapter VI: concludes the thesis with a summary of key findings, implications, and contributions, and outlines potential directions for future research, particularly in real-world applications and further AI integrations in wind energy systems.

This structure is designed to offer a comprehensive examination of AI-enhanced control and power management strategies for DFIG-based wind turbines, advancing the field of renewable energy control systems.

Chapter II
Modeling of DFIG-based wind turbine

II.1. Introduction

The integration of wind energy into the global energy mix has seen significant advancements, with technologies continually evolving to maximize efficiency and reliability [38]. A crucial component of this progress is the accurate modeling of wind turbine systems, particularly those based on Doubly Fed Induction Generators (DFIG) [39]. This chapter focuses on the detailed modeling of both the aerodynamic aspects of wind turbines and the electrical dynamics of DFIG systems.

Wind energy stands out as a promising renewable resource due to its abundance and sustainability. To harness this energy efficiently, modern wind turbines are equipped with sophisticated technologies designed to optimize performance under varying wind conditions. Among these technologies, the DFIG has gained prominence for its ability to offer flexible control over active and reactive power, thus enhancing the stability and efficiency of wind power generation [40]. As shown in Figure. II.1, the wind energy system comprises various components that work together to convert wind energy into electrical power effectively.

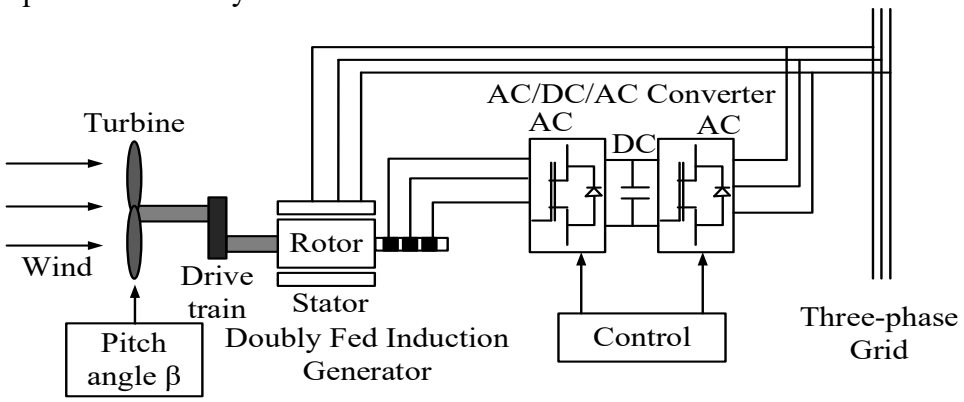

Fig. II.1 Wind energy conversion system based on DFIG [41].

The aerodynamic modeling of wind turbines is fundamental to understanding how wind energy is converted into mechanical power. This involves a comprehensive analysis of the interactions between the wind and the turbine blades. The aerodynamic forces acting on the blades, such as lift and drag, are pivotal in determining the amount of energy that can be captured from the wind. Accurate aerodynamic models incorporate factors such as blade geometry, wind speed, and atmospheric conditions to predict the performance of the turbine and optimize its design [39], [40], [42].

Blade Element Momentum (BEM) theory is one of the primary methods used in aerodynamic modeling. It combines the principles of blade element theory and momentum theory to provide a detailed understanding of the forces acting on each blade segment. This approach allows for the precise calculation of power output and helps in the design of blades that can efficiently capture wind energy. Additionally, advanced aerodynamic models account for the effects of turbulence and wind shear, which are critical for ensuring the structural integrity and performance of the turbine under real-world conditions [43].

On the electrical side, the modeling of DFIG systems is equally complex and essential for effective wind turbine operation. The DFIG technology allows for variable speed operation, which is crucial for maximizing energy capture from fluctuating wind speeds. The DFIG system consists of a wound rotor induction generator with slip rings connected to a partial-scale power converter. This setup enables the control of rotor currents, providing the ability to independently control active and reactive power [44].

The mathematical modeling of DFIG systems involves representing the generator's electrical dynamics using differential equations. These equations describe the relationships between the rotor speed, electrical frequencies, and the power exchanged with the grid. By understanding these

dynamics, engineers can optimize the performance of DFIG-based wind turbines and ensure their reliable operation [45], [46].
In summary, the modeling of aerodynamic and DFIG systems is a critical aspect of modern wind turbine technology. By developing accurate and detailed models, engineers can design and control wind turbines that maximize energy capture, ensure grid stability, and withstand the challenges posed by varying wind conditions. This chapter provides an in-depth exploration of the methodologies and principles underlying the modeling of these systems, laying the groundwork for advanced research and development in the field of wind energy.

II.2. Aerodynamic model

The aerodynamic model of a wind turbine is fundamental in understanding the conversion of wind energy into mechanical power. Accurate aerodynamic modeling is essential for predicting the performance of wind turbines under varying environmental conditions, such as wind speed, turbulence, and atmospheric density. This section delves into the key aerodynamic principles governing the interaction between wind and turbine blades, which ultimately dictates the efficiency of energy capture.
To maximize the energy extracted from the wind, modern wind turbines rely on advanced aerodynamic designs that optimize blade geometry and account for dynamic factors like wind shear and turbulence. Blade Element Momentum (BEM) theory plays a critical role in this modeling, combining the physics of blade aerodynamics with momentum conservation to compute the forces acting on individual blade elements. By applying this method, The power output can be estimated, and the optimal conditions for turbine operation can be predicted [47], [48].
This section will also introduce key parameters such as the power coefficient C_p, tip speed ratio λ and pitch angle β, which are crucial in determining the turbine's efficiency. These aerodynamic concepts will provide a comprehensive framework for simulating the energy conversion process, forming the foundation for the overall performance analysis of the wind turbine system [49], [50], [51].
The kinetic energy of wind can be calculated using the following formula:

$$E = \frac{1}{2}mv^2 \tag{II-1}$$

Where: $E$is the kinetic energy (Joule), m is the mass of air (Kg) and v is the wind speed (m/s).
Knowing that:

$$m = \rho V \tag{II-2}$$

where ρ is the air density (approximately 1.225 kg/m³ at sea level) and V is the volume of air.
and from the volumetric flow rate:

$$Q = \frac{V}{t} = Av \tag{II-3}$$

Where Q is the volumetric flow rate (m^3/s), t time (second) and A is the swept area of the turbine blades.
Solving for V from Eq.(II-3) and substituting it into Eq.(II-1) yields:

$$E = \frac{1}{2}\rho A v^3 t \tag{II-4}$$

Knowing that $E = P.t$ and $A = \pi R^2$, where P represents the power, R is the radius of the rotor, and incorporating Eq.(II-4), the available wind power is determined as follows:

$$P_w = \frac{1}{2}\rho A v_1^3 = \frac{1}{2}\rho \pi R^2 v_1^3 \tag{II-5}$$

The mass of moving air with density ρ passing through the surface S of the blades in one second is given by:

$$m = \frac{1}{2}\rho A(v_1 + v_2) \tag{II-6}$$

The power extracted by the turbine is the difference between the kinetic energy of the wind before and after passing through the turbine:

$$P_t = \frac{1}{2}m(v_1^2 - v_2^2) \tag{II-7}$$

By applying Eq.(II-6), the following expression is obtained:

$$P_t = \frac{1}{4}\rho A(v_1 + v_2)(v_1^2 - v_2^2) \quad \text{(II-8)}$$

The power coefficient C_p is the ratio of the power extracted by the turbine to the total power available in the wind:

$$C_p = \frac{P_t}{P_w} = \frac{1}{2}\frac{(v_1+v_2)(v_1^2-v_2^2)}{v_1^3} = \frac{1}{2}\left(1 + \frac{v_2}{v_1} - \frac{v_2^2}{v_1^2} - \frac{v_2^3}{v_1^3}\right) \quad \text{(II-9)}$$

By applying well-known algebraic identities, the following expression is derived:

$$C_p = \frac{1}{2}(1 + \frac{v_2}{v_1})(1 - \left(\frac{v_2}{v_1}\right)^2) \quad \text{(II-10)}$$

Utilizing the derivative of C_p and setting it to zero to find the critical point, the maximum achievable power coefficient, C_{pmax}, is found to be approximately 0.593. This value represents the Betz limit, indicating that no wind turbine can capture more than 59.3% of the kinetic energy available in the wind [52].

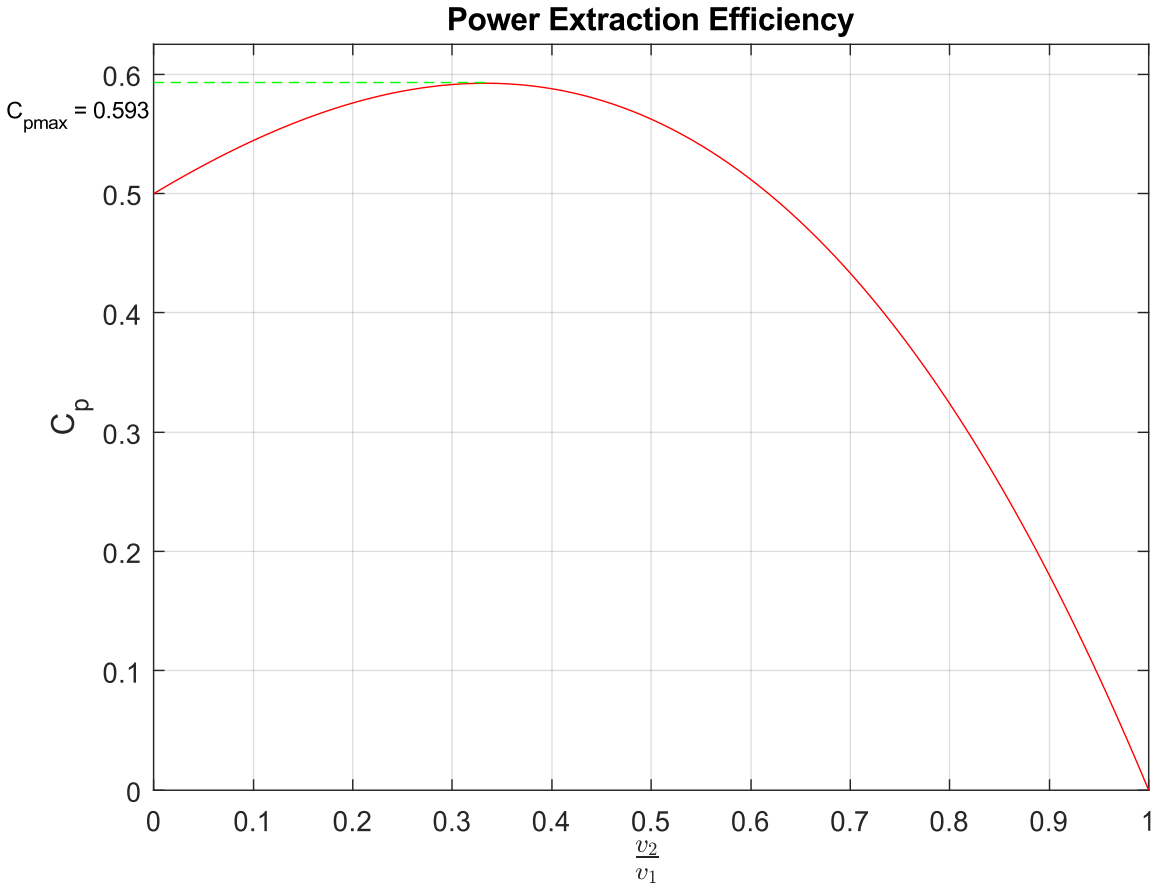

Fig. II.2 Betz limit [52].

This limit is never actually reached. In practice, the maximum C_p is 0.48 with a three-blade turbine.

The power coefficient C_p can be expressed as a function of the pitch angle β and tip speed ratio λ. The tip speed ratio λ is the ratio of the speed of the blade tips to the speed of the wind. The power coefficient and the TSR are expressed as [17]:

$$C_p(\beta,\lambda) = C_1\left(\frac{C_2}{\lambda_i} - C_3\beta - C_4\right)e^{\frac{C_5}{\lambda_i}} + C_6\lambda, \lambda = \frac{R\omega_{mech}}{v}, \frac{1}{\lambda_i} = \frac{1}{\lambda+0.08\beta} - \frac{0.035}{\beta^3+1} \quad \text{(II-11)}$$

Where $C_1, C_2, \ldots, C_6$ are constants that depend on the specific wind turbine design. In our system these constants are 0.52, 116, 0.4, 5, 21 and 0.0068 respectively, and ω_{mech} is the rotational speed of the turbine blades in radians per second, v is the wind speed.

From Eq.(II-9), the following expression is obtained:

$$P_t = \frac{1}{2} C_p(\beta, \lambda) \rho A v_1^3 = \frac{1}{2} C_p(\beta, \lambda) \rho \pi R^2 v_1^3 \quad \text{(II-12)}$$

Figure II.3 illustrates the relationship between the power coefficient C_p and the tip speed ratio λ for various pitch angle β. The graph indicates that an increase in β leads to a reduction in C_p, thereby decreasing the generated power. The maximum power coefficient, $C_p = 0.39$, is achieved at $\lambda = 9.886$ when $\beta = 0$. To achieve optimal performance, the system must regulate the rotational speed to maintain λ at its optimal value (λ_{opt}), ensuring maximum C_p, as shown in Figure II.3, The optimal power can be determined using the following equation:

$$P_t^* = \frac{1}{2} C_{pmax}(\beta, \lambda_{opt}) \rho \pi R^2 v_1^3 \quad \text{(II-13)}$$

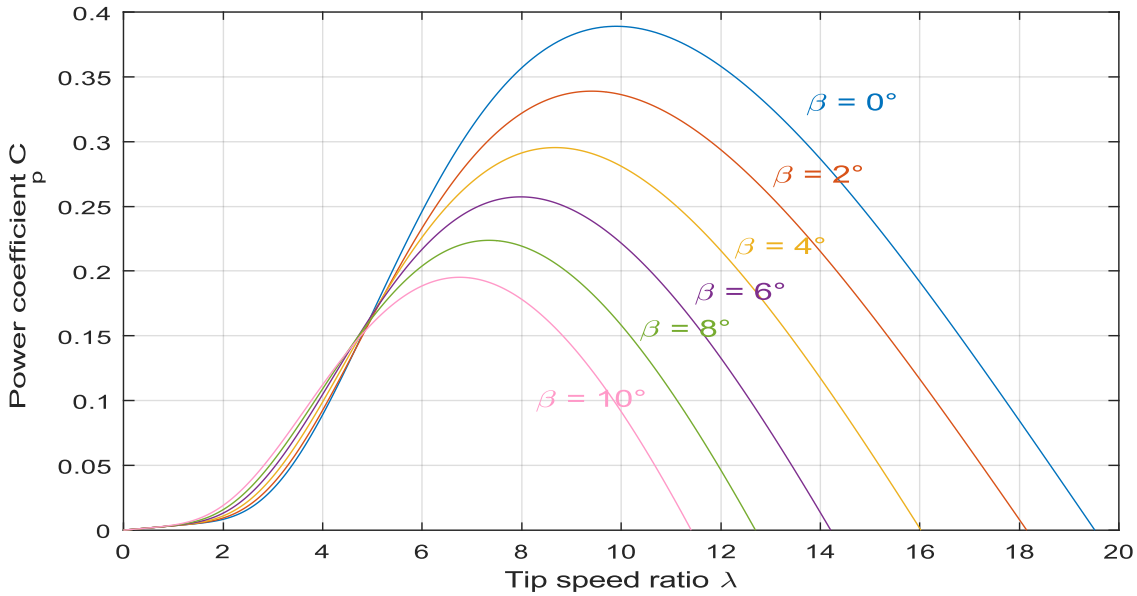

Fig. II.3 Power coefficient (C_p) vs tip speed ratio (λ) [6].

II.3. DFIG model and control system

The Doubly Fed Induction Generator (DFIG) is a key technology in modern wind turbines, valued for its efficiency and flexibility in controlling active and reactive power. This section provides a detailed model of the DFIG, covering its electrical and mechanical dynamics. Understanding the DFIG model is crucial for enhancing energy capture and ensuring stable integration into the power grid [53], [54].

The DFIG system consists of a wound rotor induction generator connected to the grid via both the stator and rotor windings. The rotor winding is connected to the grid through a back-to-back converter, which allows for variable speed operation and independent control of active and reactive power. The stator is directly connected to the grid, providing a path for power transfer [55], [56], [57], [58].

The following are some advantages of employing a DFIG in wind applications:

1. The turbine's speed can be adjusted across a broad range, allowing it to operate at its optimal power coefficient C_p.
2. The stator is connected directly to the electrical grid, while the rotor is powered through power electronics that typically account for around 30% of the turbine's rated power.
3. The reactive power supplied to the rotor is controllable and it is amplified on the stator-side.

A major drawback of DFIGs is the need for regular maintenance of the slip rings and brushes.

Figure II.4 illustrates the rotor and stator circuits of a DFIG, depicted with three-phase windings. This representation helps in understanding the electrical interactions between the rotor and stator. It also

highlights the arrangement and connection of the windings essential for DFIG operation., where Figure II.5 illustrates the stator and rotor representation by equivalent dq winding currents. This representation simplifies the analysis and control of the DFIG by transforming the three-phase stator and rotor quantities into the dq reference frame using Park transformation. This transformation allows for more straightforward modeling of the dynamic behavior of the DFIG, making it easier to implement advanced control strategies for optimal performance and stability in wind energy applications.

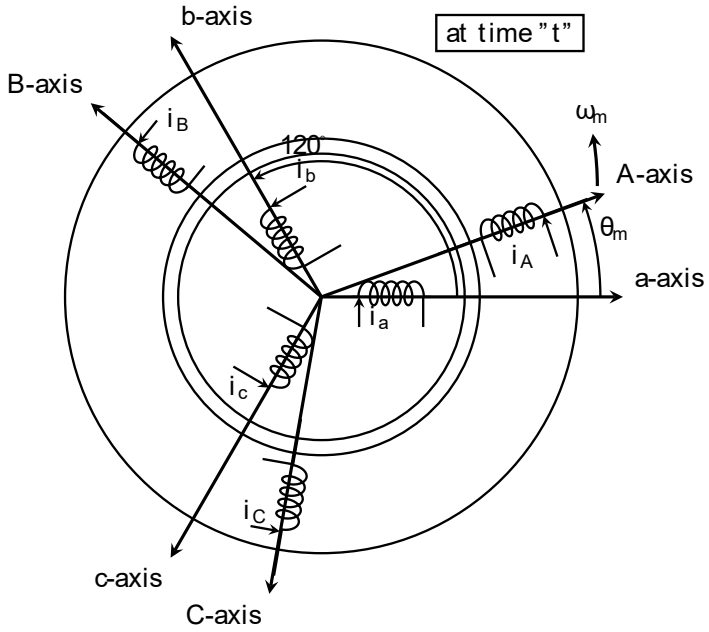

Fig. II.4 Rotor and stator circuit represented by three-phase windings [45].

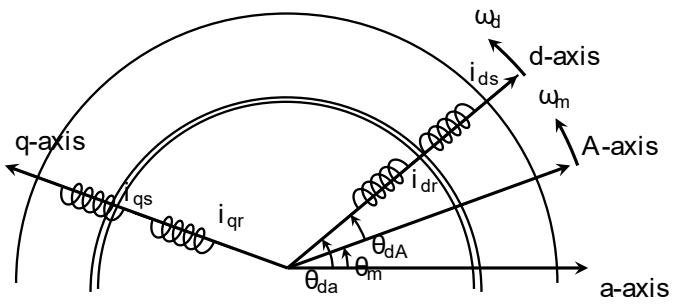

Fig. II.5 Stator and rotor representation by equivalent dq winding currents [45].

The DFIG model is developed based on the following assumptions [17]:

- The air gap is dispersed evenly.
- windage losses, friction and Eddy currentsare all negligible.
- The windings on the stator and rotor are the same.
- Under unsaturated magnetic field conditions, the induction machine functions.
- Magnetic linearity is demonstrated via the induction generator.
- A balanced three-phase sinusoidal voltage from the power grid powers the stator.
- The rotor voltage is controllable through power electronics.
- Leakage resistances and inductances from the stator and rotor are negligible and may be disregarded.

The mathematical modeling of the DFIG involves the following key components:

- Electrical equations

$$v_{ds} = R_s i_{ds} + \frac{d}{dt}\phi_{ds} - \omega_d \phi_{qs} \quad \text{(II-14)}$$

$$v_{qs} = R_s i_{qs} + \frac{d}{dt}\phi_{qs} + \omega_d \phi_{ds} \quad \text{(II-15)}$$

$$v_{dr} = R_r i_{dr} + \frac{d}{dt}\phi_{dr} - \omega_{dA} \phi_{qr} \quad \text{(II-16)}$$

$$v_{qr} = R_r i_{qr} + \frac{d}{dt}\phi_{qr} + \omega_{dA} \phi_{dr} \quad \text{(II-17)}$$

- Magentic equations

$$\phi_{ds} = L_s i_{ds} + L_m i_{dr} \quad \text{(II-18)}$$

$$\phi_{qs} = L_s i_{qs} + L_m i_{qr} \quad \text{(II-19)}$$

$$\phi_{dr} = L_r i_{dr} + L_m i_{ds} \quad \text{(II-20)}$$

$$\phi_{qr} = L_r i_{qr} + L_m i_{qs} \quad \text{(II-21)}$$

- Angular equations

The intersection angle θ_m between the a-axis and A-axis, measured in radians, is given by:

$$\theta_{dA} = \theta_{da} - \theta_m \quad \text{(II-22)}$$

$$\frac{d}{dt}\theta_{dA} = \omega_{dA} \quad \text{(II-23)}$$

$$\theta_m = \int \omega_m(t) dt + \theta_0 \quad \text{(II-24)}$$

Here ω_m represents the electrical rotational speed, while θ_0 denotes the initial angular offset between the rotor and stator coils in electrical space. From Eq.(II-22), and considering that $\omega_d = \frac{d\theta_{da}}{dt}$, the relationship can be expressed accordingly.

$$\omega_d = \omega_{dA} + \omega_m \quad \text{(II-25)}$$

The angle θ_{da} can be calculated using Clark transformation, which converts (v_a, v_b, v_c) into (v_α, v_β)

$$\theta_{da} = \tan^{-1}\frac{v\alpha}{v\beta} \quad \text{(II-26)}$$

and

$$\omega_d = \omega_{syn} = 2\pi f_{syn} \quad \text{(II-27)}$$

The mechanical angular acceleration of the wind turbine is described by:

$$\frac{d\omega_{mech}}{dt} = \frac{T_{turb} - T_{em,gen}}{J_{turb}} \quad \text{(II-28)}$$

where ω_{mech} refers to the rotational speed of the wind turbine in mechanical terms, T_{turb} represents the torque produced by the wind turbine. The term $T_{em,gen}$ denotes the electromagnetic torque generated by the combination of the wind turbine and the generator. Additionally, J_{turb} signifies the moment of inertia associated with the system that includes both the wind turbine and the integrated generator.

Since $\omega_m = \frac{P}{2}\omega_{mech}$ where P represents the number of poles, the angular acceleration equation can be derived as follows:

$$\frac{d\omega_m}{dt} = \frac{P}{2}\frac{T_{turb} - T_{em,gen}}{J_{turb}} \quad \text{(II-29)}$$

- Torque equation

The expression for the electromagnetic torque is given by:

$$T_{em} = \frac{P}{2} L_m \left(\phi_{qr} i_{dr} - \phi_{dr} i_{qr}\right) \quad \text{(II-30)}$$

- Power equation

$$P_s = v_{ds} i_{ds} + v_{qs} i_{qs} \quad \text{(II-31)}$$

$$Q_s = v_{qs} i_{ds} - v_{ds} i_{qs} \quad \text{(II-32)}$$

$$P_r = v_{dr} i_{dr} + v_{qr} i_{qr} \quad \text{(II-33)}$$

$$Q_r = v_{qr} i_{dr} + v_{dr} i_{qr} \quad \text{(II-34)}$$

From Eq.(II-18) to Eq.(II-21)

$$\begin{bmatrix}\phi_{ds}\\ \phi_{qs}\\ \phi_{dr}\\ \phi_{qr}\end{bmatrix} = \underbrace{\begin{bmatrix}L_s & 0 & L_m & 0\\ 0 & L_s & 0 & L_m\\ L_m & 0 & L_r & 0\\ 0 & L_m & 0 & L_r\end{bmatrix}}_{[M]}\begin{bmatrix}i_{ds}\\ i_{qs}\\ i_{dr}\\ i_{qr}\end{bmatrix} \quad \text{(II-35)}$$

From Eq.(II-35), the currents can be determined by applying the inverse of the matrix [M]:

$$\begin{bmatrix}i_{ds}\\ i_{qs}\\ i_{dr}\\ i_{qr}\end{bmatrix} = M^{-1}\begin{bmatrix}\phi_{ds}\\ \phi_{qs}\\ \phi_{dr}\\ \phi_{qr}\end{bmatrix} \quad \text{(II-36)}$$

From the electrical equations, fluxes can be determined using voltage as the input, expressed as follows:

$$\frac{d}{dt}\phi_{ds} = v_{ds} - R_s i_{ds} + w_d\,\phi_{qs} \quad \text{(II-37)}$$

$$\frac{d}{dt}\phi_{qs} = v_{qs} - R_s i_{qs} - w_d\,\phi_{ds} \quad \text{(II-38)}$$

$$\frac{d}{dt}\phi_{dr} = v_{dr} - R_r i_{dr} + w_{dA}\phi_{qr} \quad \text{(II-39)}$$

$$\frac{d}{dt}\phi_{qr} = v_{qr} - R_r i_{qr} - w_{dA}\phi_{dr} \quad \text{(II-40)}$$

By substituting the flux expressions in terms of rotor currents into Eq. (II-16) and Eq. (II-17), the following equation is obtained:

$v_{dr} = R_r i_{dr} + \sigma L_r \frac{d}{dt} i_{dr} - \omega_{dA}\sigma L_r i_{qr}$, where $v'_{dr} = R_r i_{dr} + \sigma L_r \frac{d}{dt} i_{dr}$, $v_{dr,comp} = -\omega_{dA}\sigma L_r i_{qr}$ (II-41)

$v_{qr} = R_r i_{qr} + \sigma L_r \frac{d}{dt} i_{qr} - \omega_{dA}\sigma L_r i_{dr}$, where $v'_{qr} = R_r i_{qr} + \sigma L_r \frac{d}{dt} i_{qr}$, $v_{qr,comp} = -\omega_{dA}\sigma L_r i_{dr}$ (II-42)

Where $\sigma = 1 - \frac{L_m^2}{L_r L_s}$

After applying the Laplace transformation, the transfer function for controlling the DFIG system is derived as follows:

$$\begin{cases} i_{dr} = \frac{1}{R_r + S\sigma L_r} v'_{dr} \\ i_{qr} = \frac{1}{R_r + S\sigma L_r} v'_{qr} \end{cases} \quad \text{(II-43)}$$

Where S indicates the parameter of complex frequency.

By applying Eq.(II-31) and considering that $v_{qs} = 0$ and $i_{ds} \approx -\frac{L_m}{Ls} i_{dr}$, the following expression is obtained:

$$P_s = v_{ds} i_{ds} \approx -\frac{L_m}{L_s} v_{ds} i_{dr} \quad \text{(II-44)}$$

By utilizing Eq.(II-32), and considering $v_{qs} = 0$, the flux expression $\phi_{qs} = L_m i_{qr} + L_s i_{qs} \approx -\frac{v_{ds}}{\omega_d}$, leads to the following equation for the stator reactive power:

$$Q_s = -v_{ds} i_{qs} \approx v_{ds}\left(\frac{v_{ds}}{\omega_d L_s} + \frac{L_m}{L_s}\right) i_{qr} \quad \text{(II-45)}$$

Considering that $\phi_{qs} = L_m i_{qr} + L_s i_{qs} \approx -\frac{v_{ds}}{\omega_d}$, $\phi_{ds} = L_m i_{dr} + L_s i_{ds} \approx 0$, $\phi_{qs} \approx -\frac{v_{ds}}{\omega_d}$ and $i_{ds} \approx -\frac{L_m}{L_s} i_{dr}$, the electromagnetic torque expression can be written as:

$$T_{em} = \frac{p}{2} L_m\left(i_{qs} i_{dr} + i_{ds} i_{qr}\right) = \frac{p}{2}\frac{L_m}{L_s}\left[\left(\phi_{qs} - L_m i_{qr}\right) i_{dr} - \left(\phi_{ds} - L_m i_{dr}\right) i_{qr}\right] \approx -\frac{p L_m v_{sd}}{2\omega_d L_s} i_{rd} \quad \text{(II-46)}$$

Given that $v_{ds} = \sqrt{\frac{2}{3}}\widehat{V_s}$ is a constant, from Eq.(II-44), (II-45) and (II-46), it is evident that we can regulate the DFIG's stator active power P_s and electromagnetic torque T_{em} by adjusting i_{dr}, while

the stator reactive power Q_s can be controller by adjusting i_{qr}. In summary, the d-axis rotor current can used to manage the stator active power and electromagnetic torque, and the q-axis rotor current can be used to control the stator flux and reactive power.

Clearly, the DFIG can be controlled using the two decoupled components i_{dr} and i_{qr}, achieving our control objectives.

The reference signal is obtained based on the target electromagnetic torque (or the desired stator active power) and the specified stator reactive power, as shown below:

$$i_{dr}^{*} \approx -\frac{L_s}{L_m v_{sd}} P_s^{*} \quad \text{(II-47)}$$

$$i_{dr}^{*} \approx -\frac{2L_s\omega_d}{pL_m v_{sd}} T_{em}^{*} \quad \text{(II-48)}$$

$$i_{qr}^{*} \approx -\frac{L_s v_{sd}}{L_m L_s \omega_d} + \frac{L_s}{L_m v_{sd}} Q_s^{*} \quad \text{(II-49)}$$

The key parameters of the DFIG-based wind turbine system used in the simulations are summarized in Table. II.1. These parameters include electrical, mechanical, and aerodynamic characteristics, which are essential for accurately modeling the turbine's behavior and evaluating the performance of the control strategies.

Tab. II.1 Parameters of the DFIG-based wind turbine system used for modeling and simulation.

Parameter	**Definition**	**Value**	**Unit**
$\boldsymbol{R_r}$	Rotor Resistance	1.5	$m\Omega$
$\boldsymbol{R_s}$	Stator Resistance	2.0	$m\Omega$
$\boldsymbol{L_r}$	Rotor leakage	0.0024	H
$\boldsymbol{L_s}$	Stator leakage	0.0024	H
$\boldsymbol{L_m}$	Mutual leakage	0.0023	H
$\boldsymbol{f_{syn}}$	Rated frequency	60	Hz
P	Poles	6	.
$\boldsymbol{J}$	Moment of inertia for DFIG	75	Kg.m^2
$\boldsymbol{J_{Turb}}$	Moment of inertia for Wind turbine	2.4x10^6	Kg.m^2
$\boldsymbol{\rho}$	Density of Air	1.2	Kg.m^3
$\boldsymbol{D}$	Rotor Diameter for the Wind Turbine (2R)	70.5	m

II.4. Simulation

The modeling of wind turbine systems and Doubly Fed Induction Generator (DFIG) dynamics provides a theoretical foundation for understanding the complex interactions between mechanical and electrical components in wind energy systems. However, to validate these models and assess their real-world performance, it is essential to implement detailed simulations. The simulation phase serves as a critical step in analyzing the behavior of wind turbines under various operational conditions, such as fluctuating wind speeds, grid disturbances, and changing load demands.

In this section, we will simulate the aerodynamic and electrical models of the wind turbine system discussed earlier. The objective is to observe the system's response to different input parameters and control strategies, particularly focusing on optimizing energy capture and improving stability. Advanced simulation tools such as MATLAB/Simulink will be employed to replicate the dynamic behavior of the wind turbine and DFIG system, enabling us to assess system performance in both steady-state and transient conditions.

Through these simulations, the efficiency of the wind turbine under various wind conditions will be evaluated, as well as the control system's ability to manage active and reactive power in a DFIG. These results will provide insights into the effectiveness of the proposed models, enabling further refinements and enhancements to achieve optimal energy generation from wind resources.

Figure. II.6 depicts the aerodynamic model of the wind turbine, showcasing the key elements involved in converting wind energy into mechanical power through blade interaction. This model is built upon the fundamental assumptions which is uniform air flow across the blades, negligible friction and eddy currents, and a linear relationship between aerodynamic forces and blade motion. These assumptions simplify the complex dynamics of wind energy capture and provide an effective framework for analyzing turbine performance under various wind conditions.

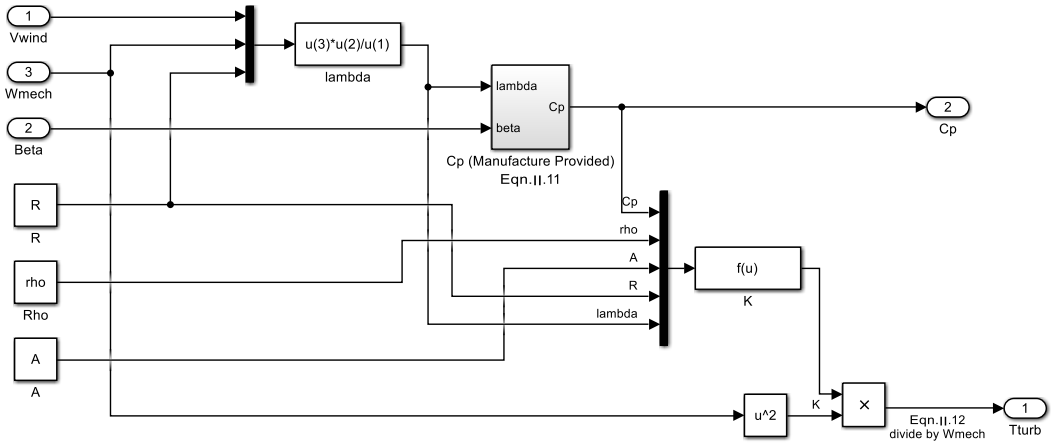

Fig. II.6 Wind turbine model.

The representation of the examined Doubly-Fed Induction Generator (DFIG) within the dq domain is illustrated in Figure II.7. This model simplifies the analysis of the DFIG by transforming the three-phase stator and rotor quantities into the dq reference frame using Park's transformation. This approach, based on the assumptions discussed earlier, allows for a more straightforward examination of the DFIG's dynamic behavior, enabling efficient control strategies for active and reactive power management. The Park and Clarke transformations, which are fundamental for simplifying the analysis of three-phase systems by converting them into the dq and αβ reference frames respectively, are presented in the following equations.

$$\begin{bmatrix} X_d \\ X_q \\ X_o \end{bmatrix} = P(\theta) \begin{bmatrix} X_a \\ X_b \\ X_c \end{bmatrix} = \sqrt{\frac{2}{3}} \begin{bmatrix} \cos\theta & \cos(\theta - 2\pi/3) & \cos(\theta + 2\pi/3) \\ \sin\theta & \sin(\theta - 2\pi/3) & \sin(\theta + 2\pi/3) \\ \frac{1}{\sqrt{2}} & \frac{1}{\sqrt{2}} & \frac{1}{\sqrt{2}} \end{bmatrix} \begin{bmatrix} X_a \\ X_b \\ X_c \end{bmatrix} \quad \text{(II-50)}$$

$$\begin{bmatrix} X_\alpha \\ X_\beta \end{bmatrix} = C \begin{bmatrix} X_a \\ X_b \\ X_c \end{bmatrix} = \begin{bmatrix} 1 & -\frac{1}{2} & -\frac{1}{2} \\ 0 & \frac{\sqrt{3}}{2} & -\frac{\sqrt{3}}{2} \end{bmatrix} \begin{bmatrix} X_a \\ X_b \\ X_c \end{bmatrix} \quad \text{(II-51)}$$

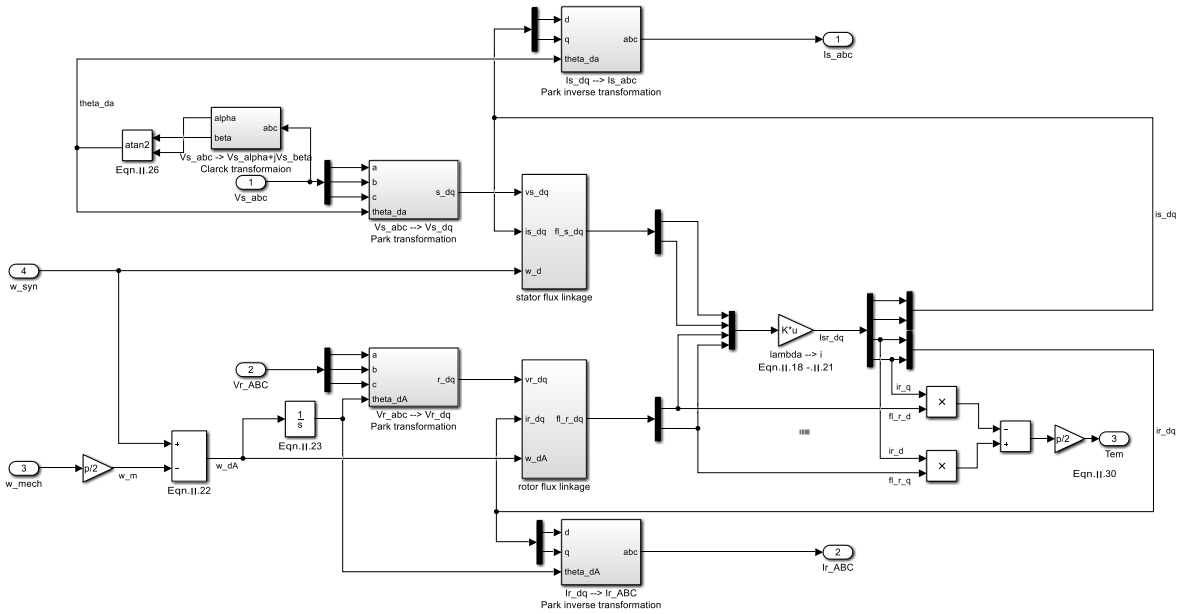

Fig. II.7 Representation of the Doubly-Fed Induction Generator (DFIG) in the dq Domain.

The estimator model, responsible for computing the variables $v_{dq,s}$, $i_{dq,s}$, $v_{dq,r}$ and $i_{dq,r}$ serves as a feedback signal for the controller. Additionally, it calculates the parameters $\theta_{da}$and θ_{dA}, which are essential for the rotor voltage compensation model and for deriving the applied rotor voltage in a three-phase frame from the dq domain voltages. This model is illustrated in Figure. II.8. Essentially, the structure of this estimator model closely resembles that of the DFIG model. however, it differs in that there is no requirement to compute the current and torque within the estimator model.

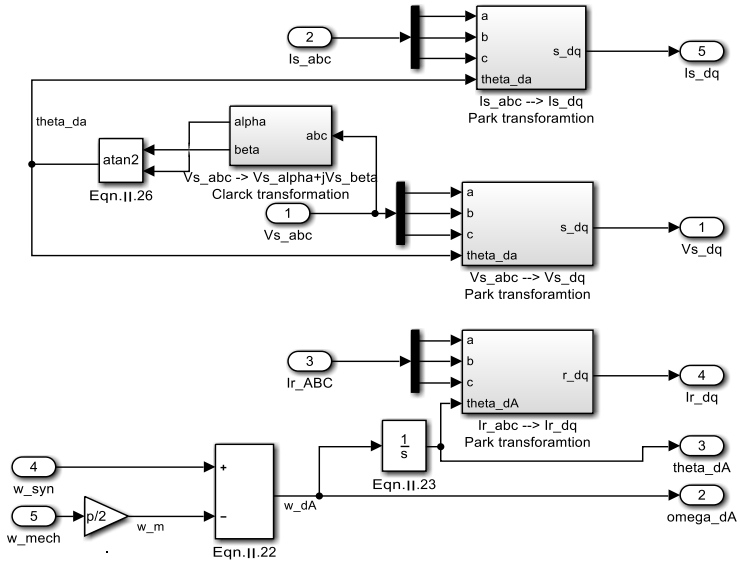

Fig. II.8 Estimator model.

Figure. II.9 presents a detailed illustration of the Doubly-Fed Induction Generator (DFIG) controller and the rotor voltage compensation model. Furthermore, the process involved in generating the reference signals for i_{qr} and i_{dr} are elaborated upon in Figure. II.10 and Figure. II.11 respectively.

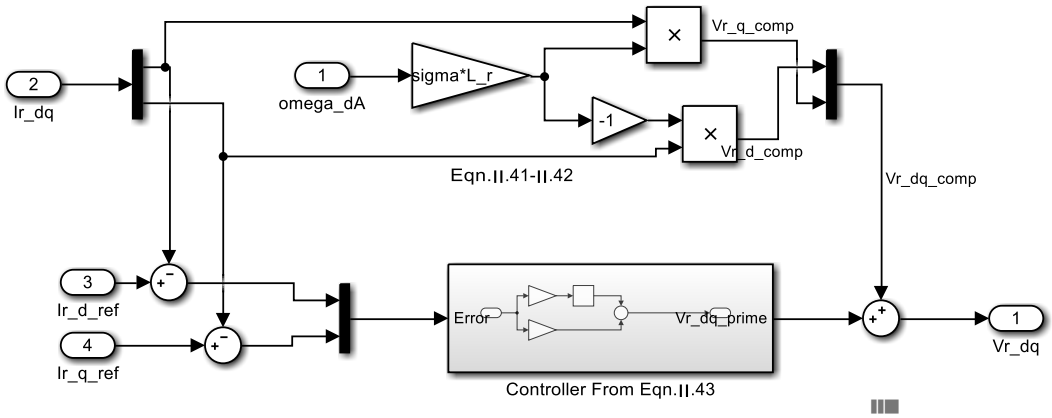

Fig. II.9 Representation of the DFIG Controller Incorporating Rotor Voltage Compensation Model.

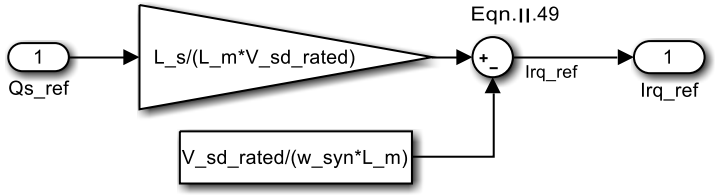

Fig. II.10 Model of deriving i_{qr}^{*} from Q_s^{*}.

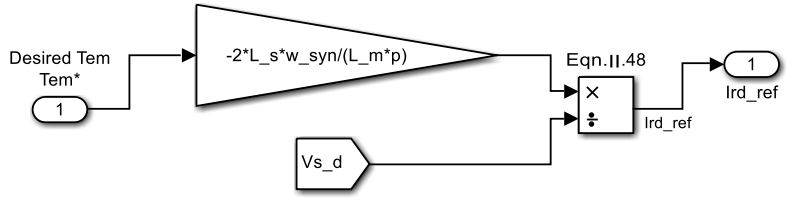

Fig. II.11 Model of reference signal generation i_{dr}^{*}.

The configuration of the Doubly-Fed Induction Generator (DFIG) in conjunction with the wind turbine is illustrated in Figure. II.12. The DFIG's stator is supplied with a balanced sinusoidal three-phase voltage, while the rotor voltage is determined using the v_{dr} and v_{qr}values provided by the controller shown in Figure. II.9. The gear ratio is configured as follows

$$GearRatio = \frac{\omega_{mech}^{rated}}{\omega_{mech}^{opt}} \tag{II-52}$$

where ω_{mech}^{rated} is the DFIG rated mechanical rotational speed defined by $\omega_{mech}^{rated} = (1-s)\omega_{syn}/(P/2)$, where s represents the slip of the DFIG under full (rated) load conditions. The optimal mechanical speed, ω_{mech}^{opt} is derived from the specified power coefficient C_p model at a wind velocity of 12m/s.

According to Eq. (II-28), the mechanical speed ω_{mech} can be regulated by adjusting the generator's electromagnetic torque $T_{em,gen}$. To achieve this, a speed-squared control strategy is employed to generate the reference signal for the generator torque $T_{em,gen}^{*}$. Our objective is to ensure that the wind turbine operates at the optimal wind power coefficient C_p^{opt}.

To derive the reference signal for the generator torque, the process begins with the equation for the Tip Speed Ratio (TSR). By substituting the wind speed expression v_{wind} in the TSR equation with $\frac{R\omega_{mech}}{\lambda}$, and incorporating it into Eq. (II-13), the equation is further simplified by dividing the entire expression by ω_{mech}. As a result, the reference signal for the generator torque can be compactly expressed as follows:

$$T_{em,gen}^{*} = \frac{1}{2}\frac{C_{pmax}(\beta,\lambda_{opt})\rho\pi R^{5}}{\lambda_{opt}}\omega_{mech}^{2} = K_{opt}\omega_{mech}^{2} \quad \text{(II-53)}$$

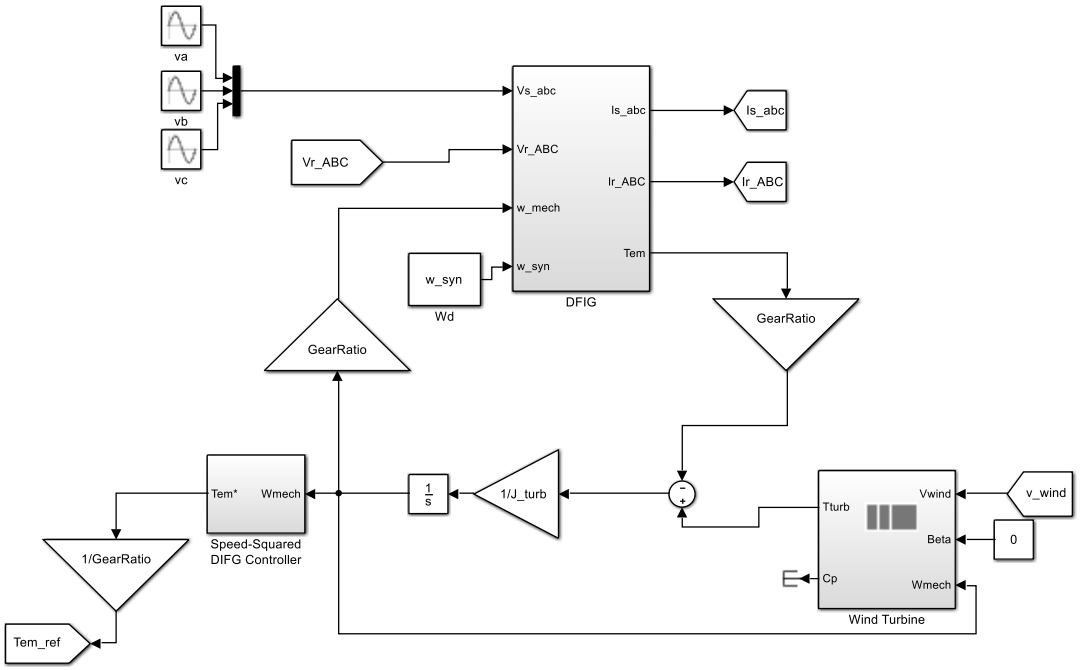

Fig. II.12 Coupling of the DFIG and the wind turbine.

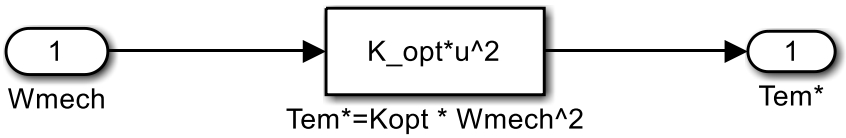

Fig. II.13 Speed-squared control model for wind turbine.

II.5. Conclusion

In this chapter, we provided a comprehensive analysis of the modeling of wind turbine systems, with a particular focus on the aerodynamic aspects and the Doubly Fed Induction Generator (DFIG). The aerodynamic model, grounded in Blade Element Momentum (BEM) theory, helped us understand how wind energy is converted into mechanical power, while the DFIG model covered the electrical and mechanical dynamics that enable efficient control of active and reactive power in modern wind turbines. Through these models, we established the essential theoretical foundation for understanding and optimizing wind energy conversion.

The detailed mathematical formulations and simulation models highlighted the importance of accurate modeling in ensuring system efficiency, grid stability, and reliable turbine operation under varying wind conditions. This chapter's insights are crucial for the development of advanced control strategies aimed at maximizing energy capture while maintaining system stability.

This modeling is crucial as it lays the groundwork for the following chapters, where we will explore the control of DFIG-based wind turbines. The models developed in this chapter will be integral to implementing advanced control strategies that ensure the reliable operation and optimal performance of wind turbines in varying wind conditions.

Chapter III
Classical & optimized PI controllers for wind turbine control

III.1. Introduction

Proportional-Integral (PI) controllers are widely used in various industrial applications due to their simplicity, robustness, and effectiveness in regulating processes [59], [60]. In the context of wind turbine control systems, the PI controller plays a critical role in maintaining system stability and optimizing power output. Wind turbines are complex, nonlinear systems subject to varying wind conditions, and maintaining optimal performance requires precise control mechanisms [61]. The PI controller, by adjusting both the proportional and integral terms, helps regulate key variables such as rotor speed and power output to ensure efficient and stable operation of the turbine [7].
The simplicity of the PI controller lies in its design as depicted in Figure III.1, where the proportional component reacts to the error between the desired and actual system output, and the integral component eliminates steady-state errors by integrating the error over time [60]. This dual-action makes the PI controller highly effective in managing disturbances and achieving the desired control objectives in wind turbines, particularly under varying wind speeds and operational conditions.

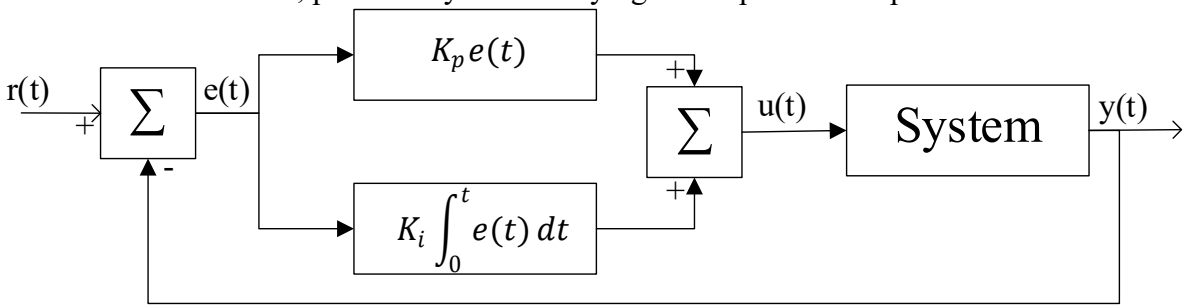

r(t) = System setpoint e(t) = Error signal u(t) = Control signal y(t) = System output

Fig. III.1 Basic Structure of a PI Controller.

Traditionally, PI controllers have been designed using classical tuning methods, such as Ziegler-Nichols or the direct synthesis approach, which rely on frequency domain techniques to define the controller parameters [62], [63]. While these classical methods are effective in many cases, they often fall short in handling the highly nonlinear behavior of wind turbines, especially under dynamic wind conditions. These limitations create the need for more advanced optimization techniques to fine-tune the PI controller for better performance.
Recent advances in artificial intelligence and optimization algorithms have introduced powerful tools for optimizing PI controller parameters. Techniques such as Grey Wolf Optimization (GWO), Particle Swarm Optimization (PSO), Ant Colony Optimization (ACO), and Genetic Algorithms (GA) have been applied to improve the tuning of PI controllers [64], [65], [66], [67]. These metaheuristic algorithms provide adaptive and flexible solutions to optimize the performance of wind turbine control systems, ensuring better handling of nonlinearities and disturbances. By exploring multiple potential solutions simultaneously, these algorithms can find optimal or near-optimal parameters for the PI controller, enhancing overall system performance.
In this chapter, both the classical PI controller design using the direct synthesis approach and the optimized methods using metaheuristic algorithms will be examined, highlighting their impact on wind turbine control.

III.2. Classical PI Controller Design Using the Direct Synthesis Approach in the Frequency Domain

III.2.1. Overiview of the Direct Synthesis Approach

The Direct Synthesis Approach is a widely used method for designing PI controllers, especially when the system's transfer function is known. This approach involves defining the desired closed-loop behavior of the system and then calculating the appropriate PI controller parameters to

achieve this behavior. The strength of the direct synthesis method lies in its ability to derive controller settings directly from the system dynamics, rather than relying on trial-and-error tuning [68].
In this method, the controller design process starts with specifying the desired closed-loop transfer function that meets the system's performance requirements, such as stability, speed of response, and robustness. By solving for the controller parameters that satisfy this desired transfer function, the PI controller is systematically tailored to the specific needs of the system [69], [70].
This approach provides a more structured and mathematically grounded alternative to empirical tuning methods, offering greater control over system response characteristics. In the following section, we will explore the key steps of the direct synthesis approach and how it can be applied to design a PI controller for wind turbine systems.

III.2.2. Methodology

The Direct Synthesis Approach for PI controller design involves several key steps (see Figure III.2). It begins by defining the desired closed-loop transfer function, which specifies the target behavior for the system in terms of frequency response, stability margins, and overall performance across a range of operating frequencies. Next, the system's transfer function is identified, representing the natural dynamics of the system. Using these two functions, a controller design equation is formulated that relates the desired closed-loop behavior to the system's dynamics. From this equation, the proportional (P) and integral (I) gains of the PI controller are derived to ensure that the system behaves as intended. Finally, the PI controller is implemented, and its performance is tested to verify that it meets the predefined objectives, ensuring a stable and efficient response under varying conditions. This method offers a systematic way to tune the PI controller based on the specific needs of the system [7], [71], [72].

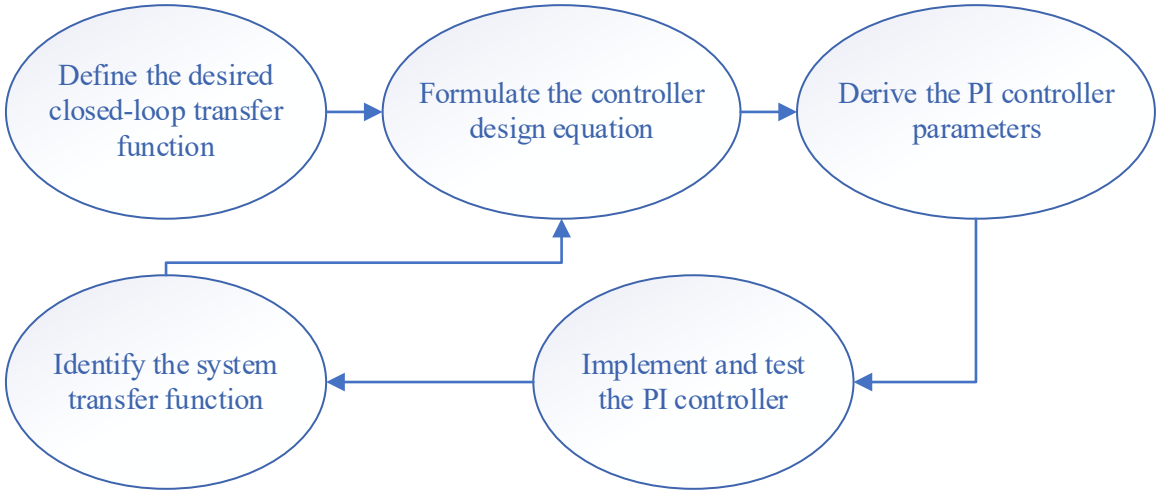

Fig. III.2 Step-by-Step process of the Direct Synthesis Approach for PI controller design.

To implement this method, the desired closed-loop transfer function is first defined based on specific design criteria. The chosen specifications include a phase margin of $PM = {}^{\pi}/_{3}$ and a crossover frequency $\omega_c = 10.2\pi$. These parameters are selected to ensure system stability and robustness while maintaining a well-defined frequency response.
At the crossover frequency ω_c, the magnitude of the open-loop transfer function must satisfy

$$|G_{ol}(j\omega_c)| = 1 \quad \text{(III-1)}$$

The phase margin of 60 degrees ensures that at this frequency, the phase lag satisfies

$$PM = \pi + \angle G_{ol}(j\omega_c) \quad \text{(III-2)}$$

Based on these requirements, the transfer function of the PI controller is expressed as

$$G_c = K_p + \frac{K_i}{s} \quad \text{(III-3)}$$

Where K_p represents the proportional gain, and K_i is the integral gain. These parameters will be derived by solving the controller design equation to ensure the system meets the desired specifications.

By cascading the PI controller transfer function from Eq. (III-3) with the system transfer function from Eq. (II-43), the overall open-loop transfer function is derived. This combined transfer function is expressed in Eq. (III-4). This combined transfer function represents the global behavior of the system when both the controller and plant dynamics are taken into account, allowing us to analyze and design the system's frequency response and stability.

$$\mathrm{G_{ol}(s)} = \left(\mathrm{K_p} + \frac{\mathrm{K_i}}{\mathrm{S}}\right)\left(\frac{1}{\mathrm{R_r}+\sigma \mathrm{L_r S}}\right) \tag{III-4}$$

$$G_{ol}(s) = \left(\frac{K_i\left(\frac{K_p}{K_i}S+1\right)}{S}\right)\left(\frac{1}{R_r+\sigma L_r S}\right) \tag{III-5}$$

In its complex form, the transfer function becomes

$$G_{ol}(j\omega) = \left(\frac{K_i\left(\frac{K_p}{K_i}j\omega+1\right)}{j\omega}\right)\left(\frac{1}{R_r+\sigma L_r j\omega}\right) \tag{III-6}$$

The phase angle of the open-loop transfer function is given by

$$\angle G_{ol}(j\omega) = \arg\big(G_{ol}(j\omega)\big) = \frac{arg\left(K_i\left({K_p}/{K_i}j\omega+1\right)\right)}{arg\big(j\omega(R_r+\sigma L_r j\omega)\big)} \tag{III-7}$$

Using the properties of the argument function

$$arg\left(\frac{a}{b}\right) = arg(a) - arg(b), arg(a.b) = arg(a) + arg(b)$$

The phase angle can be rewritten as follows:

$$\angle G_{ol}(j\omega) = \tan^{-1}\left({K_p}/{K_i}\,\omega\right) - \frac{\pi}{2} - \tan^{-1}\frac{\sigma L_r \omega}{R_r} \tag{III-8}$$

The phase margin (PM) is defined as the phase at the crossover frequency ω_c plus π

$$PM = \angle G_{ol}(j\omega_c) + \pi \tag{III-9}$$

Therefore, the phase margin can be expressed as:

$$PM = \tan^{-1}\left({K_p}/{K_i}\,\omega_c\right) + \frac{\pi}{2} - \tan^{-1}\frac{\sigma L_r \omega_c}{R_r} \tag{III-10}$$

To solve for the ratio $\frac{K_p}{K_i}$, the equation is set as follows:

$$\frac{K_p}{K_i} = \frac{1}{\omega_c}\tan\left(PM - \frac{\pi}{2} + \tan^{-1}\frac{\sigma L_r \omega_c}{R_r}\right) \tag{III-11}$$

The magnitude of the open-loop transfer function at the crossover frequency is given by

$$|G_{ol}(j\omega_c)| = 1 = \frac{K_i\sqrt{\left(\frac{K_p}{K_i}\omega_c\right)^2+1}}{\omega_c\sqrt{(\sigma L_r\omega_c)^2+{R_r}^2}} \tag{III-12}$$

Solving for K_i, the following expression is obtained:

$$K_i = \frac{\omega_c\sqrt{(\sigma L_r\omega_c)^2+{R_r}^2}}{\sqrt{\left(\frac{K_p}{K_i}\omega_c\right)^2+1}} \tag{III-13}$$

Finally, K_p is expressed in terms of K_i and the ratio $\frac{K_p}{K_i}$ from Eq.(III-13), Eq.(III-11) respectively:

$$K_p = \frac{K_p}{K_i}K_i \tag{III-14}$$

For the given phase margin $PM = \frac{\pi}{3}$ and crossover frequency $\omega_c = 10.2\pi$, the parameters of the PI controller are determined using the direct synthesis approach in the frequency domain.

$$\left(\frac{K_p}{K_i} = 0.0224, K_i = 0.5743, K_p = 0.0129\right)$$

III.2.3. Simulation results

In this section, the performance of the proposed indirect wind turbine power control techniques is evaluated through numerical simulations conducted using MATLAB Simulink software. The model used for the simulation is based on the modeling presented in Chapter II, where the system dynamics and control strategies for the wind turbine and DFIG are detailed. The key specifications of the Doubly-Fed Induction Generator (DFIG) and the wind turbine used in the simulations are provided in Annex A. The wind turbine model used for this study is based on a GE wind turbine, ensuring realistic and industry-standard system parameters.

To assess the controller performance, a realistic wind speed profile was employed (as depicted in Figure III.3), simulating variable wind conditions to reflect real-world operational environments. This profile was used to test the system's response to changing wind speeds and its ability to maintain optimal power generation.

The reference for active power $P_{sref}$was generated through the Maximum Power Point Tracking (MPPT) strategy, ensuring that the wind turbine operates at its maximum efficiency by dynamically adjusting the power reference based on the wind speed.

Additionally, for the reactive power reference Q_{sref}, we imposed a constant reference value to evaluate the system's performance. The reference was then varied to observe whether the real signal could follow the desired trajectory, allowing us to test the system's dynamic response to changes in the reactive power demand.

The results of the simulation, presented in Figures III.4 through III.7, demonstrate the performance of the classical PI controller in stabilizing the system and providing effective control over both the rotor currents and the stator power.

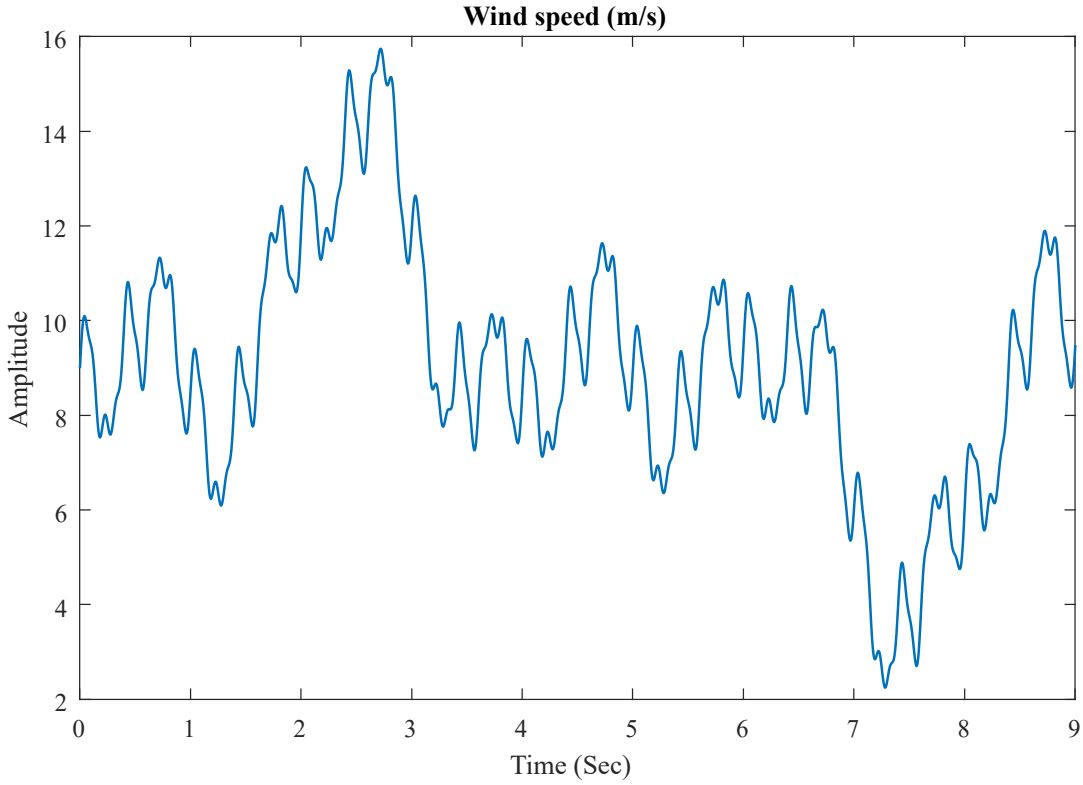

Fig. III.3 Simulation of wind speed profile.

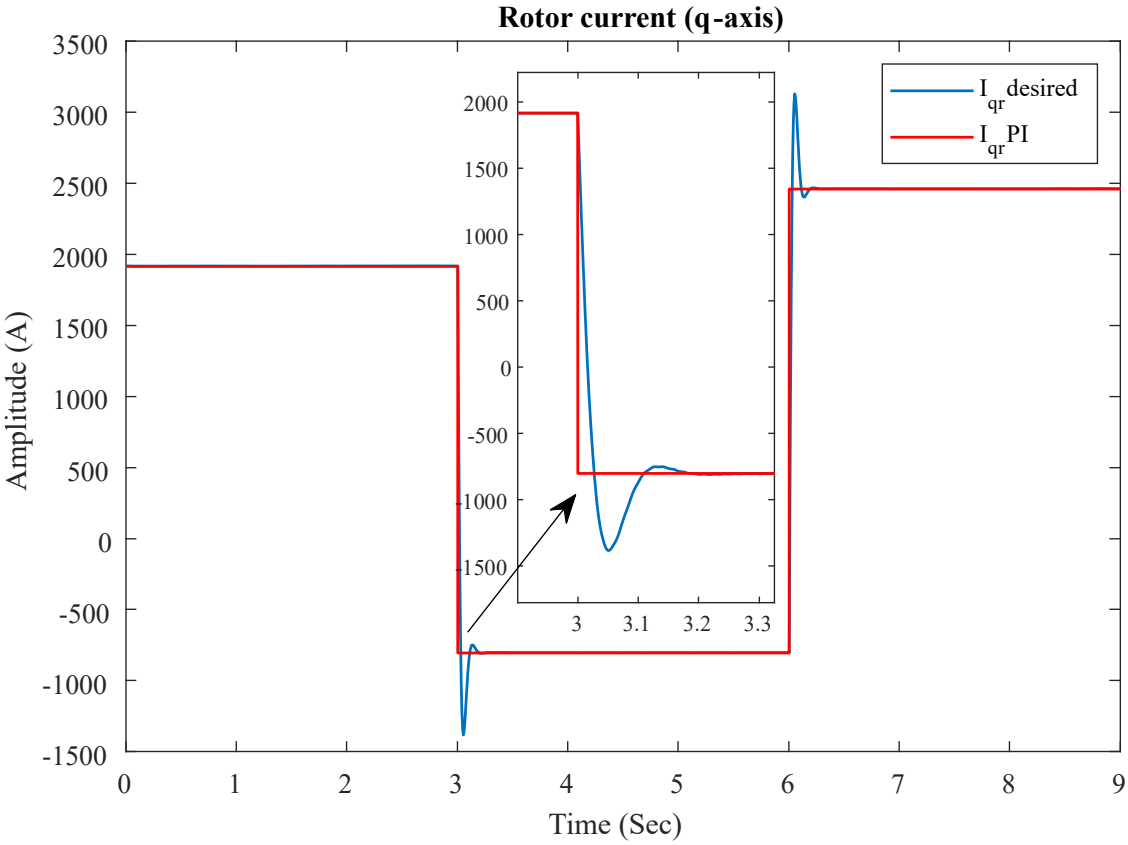

Fig. III.4 Rotor current response (q-axis).

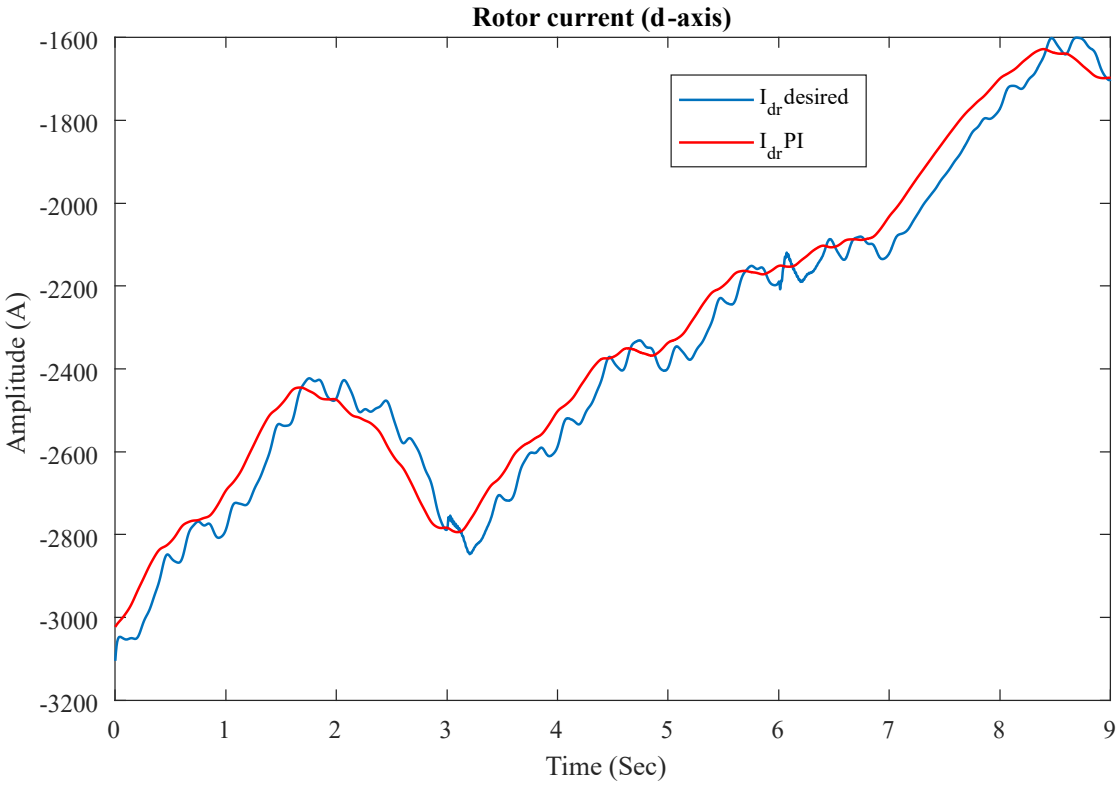

Fig. III.5 Rotor current response (d-axis).

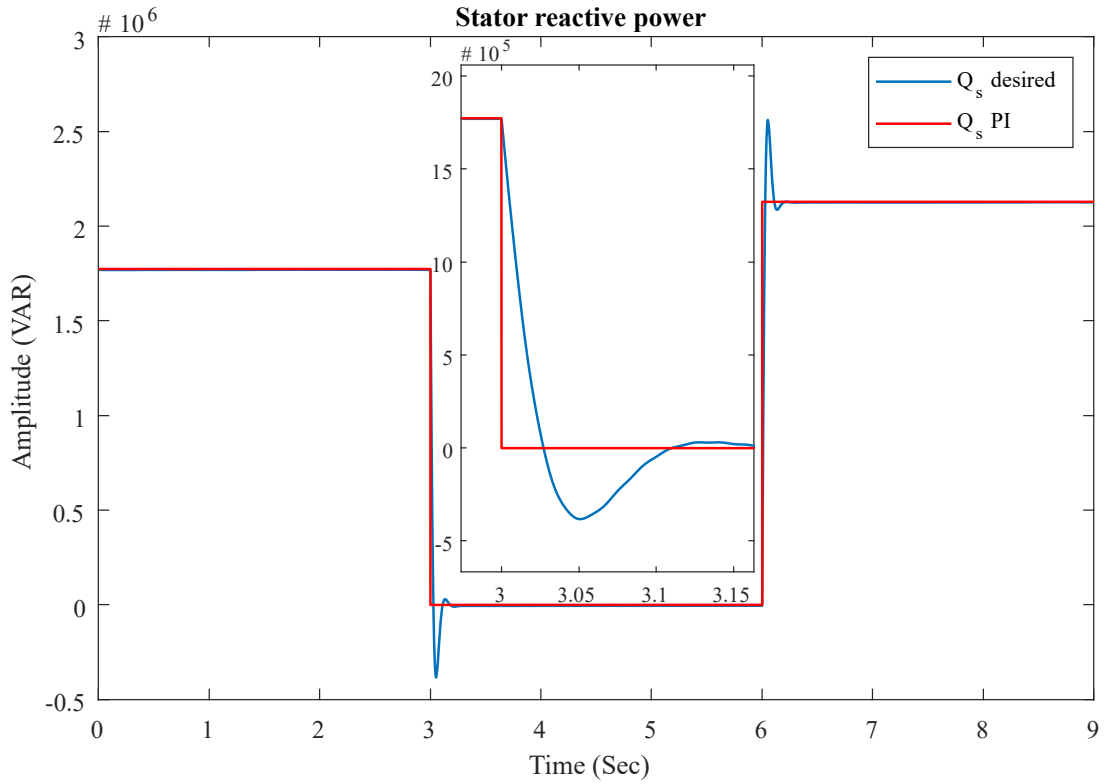

Fig. III.6 Stator reactive power dynamics.

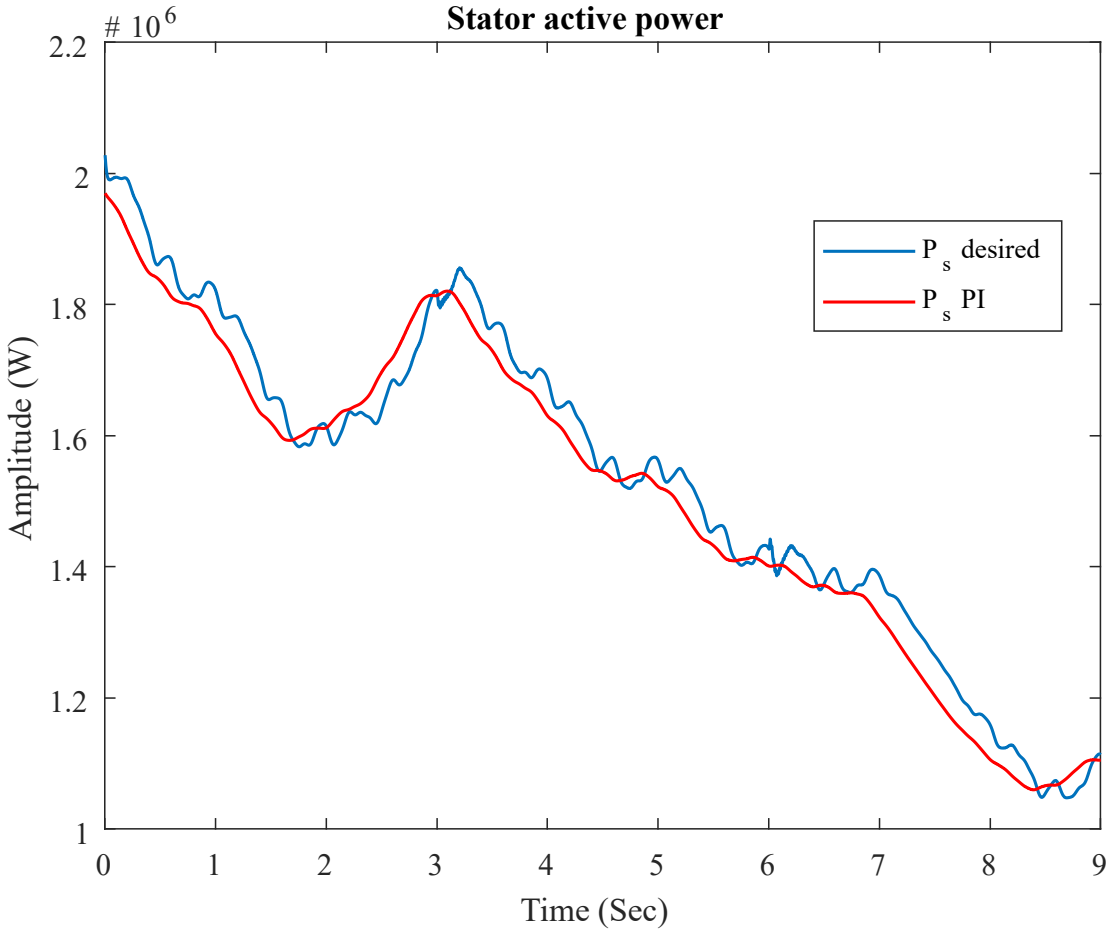

Fig. III.7 Stator active power dynamics.

Figure III.4 and Figure III.5 show the rotor current responses. From these figures, we can observe that the classical PI controller successfully stabilizes both currents, maintaining system balance. However, there is a noticeable overshoot when the reference is changed, indicating that while the controller is effective in reaching the desired setpoint, it briefly exceeds the target before settling. Additionally, a delay of approximately 0.12 seconds is seen before the system reaches the desired point, which affects the system's dynamic performance. Despite the delay, the steady-state response is achieved with minimal error, ensuring stability in the rotor currents.
Figure III.6 and Figure III.7 show the stator power responses. further confirm the controller's effectiveness. The stator reactive power tracks the imposed constant reference with good accuracy, but similarly to the rotor currents, we observe a small overshoot and a delay before the system fully converges to the desired reference. The stator active power is controlled well, showing that the PI controller can maintain system performance under varying wind conditions. However, as with the rotor currents, a small steady-state error persists, although it remains within acceptable limits.
In conclusion, while the classical PI controller demonstrates good control and performance across the system, overshoot and delay (0.12 seconds) during reference changes affect its dynamic response. The system is stable overall, with only a minor steady-state error, which suggests that further optimization of the PI controller could improve performance by reducing these transient effects.

III.3. Optimized PI controller

III.3.1. Overview of Optimization methods

While the classical PI controller is widely used in wind turbine control due to its simplicity and effectiveness, it exhibits certain limitations, particularly in dynamic environments where wind speed and system conditions vary rapidly. These limitations often manifest as overshoot, delays in reaching the desired reference point, and steady-state errors, as seen in the previous simulation results. To address these challenges, optimization techniques are employed to enhance the performance of the PI controller. By adjusting the proportional (P) and integral (I) gains more intelligently, optimization algorithms aim to improve the controller's ability to handle system dynamics, reduce overshoot, minimize steady-state error, and shorten the response time [73]. Various optimization techniques such as Grey Wolf Optimization (GWO), Particle Swarm Optimization (PSO), and Genetic Algorithms (GA) are often applied to tune the PI controller gains based on specific performance criteria.
The objective of these optimization methods is to find the optimal set of parameters that maximize the controller's effectiveness in varying operating conditions. This ensures the wind turbine operates more efficiently, with improved stability, faster convergence to the desired reference, and reduced energy losses. In this section, we will explore the use of these optimization techniques and evaluate their impact on the PI controller's performance for wind turbine control [74], [75].
In the context of optimizing the PI controller for wind turbine control, the optimization algorithm follows a systematic approach to fine-tune the controller parameters. The goal of the algorithm is to iteratively adjust the proportional (P) and integral (I) gains to achieve the best possible control performance, as measured by a specific cost function [76], [77], [78]. The optimization process proceeds as follows [79], [80]:

- The first step is to define the search space or the range for the parameters to be optimized. In this case, the ranges for the proportional gain K_p and the integral gain K_i are specified. These ranges set the boundaries within which the algorithm will search for the optimal values.
- Once the parameter ranges are defined, the algorithm initializes a set of parameters within the given bounds. This initial set of parameters acts as the starting point for the optimization process.
- The next step is to run a simulation of the system using the initialized parameters. After each simulation, a cost function is evaluated to determine the performance of the controller. In this

context, the cost function used is the Integral Time Absolute Error (ITAE), which penalizes deviations of the system response from the reference signal over time, emphasizing both the magnitude and the duration of the error. The ITAE performance index is defined as:

$$ITAE = \int t|e(t)|dt$$

Where $e(t)$ represents the error between the reference signal and the system output and t is time.

- After evaluating the cost function, the algorithm checks whether the optimization process has met the predefined end criteria. This could be based on a minimum cost value or the maximum number of iterations allowed.
- If the end criteria are not met, the optimization algorithm updates the parameters based on its specific strategy (e.g., Grey Wolf Optimization, Particle Swarm Optimization, etc.). The updated parameters are then used to run the simulation again, and the process repeats.
- The optimization process continues iteratively, with the algorithm updating the parameters and re-running the simulation until the end criteria are satisfied. Once the criteria are met, the algorithm terminates, and the optimal PI controller parameters are determined.

This general optimization algorithm (as summarized in Figure III.8) provides an efficient way to automatically adjust the PI controller's gains to achieve better control performance, reducing overshoot, minimizing steady-state error, and improving the overall system response.

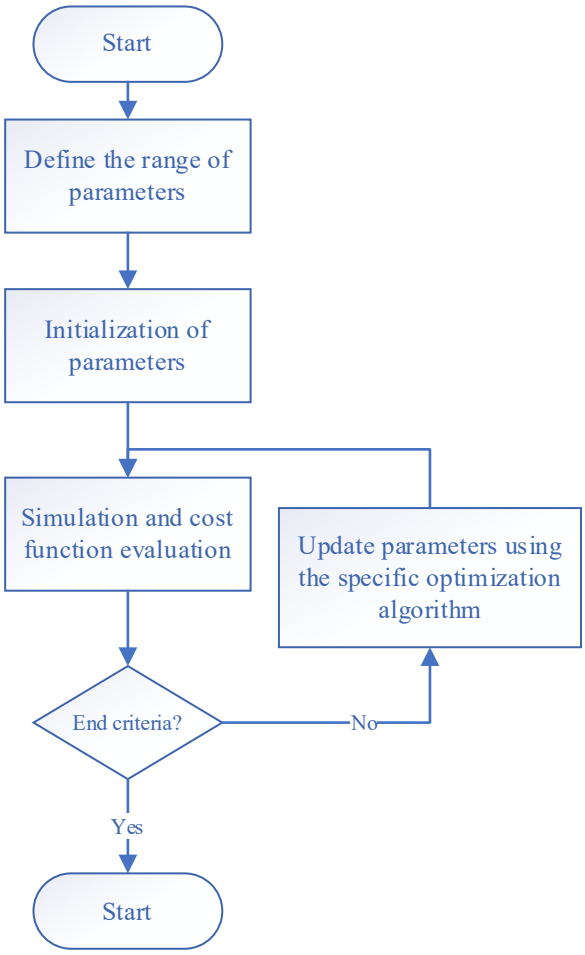

Fig. III.8 Flowchart of the general optimization algorithm.

III.3.2. Grey Wolf Optimization

Grey Wolf Optimization (GWO) is a bio-inspired algorithm that mimics the social hierarchy and hunting behavior of grey wolves. This algorithm solves optimization problems by translating the wolves' predatory strategies into a computational model. In GWO, the hierarchical structure of the wolf pack plays a key role in the optimization process. The pack is divided into four roles: alpha (α), beta (β), delta (δ), and omega (ω) wolves [67]. Each of these roles contributes uniquely to the search process

- Alpha wolves lead the pack, guiding the search towards promising regions of the solution space.
- Beta and delta wolves assist in refining the search process, balancing exploration and exploitation.
- Omega wolves primarily focus on exploring new regions, ensuring that the search does not prematurely converge to suboptimal solutions.

One of the core behaviors in GWO is encircling the prey, which models how wolves surround their prey during hunting. This behavior is mathematically modeled by updating the wolves' positions dynamically based on the prey's position. The wolves gradually adapt their positions until they are ready to attack, this process represents refining the potential solutions [67], [81]. Figure III.9 illustrates the wolf position updating pattern, which is based on random vectors and highlights the adaptability of the algorithm in navigating the search space.

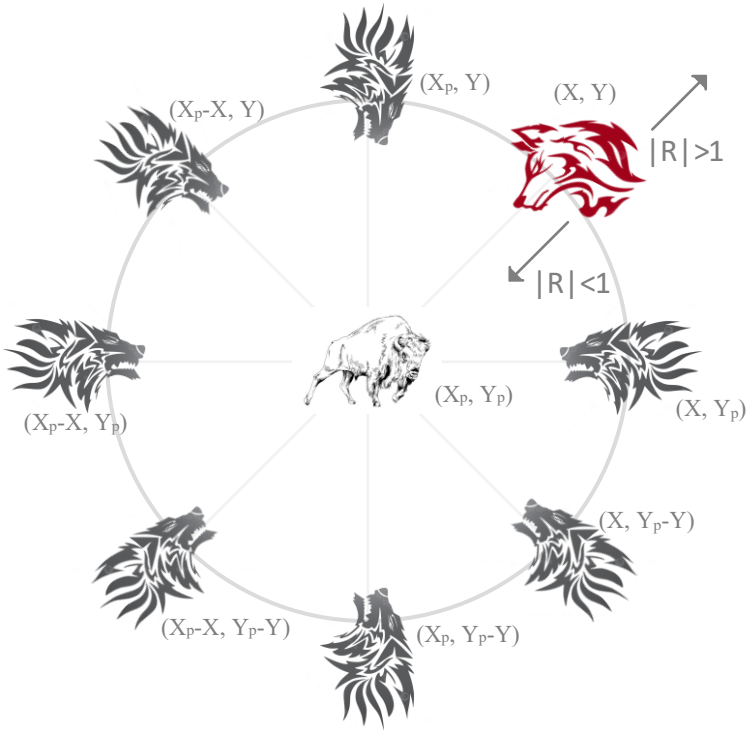

Fig. III.9 Wolf position updating pattern based on random vectors [67].

The GWO algorithm operates by distinguishing between two phases: exploration and exploitation. During the exploration phase, wolves search the solution space by maintaining a cautious distance, exploring various possibilities. As the algorithm progresses, it shifts into the exploitation phase, where the wolves close in on their prey and fine-tune the best solutions identified so far. The general workflow of the GWO algorithm is depicted in Figure III.10, which demonstrates how the wolves transition between these phases to optimize the search.

The following mathematical model describes the prey (solution) encirclement by the wolves

$$\vec{N} = \left|\vec{M} \cdot \overrightarrow{X_p}(\text{iter}) - \vec{X}(\text{iter})\right| \quad \text{(III-15)}$$

$$\vec{X}(\text{iter}+1) = \overrightarrow{X_p}(\text{iter}) - \vec{R} \cdot \vec{N} \quad \text{(III-16)}$$

Here iter is the current iteration, $\vec{R} = 2\vec{k}.\overrightarrow{u_1} - \vec{k}$, $\vec{M} = 2\overrightarrow{u_2}$, where $\overrightarrow{X_p}$ represent the position vectors of prey and the wolf respectively. $\overrightarrow{u_1}$, $\overrightarrow{u_2}$ are random vectors within [0 1] while the component $\vec{k}$ linearly decreases from 2 to 0 across iterations.

The position updates of the wolves, including alpha, beta, and delta, are further refined by

$$\overrightarrow{N_{\alpha,\beta,\delta}} = \left|\overrightarrow{M_{1,2,3}} \cdot \overrightarrow{X_{\alpha,\beta,\delta}} - \vec{X}\right| \quad \text{(III-17)}$$

$$\overrightarrow{X_{1,2,3}} = \overrightarrow{X_{\alpha,\beta,\delta}} - \overrightarrow{R_{1,2,3}} \cdot \overrightarrow{N_{\alpha,\beta\cdot\delta}} \quad \text{(III-18)}$$

$$\vec{X}(\text{ iter } + 1) = \frac{\overrightarrow{X_1}+\overrightarrow{X_2}+\overrightarrow{X_3}}{3} \quad \text{(III-19)}$$

Where $\overrightarrow{X_{\alpha,\beta,\delta}}$ is the position of alpha, beta and delta respectively. These equations define how the distances between the current solution and the positions of the alpha, beta, and delta wolves are determined. The final position of the wolves is calculated by averaging their individual updates, ensuring that the solution is optimally refined through collaboration.

Applying the GWO algorithm to optimize the Proportional-Integral (PI) controller gains enhances wind turbine performance by minimizing the Integral Time Absolute Error (ITAE). This leads to improved system response and stability. After optimization, the optimal PI gains obtained are $K_p = 50.001$ and $K_i = 4885.001$.

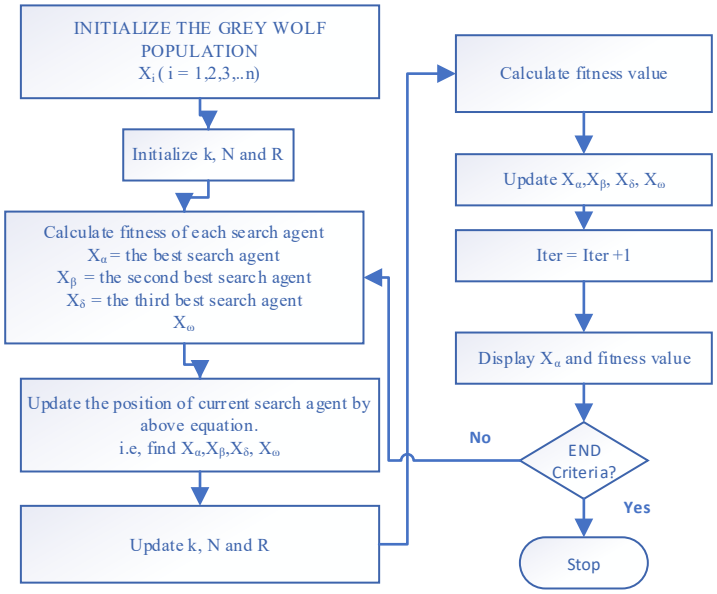

Fig. III.10 GWO algorithm.

III.3.3. Genetic Algorithm

The Genetic Algorithm (GA) is a powerful optimization technique inspired by the process of natural selection in evolutionary biology. It is designed to solve complex optimization problems by mimicking biological evolution, utilizing concepts such as chromosomes, fitness, selection, crossover, and mutation [64], [82], [83]. In the context of PI controller optimization for wind turbine control, the GA is used to optimize the proportional (K_p) and integral (K_i) gains, leading to improved control performance, stability, and response time [84], [85]. Figure III.11 presents the core components of a Genetic Algorithm.

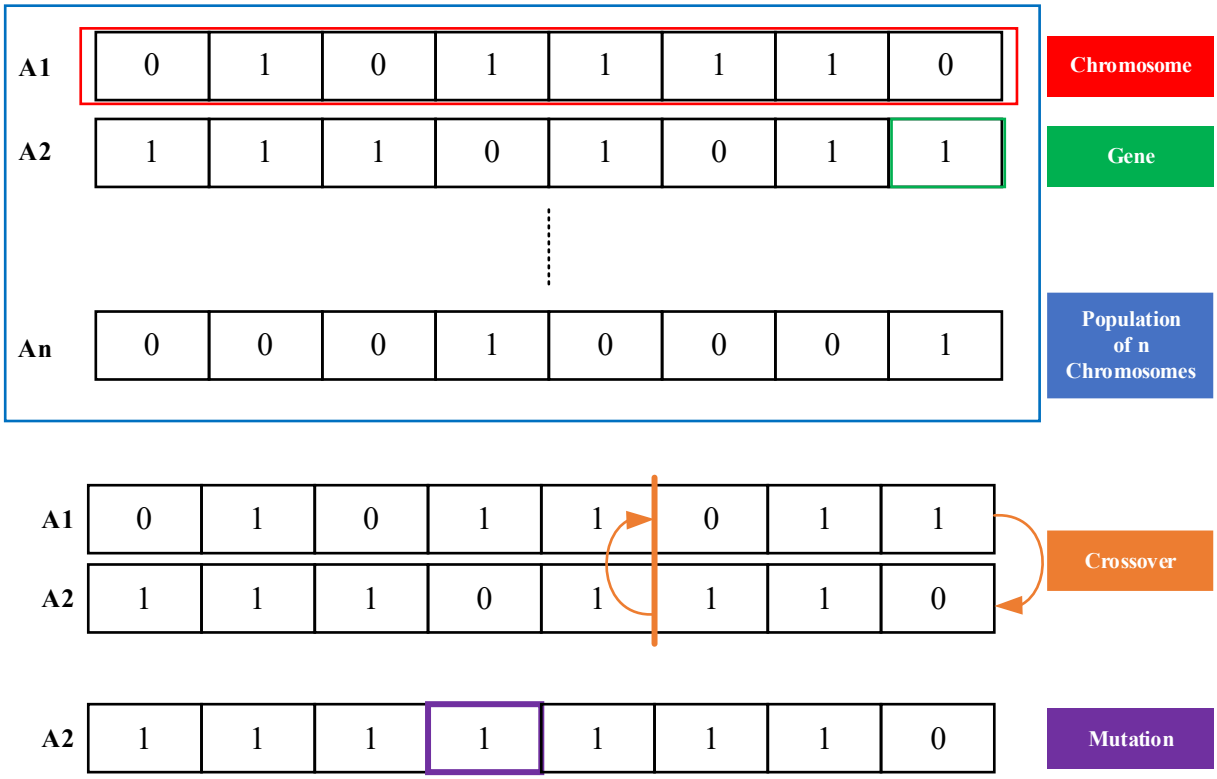

Fig. III.11 The primary elements of a Genetic Algorithm [86].

- Chromosomes and Population Initialization

In a Genetic Algorithm, each potential solution is represented as a chromosome, which in this case consists of the PI controller parameters K_p and K_i. A population of chromosomes is initially generated, with each chromosome representing a unique set of controller gains. These chromosomes form the initial search space, providing a diverse set of solutions from which the algorithm can evolve toward an optimal solution.

- Fitness evaluation

Once the population is initialized, each chromosome is evaluated using a fitness function. For PI controller optimization, the fitness function is typically the Integral Time Absolute Error (ITAE), which penalizes the system's response based on the magnitude and duration of the error between the desired and actual outputs. Chromosomes that result in better controller performance, such as minimizing overshoot, reducing steady-state error, and improving response time, are assigned higher fitness scores.

- Selection: Roulette Wheel Selection

One of the key processes in GA is selection, where chromosomes with higher fitness are more likely to be chosen to pass on their genes (controller parameters) to the next generation. The roulette wheel selection method is commonly used for this purpose. In this method, each chromosome is assigned a section of a virtual roulette wheel, proportional to its fitness score. Chromosomes with better performance occupy larger portions of the wheel, increasing their chances of being selected. The wheel is "spun" multiple times to select individuals that will form the mating pool for the next generation.

- Crossover and Mutation

After selection, the crossover operation is performed on pairs of selected chromosomes. In crossover, segments of two parent chromosomes are exchanged to create new offspring, combining the strengths of both parents. This recombination introduces diversity into the population and explores

new regions of the solution space. In addition to crossover, mutation is applied to some individuals. Mutation introduces random changes to certain genes (controller gains) within a chromosome, preventing the population from converging prematurely on local minima and ensuring that the algorithm continues to explore new solutions. The mutation rate is typically kept low to maintain the balance between exploration and exploitation. The general process of the Genetic Algorithm is summarized in Figure III.12.

- Evaluation and Convergence

This process of selection, crossover, and mutation is repeated over several generations. With each generation, the population of chromosomes evolves, and the overall fitness improves. The algorithm continues until a stopping criterion is met, such as a maximum number of generations or a sufficiently small error in the fitness function.

When applied to the optimization of PI controller gains, the Genetic Algorithm searches through a wide range of possible solutions, ultimately converging on the optimal set of K_p and K_i values that minimize the error and maximize system stability. The final set of gains obtained through this process are $K_p = 394.7075$ and $K_i = 869.9410$.

The optimized gains result in a controller that provides faster response times, reduced overshoot, and enhanced performance under varying wind conditions. Genetic Algorithms are particularly effective for this type of optimization due to their ability to handle large search spaces and avoid being trapped in local minima, making them ideal for tuning PI controllers in complex, dynamic systems like wind turbines.

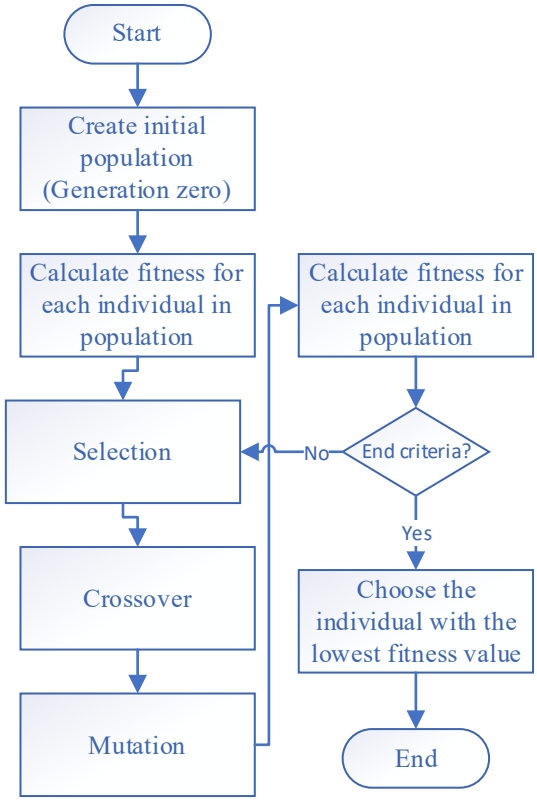

Fig. III.12 Genetic Algorithm.

III.3.4. Particle Swarm Optimization

Particle Swarm Optimization (PSO) is a popular optimization algorithm inspired by the social behavior of birds flocking or fish schooling. It was introduced by Kennedy and Eberhart in 1995 and has since been widely applied to solve complex optimization problems, including tuning the parameters of control systems such as PI controllers [66]. In the context of PI controller optimization

for wind turbine control, PSO is used to adjust the proportional (K_p) and integral (K_i) gains to minimize error and improve system performance.
PSO works by simulating a swarm of particles, where each particle represents a potential solution to the optimization problem. In this case, each particle corresponds to a pair of controller gains K_p and K_i. The particles "fly" through the solution space by updating their positions and velocities based on their own experience and the experience of neighboring particles [87], [88], [89].
The main features of PSO include:

- Initialization: A population of particles (candidate solutions) is randomly initialized in the solution space. Each particle has a position (representing K_p and K_i) and a velocity that guides its movement.
- Fitness Evaluation: Each particle's position is evaluated using a fitness function, typically the Integral Time Absolute Error (ITAE), to assess the quality of the solution. The particles strive to find positions that minimize the fitness function, reducing the system error.
- Personal Best and Global Best: As the particles move through the search space, each particle keeps track of its personal best position (the best solution it has found so far). Additionally, the global best position, which is the best solution found by any particle in the swarm, is shared with the entire population.
- Velocity and Position Update: Each particle's velocity and position are updated based on three components: inertia (previous velocity), personal best attraction, and global best attraction. These components guide the particles toward the optimal solution.

The equations governing the velocity and position updates of each particle are shown in Figure III.13 and are defined as follows

$$v_i(t+1) = \omega v_i(t) + c_1 r_1\big(Pbest - x_i(t)\big) + c_2 r_2(Gbest - x_i(t)) \quad \text{(III-20)}$$

$$x_i(t+1) = x_i(t) + v_i(t+1) \quad \text{(III-21)}$$

Where

- $v_i(t)$ is the velocity of particle i at iteration t.
- $x_i(t)$ is the position of particle i.
- $Pbest$ is the personal best position of particle i.
- $Gbest$ is the global best position among all particles.
- ω is the inertia weight.
- c_1, c_2 are acceleration coefficients with random values r_1 and r_2 in the range [0 1].

The Particle Swarm Optimization algorithm is illustrated in Figure III.14, which provides a visual overview of the optimization process.
The PSO process continues iteratively until the swarm converges on an optimal or near-optimal solution. The algorithm is particularly effective in balancing exploration (searching new areas of the solution space) and exploitation (refining known good solutions).
By applying PSO to PI controller tuning, the algorithm efficiently identifies the optimal controller gains that minimize error, improve response time, and stabilize the system under varying conditions. After applying PSO, the optimal controller gains obtained were $K_p = 10000$ and $K_i = 3575.7$. PSO's ability to avoid local minima and converge quickly makes it ideal for complex control problems like wind turbine systems.

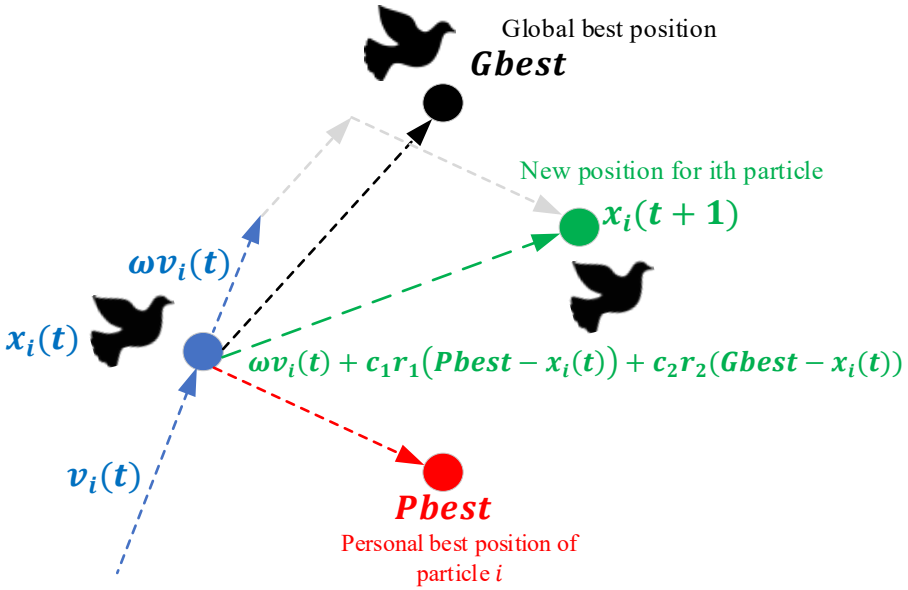

Fig. III.13 The schematic illustration of a flight in the PSO [90].

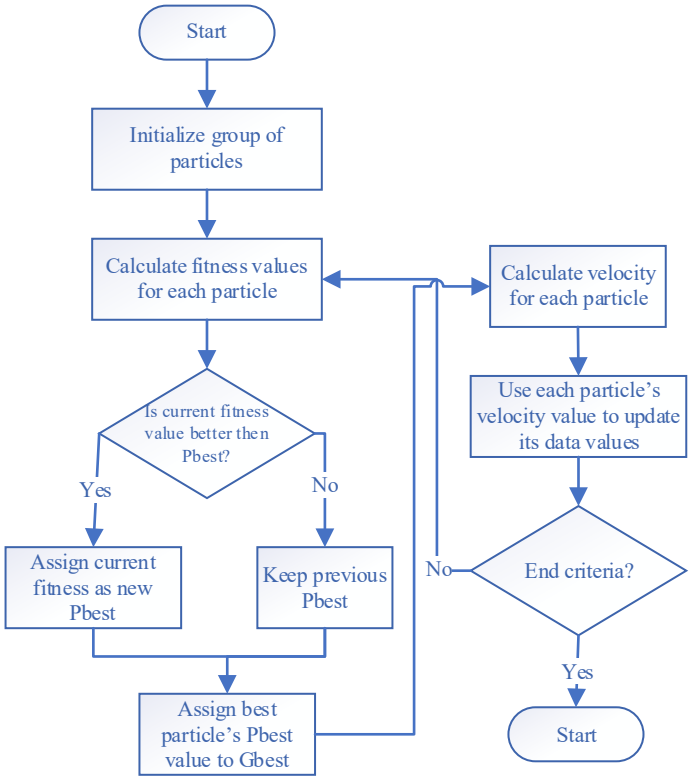

Fig. III.14 PSO algorithm.

III.3.5. Simulation results

In this section, we compare the performance of the optimization methods-Grey Wolf Optimization (GWO), Genetic Algorithm (GA), and Particle Swarm Optimization (PSO) against the classical Direct Synthesis Approach (DSA). The figures presented provide insights into the behavior of key control parameters, including rotor current (d-axis and q-axis), stator powers, and rotor powers.

III.3.5.1. Comparison of optimization methods response behavior

- Figure III.15 show the rotor current behavior of d-axis, this figure shows that all optimization methods (GWO, GA, PSO) yield powerful results, especially when compared to the PI

controller using the Direct Synthesis Approach. Among the optimization methods, PSO exhibits the best alignment with the desired signal, followed by GA and lastly GWO.

- Figure III.16 show the stator active power and that all the three optimization methods display similar response behavior in terms of stator active power, with no significant differences in performance.
- Figure III.17 show the rotor current behavior of q-axis, we remark that PSO provides the most accurate response, with an error of just 0.0003, while GA has an error of 0.01, and GWO shows the least accurate performance, with an error of 0.9.
- Figure III.18 show the stator reactive power and that all optimization methods demonstrate significantly faster response times compared to the Direct Synthesis Approach. GWO achieves a response time of 0.00002 seconds, GA improves on that with 0.0000035 seconds, and PSO delivers the most exceptional result with a response time of 0.0000001 seconds, which is 200 times faster than GWO.

The Table. III.1 summarizes the performance results obtained using the different optimization-based control methods. The comparison is carried out in terms of response time, overshoot, and steady-state error to evaluate the effectiveness of each algorithm in regulating the system.

Tab. III.1 Performance Comparison of Optimization-Based Control Methods.

Control Method	Response Time (s)	Overshoot (%)	Steady-State Error (W)
GWO	0.00002	≈0%	480 (0.00044%)
GA	0.0000035	≈0%	415 (0.00027%)
PSO	0.0000001	≈0%	374 (0.00018%)

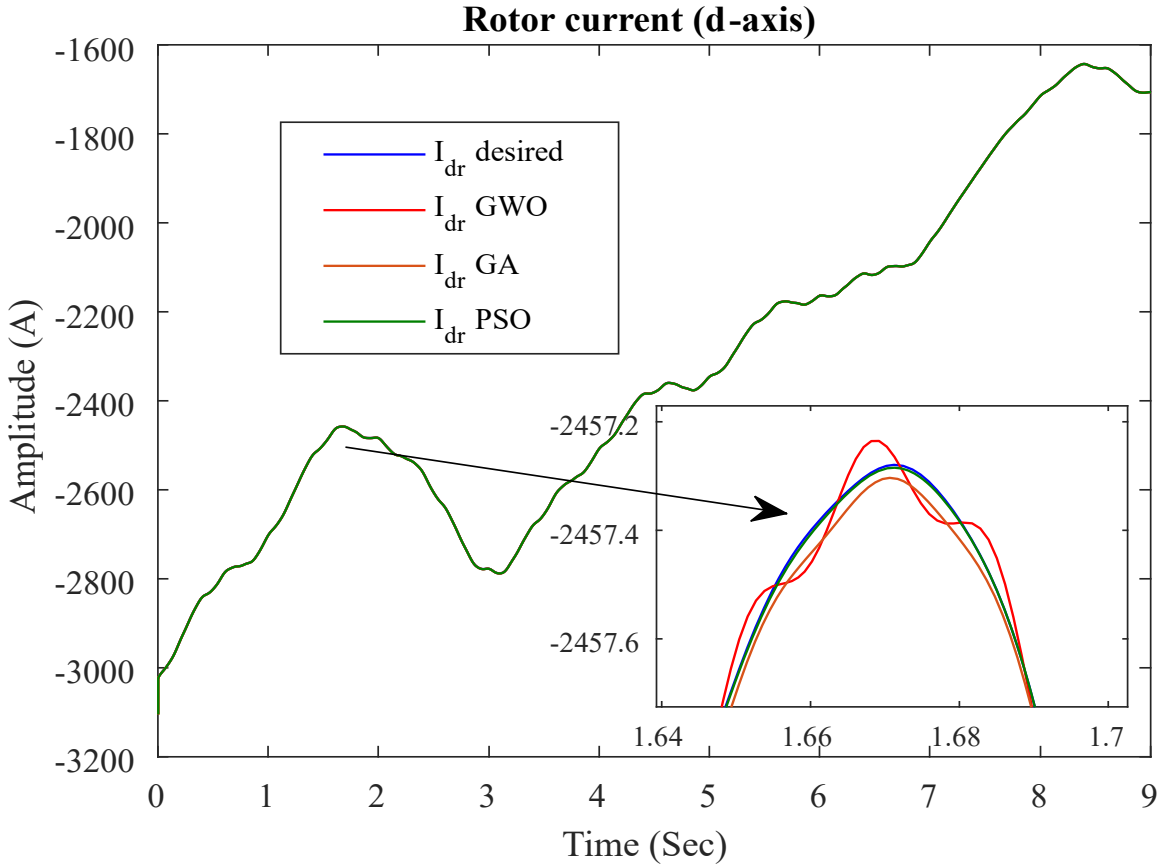

Fig. III.15 Rotor current response (d-axis).

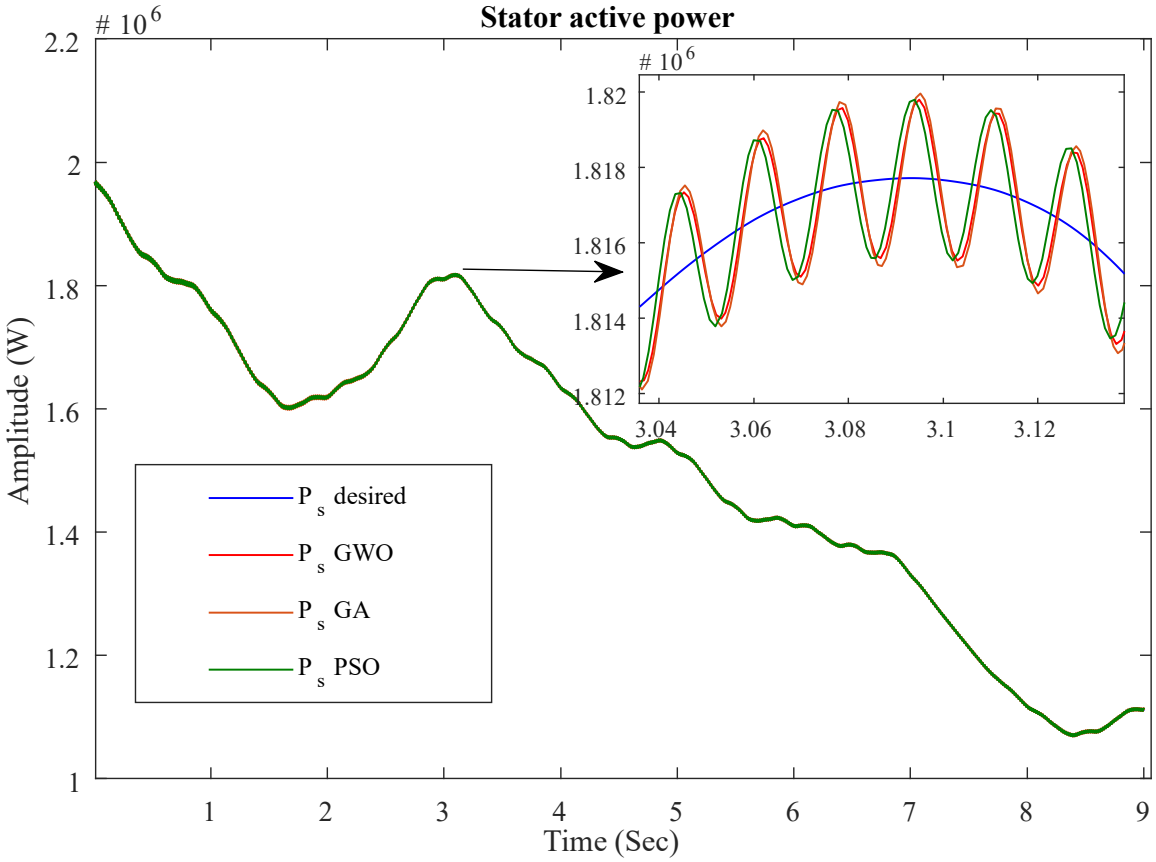

Fig. III.16 Stator active power dynamics.

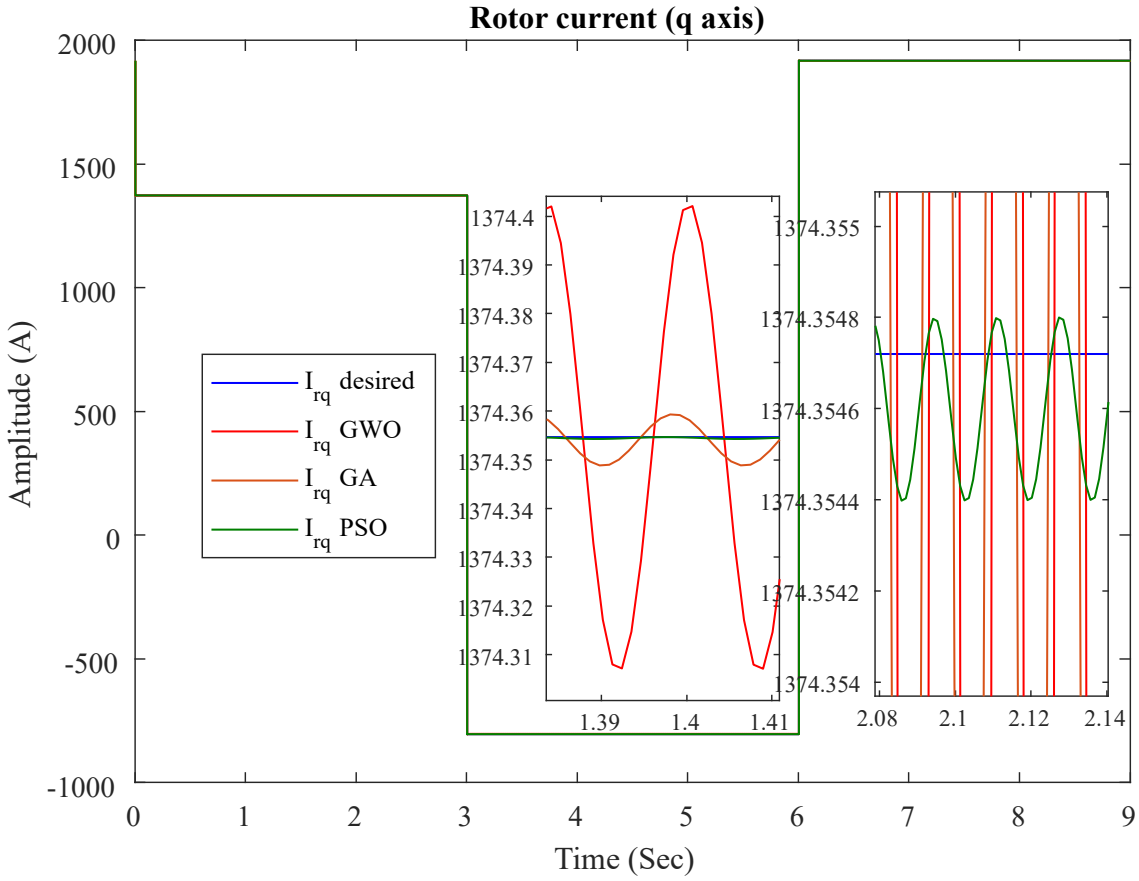

Fig. III.17 Rotor current response (q-axis).

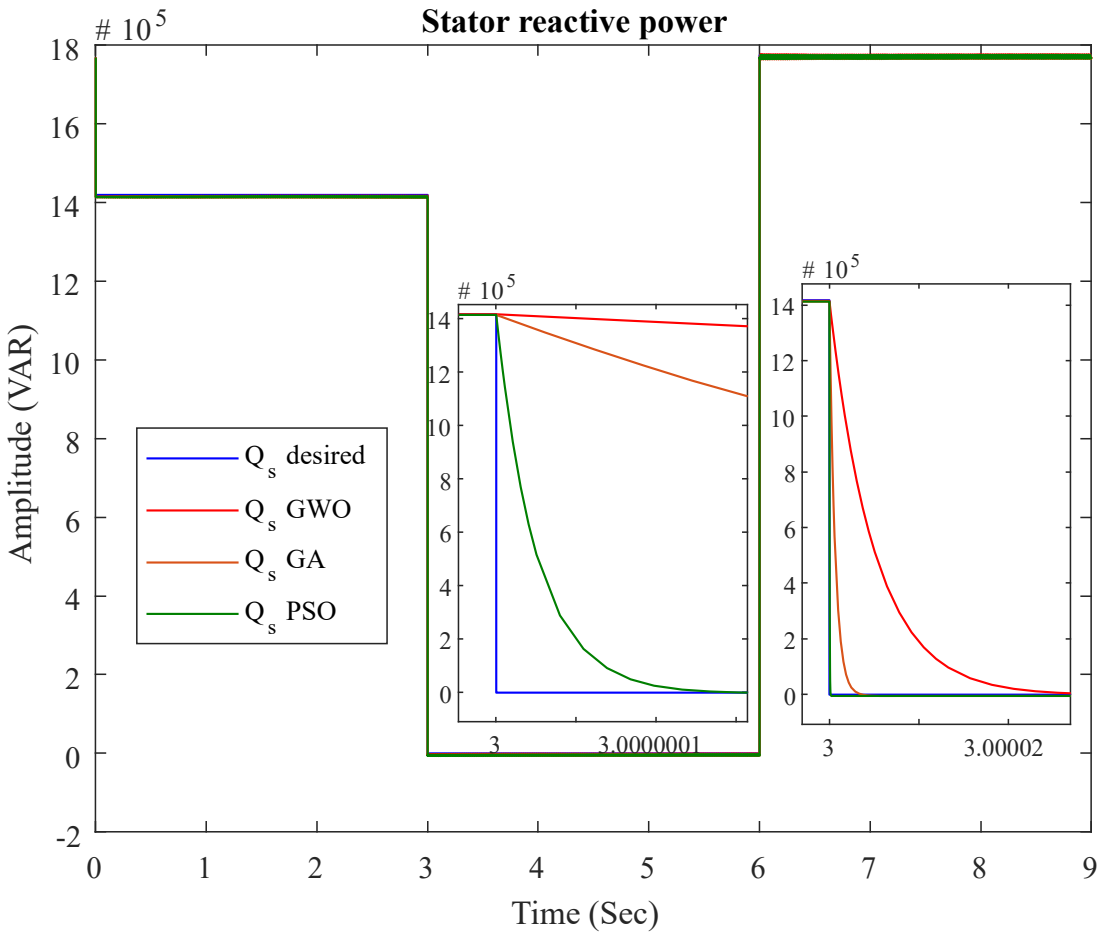

Fig. III.18 Stator reactive power dynamics.

III.3.5.2. Comparison of classical PI (DSA) and optimized PI

Figure III.19 and Figure III.20 show the rotor active and reactive power. Both figures compare the performance of the classical PI controller (DSA) with the optimized PI controllers (GWO, GA, PSO). The results show that while the optimization methods offer superior response performance in terms of speed and accuracy, they introduce oscillations in the rotor power, which are absent in the Direct Synthesis Approach. The DSA provides a smooth, steady response with no oscillations, indicating no vibrations in the system.

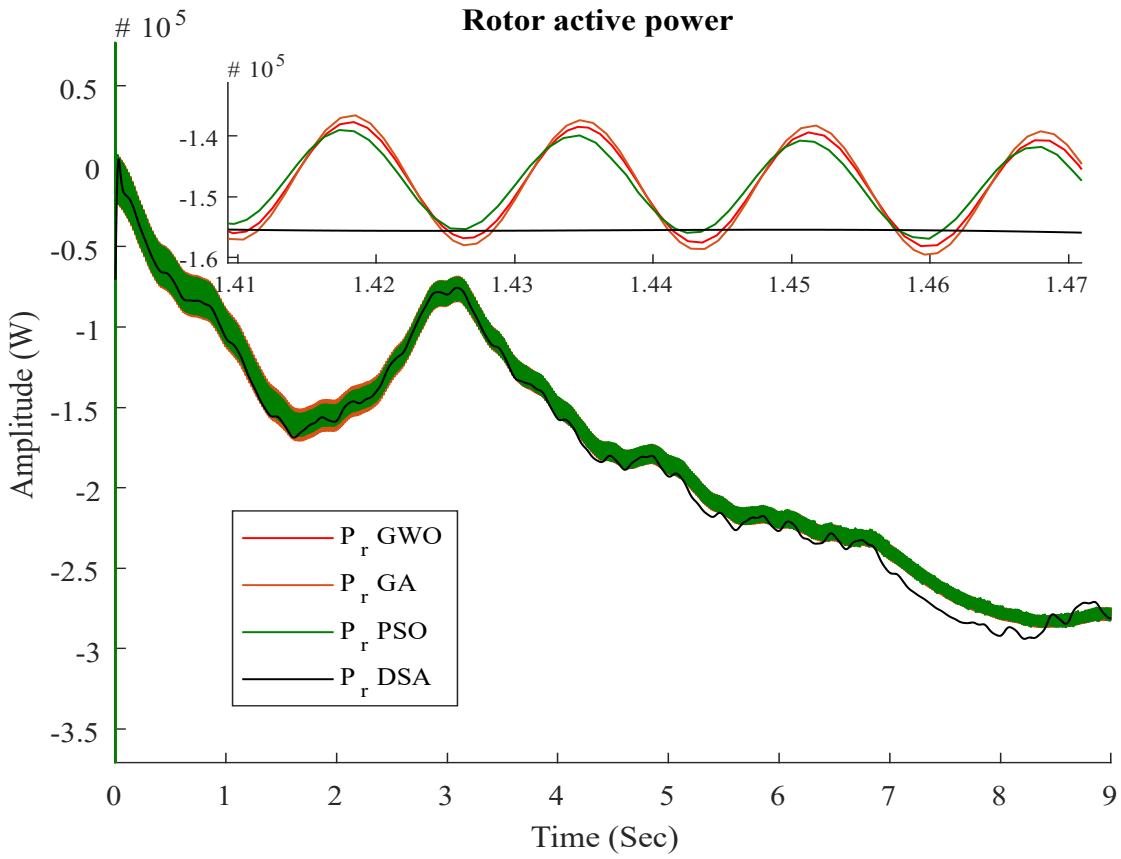

Fig. III.19 Rotor active power dynamics.

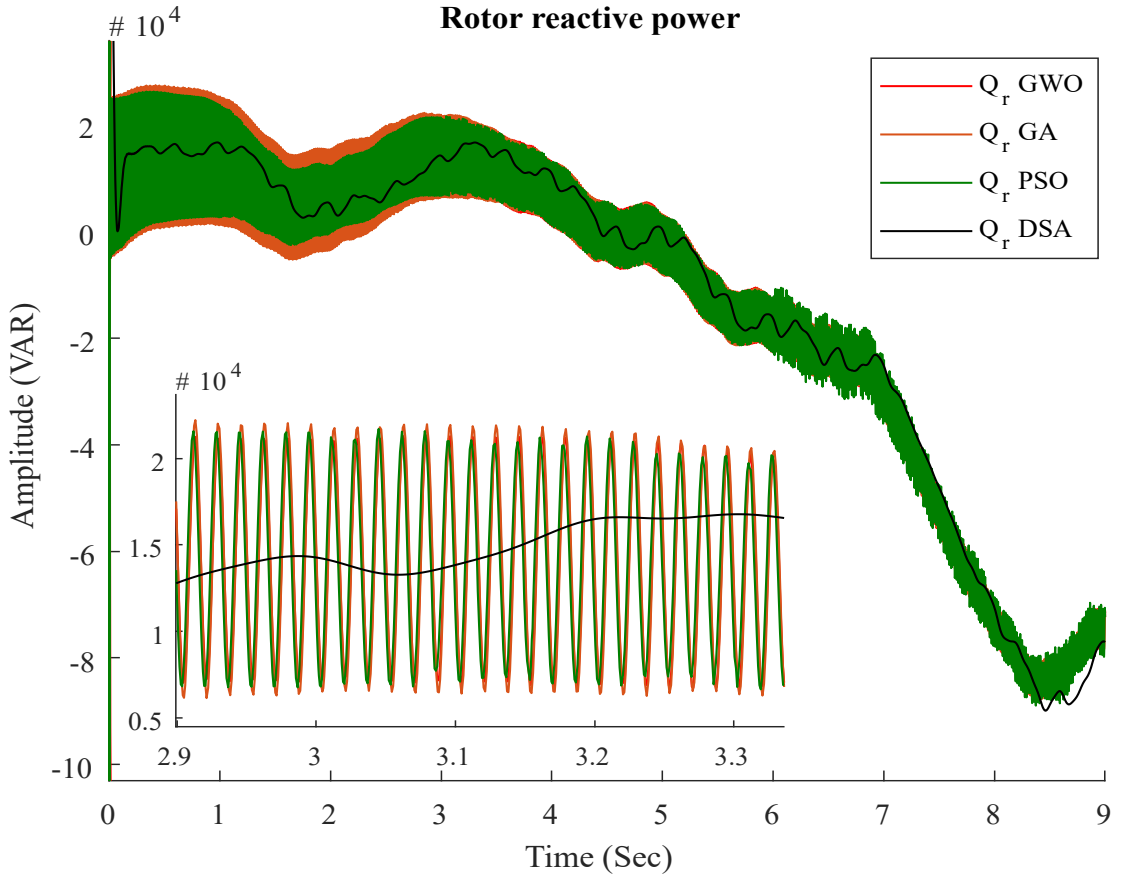

Fig. III.20 Rotor reactive power dynamics.

From the results presented in Figures III.15 to III.20, it is clear that the optimization methods-particularly PSO-offer significant advantages in terms of response time and accuracy. These methods provide powerful performance in terms of both precision and response speed, with all three optimization techniques significantly outperforming the classical PI controller using the Direct Synthesis Approach (DSA). The optimized PI controllers also demonstrate an absence of overshoot, further highlighting their effectiveness in dynamic control scenarios.
However, while the optimization methods provide these clear improvements, they also introduce oscillations in the rotor power, as seen in Figures III.19 and III.20. These oscillations could potentially lead to vibrations in the system, a behavior that is not present in the DSA. The DSA, while slower and less precise in terms of response, maintains a smooth and stable rotor power output, with no oscillations.
In conclusion, while the optimization methods excel in terms of response performance and accuracy, they do come with the drawback of rotor power oscillations, a factor that must be considered in applications where power stability is essential.

III.4. Conclusion

This chapter delved into the design, implementation, and optimization of PI controllers for wind turbine systems, focusing on the comparison between classical methods and modern optimization techniques. The Direct Synthesis Approach (DSA) was examined first, providing a structured methodology for designing PI controllers based on the system's transfer function. This classical method has long been favored for its simplicity, ease of implementation, and effectiveness in achieving basic control objectives like stability and steady-state accuracy.

In wind turbine control systems, maintaining a balance between the rotor current and power output is crucial, particularly under varying wind conditions. The Direct Synthesis Approach achieved reasonable success in stabilizing the system. However, as we observed in the simulation results, this approach exhibited certain limitations, particularly in dynamic environments. These limitations were most apparent in terms of slower response times, noticeable overshoot, and minor steady-state errors. While the system maintained overall stability, the transient behavior left room for improvement, especially when responding to rapid changes in wind speed or power demand.

To address these performance gaps, we introduced several metaheuristic optimization algorithms-Grey Wolf Optimization (GWO), Genetic Algorithm (GA), and Particle Swarm Optimization (PSO)-as more dynamic alternatives to the classical PI tuning methods. These optimization techniques are particularly suited for complex, nonlinear systems like wind turbines, where traditional methods may struggle to cope with the intricate dynamics and variability in operating conditions.

The performance of these optimization methods was evaluated through simulations, revealing several important findings:

- PSO emerged as the best performer among the optimization methods, offering rapid convergence to the desired control points with minimal error. It demonstrated the ability to quickly adapt to changing wind conditions, reducing response time and eliminating overshoot. This precision in control makes PSO a highly effective solution for improving wind turbine efficiency, especially in dynamic and fluctuating wind environments.
- GA performed well in optimizing the PI controller but showed moderate accuracy and response speed compared to PSO. It was more stable than GWO but fell short in achieving the same level of precision as PSO.
- GWO, while effective, lagged behind the other two methods in terms of speed and accuracy, demonstrating slower convergence and higher steady-state error.

However, while the optimization methods-especially PSO-provided substantial improvements in terms of response time, precision, and the elimination of overshoot, they introduced a new challenge: oscillations in rotor power. These oscillations, absent in the Direct Synthesis Approach, could lead to system vibrations, potentially affecting the long-term stability and reliability of the wind turbine

system. In contrast, the DSA, though slower and less precise, maintained a smooth and steady rotor power response with no oscillations, indicating that it may be better suited for applications where rotor stability and vibration minimization are critical considerations.
The results of this chapter highlight a key dilemma between the classical and optimized PI control methods:

- Optimized PI controllers provide faster, more accurate control responses, making them ideal for applications where rapid changes in wind conditions or power output are expected. However, they come with the drawback of potential oscillations in rotor power, which could impact mechanical wear and overall system durability over time.
- Classical PI controllers using the Direct Synthesis Approach, while less responsive and slightly less accurate in dynamic conditions, offer the advantage of a smooth, oscillation-free power output. This makes them more suitable for systems where stability and long-term reliability are prioritized over immediate responsiveness.

These findings underscore the importance of selecting the appropriate control strategy based on the specific operational needs of the wind turbine system. For instance, in high-performance wind turbines operating in rapidly changing environments, optimization methods like PSO may be ideal for maximizing energy capture and improving system responsiveness. On the other hand, in systems where mechanical stability and vibration control are more critical, a more conservative approach like DSA may be preferred.

Looking ahead, the next chapter will explore Intelligent Control, which represents the frontier of advanced control strategies for wind turbines. By leveraging artificial intelligence (AI) and machine learning (ML), intelligent control systems promise to go beyond the limitations of traditional and optimization-based methods. These systems can adapt to real-time changes in wind conditions, turbine health, and operational demands, providing a more proactive and autonomous form of control. Through intelligent algorithms, wind turbines can continuously learn from their environment, predict future conditions, and make real-time adjustments to optimize performance, stability, and longevity.

In conclusion, while this chapter demonstrated the potential of optimization algorithms to significantly enhance PI controller performance, it also highlighted the need for careful consideration of dilemma between speed, accuracy, and stability. The findings serve as a foundation for the exploration of more advanced, AI-driven control strategies that will be discussed in the following chapter.

Chapter IV
Advanced control strategies for wind turbine control

IV.1. Introduction

In recent years, wind turbine systems have grown in complexity, requiring more advanced control strategies to maintain stability, optimize performance, and handle the nonlinearities and uncertainties associated with fluctuating wind conditions. Traditional control methods, such as the Proportional-Integral (PI) controller, have proven effective in basic scenarios but often fall short when managing complex dynamics, unpredictable disturbances, and rapidly changing environments [91].

To address these challenges, a range of intelligent control techniques has emerged, offering more robust, adaptive, and efficient control solutions. These methods are capable of handling the nonlinear and time-varying nature of wind turbines, improving system response, reducing energy loss, and enhancing the overall performance of the wind energy conversion system. In this chapter, we explore several advanced control strategies and their application to wind turbine systems, including:

- Sliding Mode Control (SMC): A robust control method known for its ability to handle uncertainties and disturbances by forcing the system to "slide" along a predefined surface in the state space. It provides excellent tracking performance but may suffer from chattering, which can affect mechanical components.
- Super Twisting Sliding Mode Control (STSMC): An enhanced version of SMC that mitigates the chattering effect by introducing a continuous control law. This method improves the smoothness of the control action while maintaining robustness.
- Fuzzy Logic Control (FLC): A control strategy based on human reasoning, capable of dealing with uncertainties and nonlinearities without requiring a precise mathematical model of the system. FLC is particularly useful in systems with variable operating conditions.
- Artificial Neural Networks (ANN): A data-driven control approach inspired by the human brain's learning process. ANN-based controllers can learn complex relationships between inputs and outputs, making them highly effective in adaptive control scenarios for wind turbines.
- Hybrid Control (SMC-FLC, STSMC-FLC): A combination of different intelligent control strategies, such as integrating Sliding Mode Control with Fuzzy Logic Control (SMC-FLC) or Super Twisting Sliding Mode Control with Fuzzy Logic Control (STSMC-FLC). These hybrid methods leverage the strengths of both techniques, offering a balance between robustness and adaptability, while mitigating the weaknesses of individual methods.

The primary focus of this chapter is to explore the design, implementation, and performance of these intelligent control strategies. Through simulations and comparative analyses, we will evaluate their effectiveness in improving the stability, performance, and efficiency of wind turbine systems under various operational conditions. As wind energy continues to expand as a critical component of global renewable energy, the application of intelligent control becomes essential in achieving optimal system performance and reliability.

IV.2. Sliding Mode Control

IV.2.1. Overview of the SMC

Sliding Mode Control (SMC) is a robust nonlinear control technique widely used for systems with uncertainties and external disturbances. The core concept behind SMC is to force the system's trajectory to "slide" along a predefined surface in the state space, known as the sliding surface, where the system exhibits desired dynamic behavior (as depicted in Figure IV.1). The system is driven towards this sliding surface by a discontinuous control action, ensuring that the system remains on the surface despite disturbances or model inaccuracies [92].

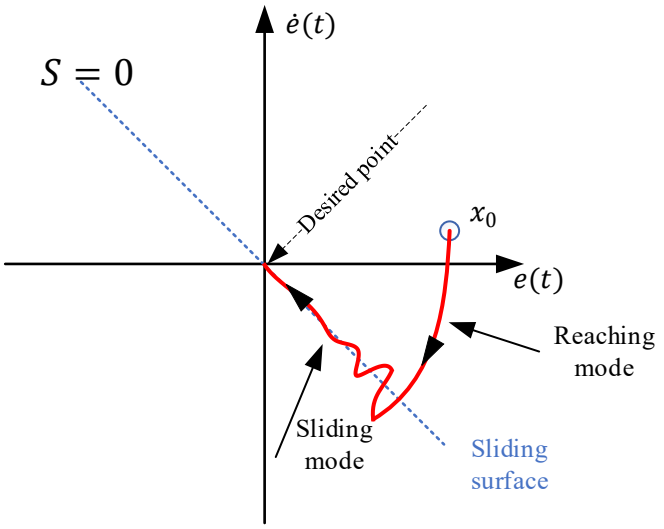

Fig. IV.1 Phase plane trajectory modes [93].

The key characteristics of SMC are [92], [94]:

- Sliding Surface Design: The design of the sliding surface is crucial to the performance of SMC. The surface is defined based on system states and is typically chosen to ensure desirable dynamic behavior, such as fast convergence, reduced overshoot, and minimized steady-state error.
- Control Law: The control input in SMC is composed of two parts: an equivalent control that maintains the system on the sliding surface, and a switching control that drives the system towards the surface. The switching control introduces discontinuity to ensure robustness but also leads to the below mentioned chattering problem.
- Robustness: SMC is highly effective in handling system uncertainties, parameter variations, and external disturbances. Once the system reaches the sliding surface, the control law guarantees that the system behavior remains insensitive to disturbances, making it particularly attractive for controlling wind turbines, where wind conditions can change unpredictably.
- Chattering: A common issue with SMC is the chattering effect, where the control signal switches rapidly, causing high-frequency oscillations in the control input. This can result in wear and tear on mechanical components, such as the turbine's gearbox or actuators. Mitigating chattering is a key challenge in SMC, often addressed through modifications like boundary layer approaches or advanced techniques such as Super Twisting Sliding Mode Control (STSMC).

In the context of wind turbine control, SMC can be applied to regulate key parameters such as rotor speed, power output, and mechanical stresses. The robustness of SMC allows it to handle the nonlinearities and uncertainties inherent in wind turbines, making it a suitable choice for improving system performance under varying wind conditions. However, careful design of the control law and sliding surface is necessary to minimize the negative effects of chattering and ensure smooth system operation [6], [95].

In the following sections, we will explore the detailed formulation of the SMC control law, the sliding surface design, and how SMC is applied to wind turbine systems to enhance performance and robustness.

IV.2.2. Methodology

The control design has three highly dependent phases:

- Design of the Sliding Surface: The sliding surface defines the desired behavior of the system and the region where the system will "slide" to ensure optimal performance. J.J. Slotine [92] proposed to develop a scalar function of the sliding surfaces in the phase plane to ensure the convergence of a state variable x towards its set value S, as shown in following equation:

$$S(x) = \left(\frac{d}{dt} + \lambda\right)^{r-1} e(x) \quad \text{(IV-1)}$$

  Where
  $e(t) = x_{ref}(t) - x(t)$ is the tracking error between the system's actual state $x(t)$ and the reference state x_{ref}.
  $\dot{e}(t)$ is the derivative of the error.
  λ is a positive constant that defines the slope of the sliding surface and determines the convergence rate. Higher values of λ lead to faster convergence, but might induce higher control effort.
  r is the order of the system.
- Formulation of the SMC control low: The control law is designed to drive the system to the sliding surface $S(x) = 0$ and maintain it there, even in the presence of distrubances. The SMC control law is typically composed of two parts:
  - Equivalent control: This component maintains the system on the sliding surface. It is derived from the system dynamics and ensures that the system follows the desired trajectory once it reaches the sliding surface. The equivalent control u_{eq} can be derived from the system dynamics by ensuring that the derivative of the sliding surface equals zero.

$$\dot{S}(x) = 0 \quad \text{(IV-2)}$$

  - Switching control: This component drives the system toward the sliding surface by switching between control inputs. It typically takes the form of a discontinuous function, such as $u(t) = u_{eq} + u_{sw}$, where u_{eq} is the equivalent control, and u_{sw} is the switching control. The switching control law is typically defined as

$$u_{sw} = -k.sign(S(x)) \quad \text{(IV-3)}$$

    Where k is a positive constant and $sign(S(x))$ is the signum function. This discontinuous control ensures that the system reaches and stays on the sliding surface, but it can introduce chattering.
- Stability analysis: After defining the control law, the stability of the closed-loop system is analyzed. The Lyapunov stability criterion is commonly used to prove that the system

will converge to the sliding surface and remain stable [96]. The Lyapunov function $V(S)$ is chosen such that:

$$V(S) = \frac{1}{2}S^2(x) \quad \text{(IV-4)}$$

The derivation of $V(S)$ along the system trajectory should satisfy $\dot{V}(S) < 0$, guaranteeing that the system will converge to the sliding surface and remain stable.

- Chattering Reduction Technique using Super Twisting Sliding Mode Control (STSMC): A significant challenge in SMC is the chattering phenomenon, caused by the high-frequency switching of the control input. This chattering can lead to mechanical wear in systems like wind turbines and reduced efficiency.

  To address this, Super Twisting Sliding Mode Control (STSMC) is introduced as an advanced technique that reduces chattering while maintaining the robustness and accuracy of conventional SMC. The STSMC approach uses continuous control signals to smooth out the switching behavior, significantly reducing high-frequency oscillations in the control signal [26], [97], [98].

  The STSMC control law is composed of two parts:

  - A continuous control term:

  $$u_1 = -k_1|S(x)|^{1/2}.Sign(S(x)) \quad \text{(IV-5)}$$

    This term reduces chattering by applying a control action proportional to the square root of the sliding surface.

  - A discontinuous control term:

  $$u_2 = -k_2 \int Sign(S(x))\, dt \quad \text{(IV-6)}$$

    This integrates the sign function over time, further reducing the chattering effect by smoothing the control signal.

  The total control law for STSMC is:

  $$u = u_{eq} + u_1 + u_2 \quad \text{(IV-7)}$$

  Where u_{eq} is the equivalent control ensuring the system stays on the sliding surface, u_1 and u_2 reduce the chattering through smooth control actions.

  By applying STSMC, the system can achieve superior control performance with reduced chattering, making it an ideal method for wind turbine control applications where mechanical stress and precision are critical.

To apply the Sliding Mode Control (SMC) to the system modeled by the transfer function in Eq. (II-43), the following steps are taken:

The System model to be controlled is $i_{dqr} = \frac{1}{R_r + S\sigma L_r} v'_{dqr}$. This first-order system represents the dynamics of the rotor current in response to the control input v'_{dqr}.

The sliding surface is defined as

$$S(i_{dqr}) = e(t) = i_{dqr\,ref}(t) - i_{dqr}(t) \quad \text{(IV-8)}$$

Where $e(t)$ is the error between the actual rotor current and the reference current.

To maintain the system on the sliding surface $S = 0$, the equivalent control is derived by setting $\dot{S} = 0$, which means driving $e(t)$ to zero.

From Eq. (IV-8)

$$\dot{S}(i_{dqr}) = \dot{e}(t) = \dot{i}_{dqr\,ref}(t) - \dot{i}_{dqr}(t) \quad \text{(IV-9)}$$

Using the system dynamics $\dot{i}_{dqr} = \frac{v_{dqr} - R_r I_{dqr}}{\sigma L_r}$, the equivalent control expression is derived as follows:

$$u_{eq} = \sigma L_r \dot{i}_{dqr\,ref}(t) + R_r I_{dqr}(t) \quad \text{(IV-10)}$$

This ensures the system follows the desired reference current.

The switching control drives the system towards the sliding surface. It is defined as:

$$u_{sw} = -k.sign(e(t)) \quad \text{(IV-11)}$$

The total control input is the sum of the equivalent and switching controls:

$$u = u_{eq} + u_{sw} = \sigma L_r \dot{i}_{dqr\,ref}(t) + R_r I_{dqr}(t) - k.sign(e(t)) \quad \text{(IV-12)}$$

This control law ensures that the system is driven to the sliding surface and remains there, robustly tracking the reference current $\dot{i}_{dqr\,ref}$.

The total control input for STSMC using Eq. (IV-7) is:

$$u = \sigma L_r \dot{i}_{dqr\,ref}(t) + R_r I_{dqr}(t) - k_1 |S(x)|^{1/2}.Sign(S(x)) - k_2 \int Sign(S(x))\, dt \quad \text{(IV-13)}$$

IV.2.3. Simulation results

In this section, we present the simulation results comparing the performance of Sliding Mode Control (SMC) and Super Twisting Sliding Mode Control (STSMC) for wind turbine control. The simulations were carried out using MATLAB/Simulink, with the system model based on the modeling developed in Chapter II. The objective is to evaluate the response of rotor currents and stator power under varying wind speed conditions and reactive power reference changes, while analyzing the impact of chattering. The primary goal is to determine if STSMC can effectively mitigate the chattering problem inherent in SMC, while maintaining or improving system performance.

The following figures illustrate the behavior of rotor current (d-axis and q-axis), stator active power, and stator reactive power for both SMC and STSMC. Additionally, we analyze the rotor active power to assess the extent of chattering in both methods.

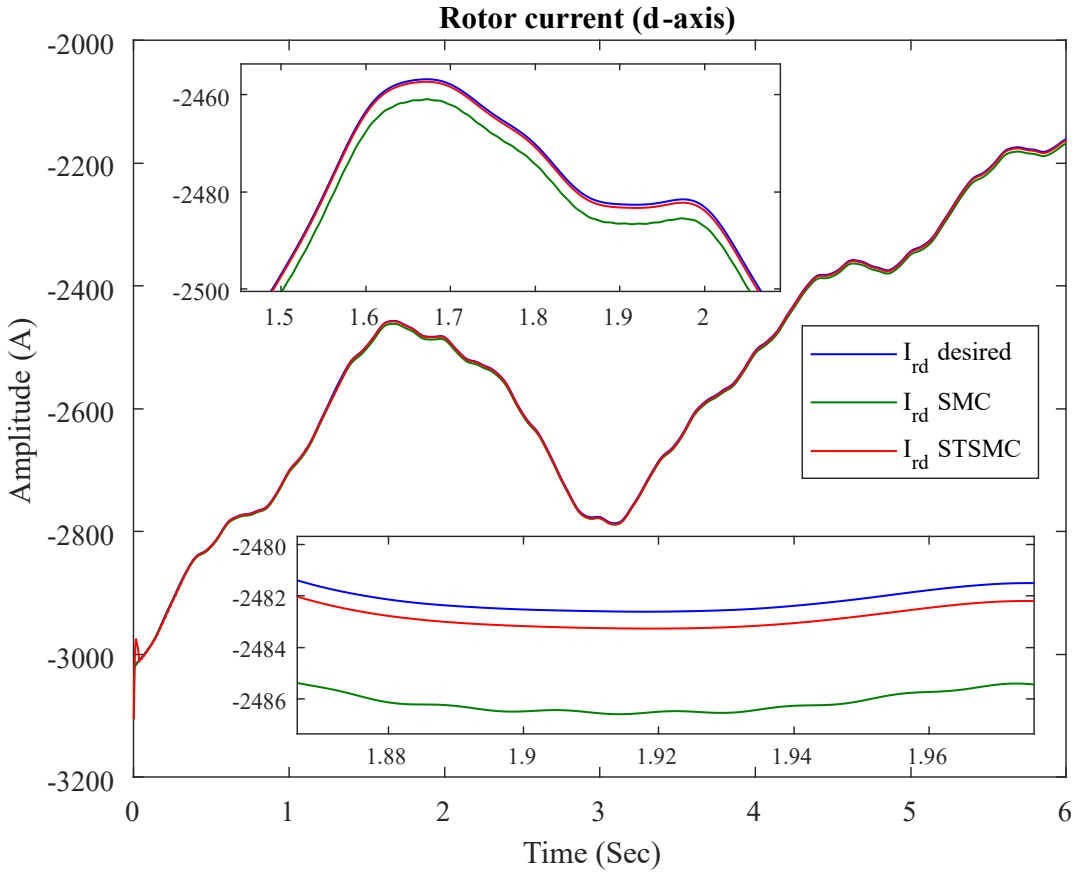

Fig. IV.2 Rotor current response (d-axis).

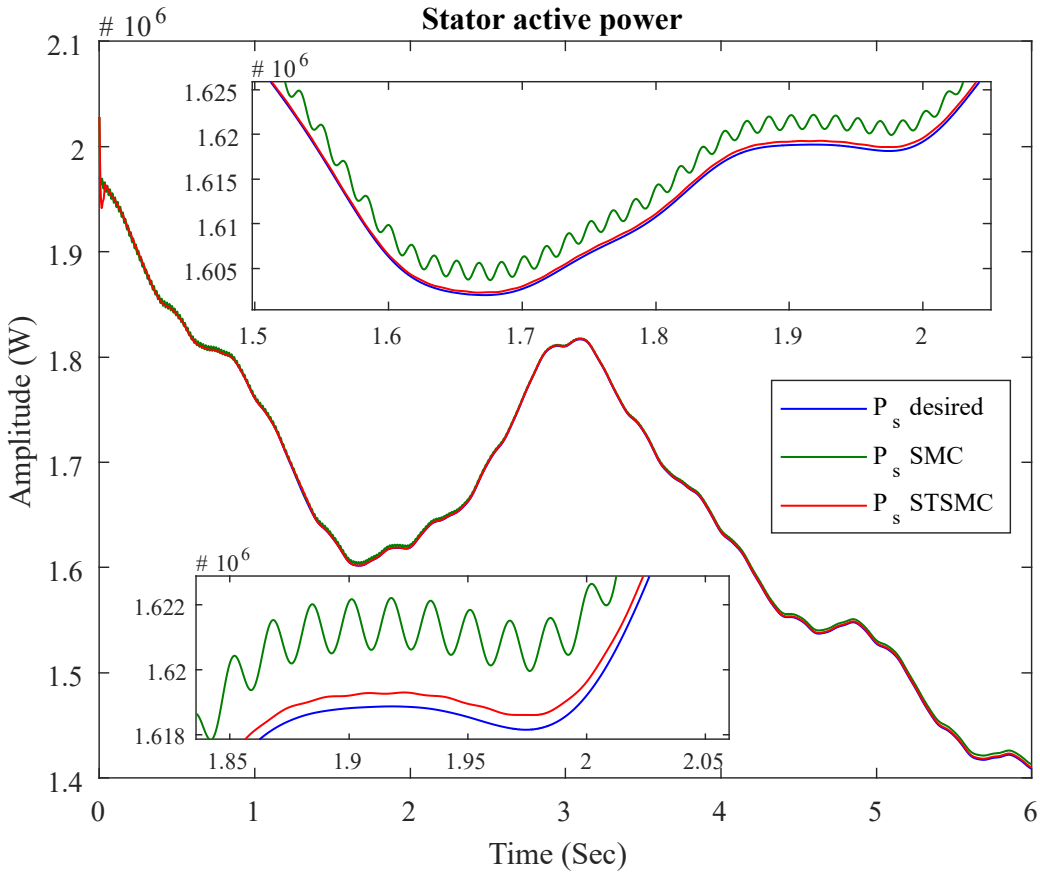

Fig. IV.3 Stator active power dynamics.

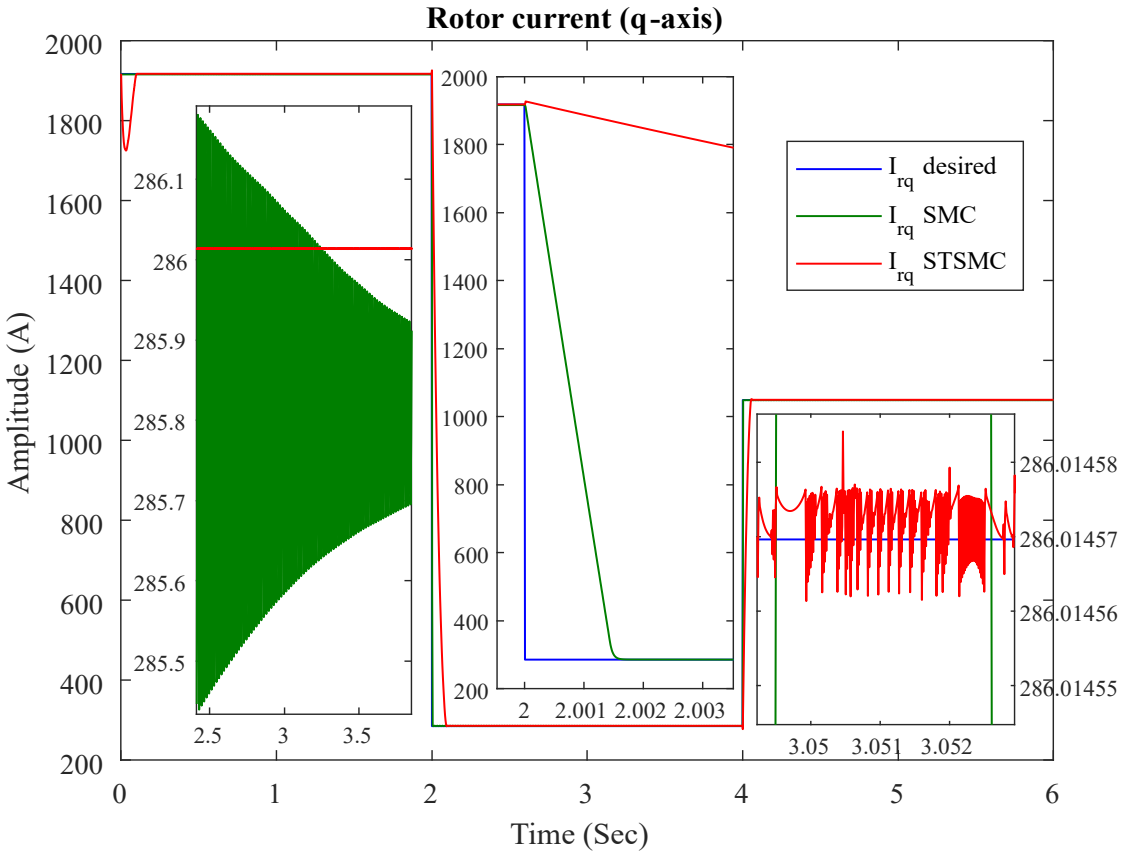

Fig. IV.4 Rotor current response (q-axis).

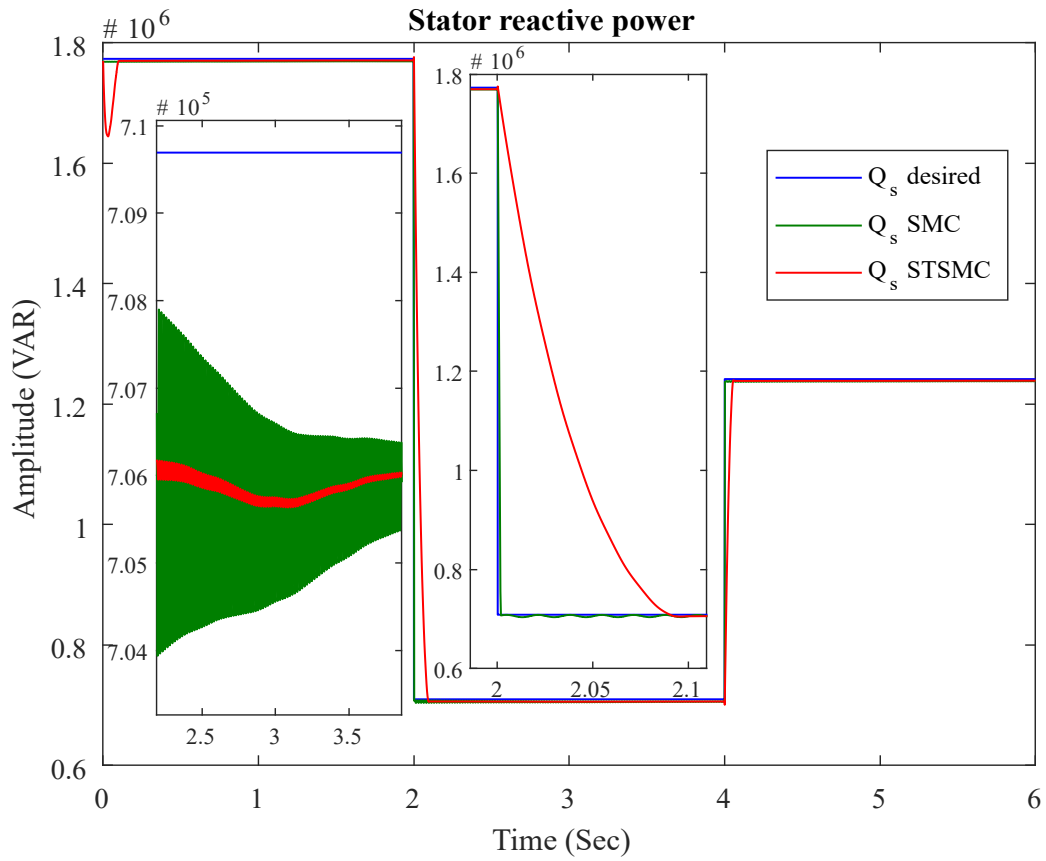

Fig. IV.5 Stator reactive power dynamics.

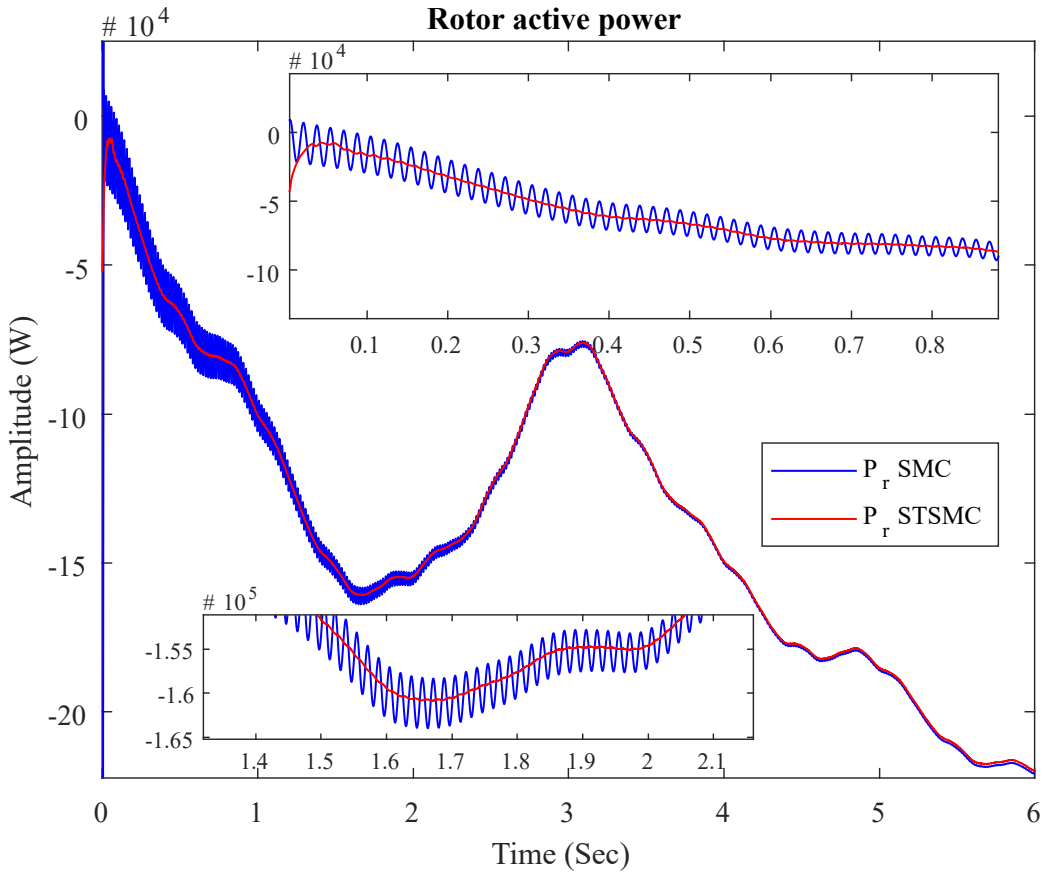

Fig. IV.6 Rotor active power dynamics.

The results of Figure IV.2 for rotor current (d-axis) show that STSMC provides a response much closer to the desired reference signal than SMC. The SMC exhibits minor oscillations (chattering), although they are not prominent. In contrast, STSMC eliminates this chattering effect, offering a smoother response. However, STSMC experiences a small delay in the initial response, which is not observed in SMC. This trade-off between improved accuracy and slight delay is an important observation when comparing the two control strategies.

In the stator active power dynamics (Figure IV.3), the chattering effect is more pronounced when using SMC. This is evident from the significant oscillations in the SMC signal, which could potentially lead to inefficiencies and mechanical stress in real-world applications. On the other hand, STSMC successfully suppresses this chattering, providing a smoother and more stable power response. This shows that STSMC is highly effective in mitigating the chattering issue without sacrificing performance.

The Figure IV.4 and Figure IV.5 confirm the observations made in Figs. IV.2 and IV.3. The rotor current (q-axis) and stator reactive power dynamics demonstrate the same trend: STSMC is much closer to the desired signal compared to SMC, with significantly reduced chattering. Furthermore, the response time for STSMC is slightly slower at approximately 0.85 seconds, while SMC responds almost instantaneously at 0.002 seconds. However, the SMC response exhibits a larger error margin compared to STSMC. This reaffirms that while SMC offers faster initial response, its precision is compromised, and it suffers from chattering issues. In the final figure (Figure IV.6), the chattering effect in the rotor active power is clearly visible in the SMC response. The oscillations caused by SMC are substantial and could introduce undesirable vibrations in the system. In contrast, STSMC completely resolves this issue, as the rotor active power under STSMC control shows no oscillations and exhibits a smooth, stable output. This confirms the superior performance of STSMC in eliminating chattering while maintaining accurate control.

In conclusion, the simulation results clearly demonstrate that Super Twisting Sliding Mode Control (STSMC) outperforms standard Sliding Mode Control (SMC) in terms of reducing chattering and providing a more precise response. STSMC not only eliminates the oscillations caused by SMC, particularly in rotor and stator power dynamics, but also offers greater accuracy in tracking the reference signals. The main drawback of STSMC is a small delay in response time compared to SMC, which responds more quickly but at the cost of higher error and significant chattering.

Overall, STSMC proves to be a more effective control strategy for wind turbine systems, particularly in scenarios where precision and stability are critical. By mitigating the chattering issue inherent in SMC, STSMC enhances the longevity and performance of mechanical components while maintaining robust control under varying operational conditions.

IV.3. Hybrid Fuzzy Logic and Super Twisting Sliding Mode Control

IV.3.1. Overview of Hybrid Fuzzy-STSMC

The Hybrid Fuzzy Logic and Super Twisting Sliding Mode Control (Fuzzy-STSMC) approach combines the strengths of two robust control techniques to improve system performance in dynamic and uncertain environments [95], [99], [100]. Fuzzy Logic Control (FLC) is well-known for its ability to handle uncertainty and nonlinearities by using a rule-based system that mimics human decision-making. It offers smooth control actions, especially in systems where precise mathematical modeling is difficult. However, FLC alone may lack the robustness required for systems with high variability or external disturbances [101], [102], [103].

Super Twisting Sliding Mode Control (STSMC), on the other hand, provides strong robustness against disturbances and model uncertainties by forcing the system trajectory to remain on a predefined sliding surface. The main advantage of STSMC over conventional sliding mode control is its ability to mitigate the chattering effect, making it suitable for applications requiring smooth control. However, while STSMC ensures robustness, it may sometimes result in high control efforts or slower convergence [104], [105].
The Fuzzy-STSMC hybrid approach leverages the adaptive nature of fuzzy logic to enhance the sliding mode control by tuning the parameters of the sliding mode controller based on the system's state. This combination improves the overall performance of the control system by providing smoother control actions and faster convergence while maintaining robustness against disturbances. This section will explore the implementation of this hybrid control strategy and its impact on the control of wind turbines, demonstrating how it balances precision, stability, and robustness in variable wind conditions.

IV.3.2. Fuzzy Logic Control

Fuzzy Logic Control (FLC) is an intelligent control method that mimics human reasoning and decision-making processes to handle complex systems that are difficult to model mathematically. Unlike traditional control techniques, which rely on precise mathematical models, FLC uses linguistic variables and rule-based logic to manage uncertainty and nonlinearity within a system. This makes FLC particularly effective in dealing with imprecise, vague, or uncertain data [102].
The key idea behind fuzzy logic is to interpret values that fall between binary extremes of "true" and "false." In FLC, inputs are expressed in degrees of truth rather than absolute binary values, and control rules are expressed as IF-THEN statements. These fuzzy rules, based on expert knowledge or heuristics, allow the controller to infer decisions in ambiguous situations where conventional control methods may struggle [101], [103].
The main components of a fuzzy logic controller include:

- Fuzzification: Converts crisp input data (exact numerical values) into fuzzy sets, which represent the degree of truth in linguistic terms such as “low,” “medium,” or “high.”
- Inference Engine: Uses a rule base to process the fuzzy inputs and applies the fuzzy rules to generate fuzzy outputs based on the IF-THEN logic.
- Defuzzification: Converts the fuzzy output back into a crisp value, providing a precise control signal to the system.

The overall structure of a fuzzy logic controller is depicted in Figure IV.7, which provides an overview of how these components interact within the system.

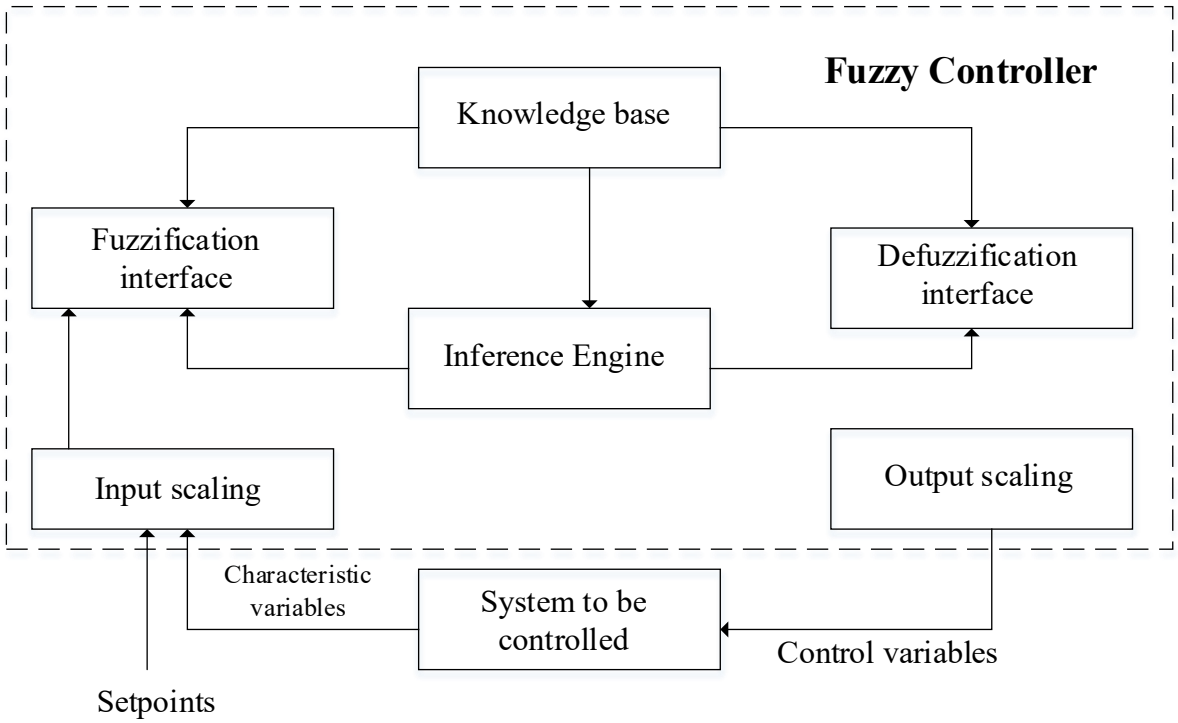

Fig. IV.7 Fuzzy controller: Basic structure overview [106].

Fuzzy logic control is particularly suited for systems with nonlinearity, such as wind turbines, where the dynamics are subject to constant variability and change. It provides smooth and adaptive control, offering the flexibility to handle uncertain and imprecise conditions that are inherent in wind turbine operations [6]. However, while FLC is adaptive and easy to implement, it may lack robustness in handling external disturbances, which is why it is often combined with other control methods like Sliding Mode Control (SMC) or Super Twisting Sliding Mode Control (STSMC) for improved performance.

IV.3.3. Methodolgy

The Fuzzy Logic Controller (FLC) is designed to improve the performance of the wind turbine system by enhancing control precision and stability under varying wind conditions. Traditionally, FLC requires an expert to manually define the membership function ranges and create the fuzzy rules, which can be a complex and subjective process. The effectiveness of the FLC largely depends on the chosen ranges for the input and output variables and the rules governing the controller's behavior.

One significant challenge in using FLC is determining the appropriate ranges for the membership functions and crafting accurate rules that effectively govern the control system. These decisions are often based on trial and error or expert knowledge, which introduces a potential source of inaccuracy or inconsistency.

To address this problem, the Proportional-Integral (PI) controller developed using the Direct Synthesis Approach (DSA) in Chapter III provides valuable input-output data that can be leveraged to design the FLC without requiring extensive expert knowledge. By analyzing the input-output relationships of the PI-DSA controller, we can derive the appropriate ranges for the membership functions and create data-driven fuzzy rules, removing the need for manual tuning [107].

- Data extraction from PI-DSA controller: To overcome the need for expert-defined ranges and rules, the input-output data of the PI-DSA controller is used as the

foundation for defining the FLC. The wind turbine is operated under varying wind conditions using the PI-DSA controller, and data is collected.

- Input data: The error signal of rotor currents, representing the difference between the desired system state and the actual response, is extracted from the PI-DSA controller. This data forms the basis for determining the appropriate input membership function ranges. This is shown in Figure IV.8.

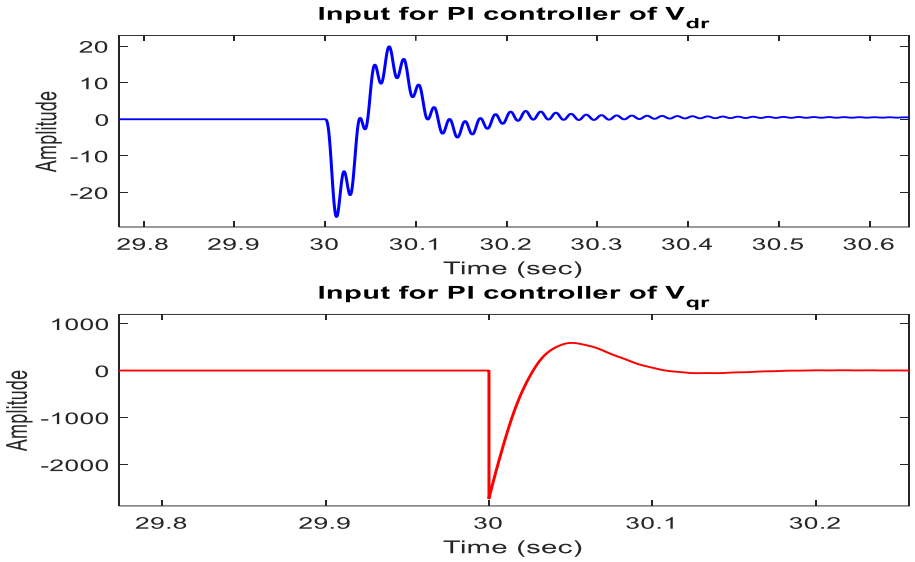

Fig. IV.8 Data Input for PI Controller

- Output data: The control signals (voltage adjustment) generated by the PI-DSA controller to minimize error and stabilize the system are used to define the output membership function ranges. This data is illustrated in Figure IV.9.

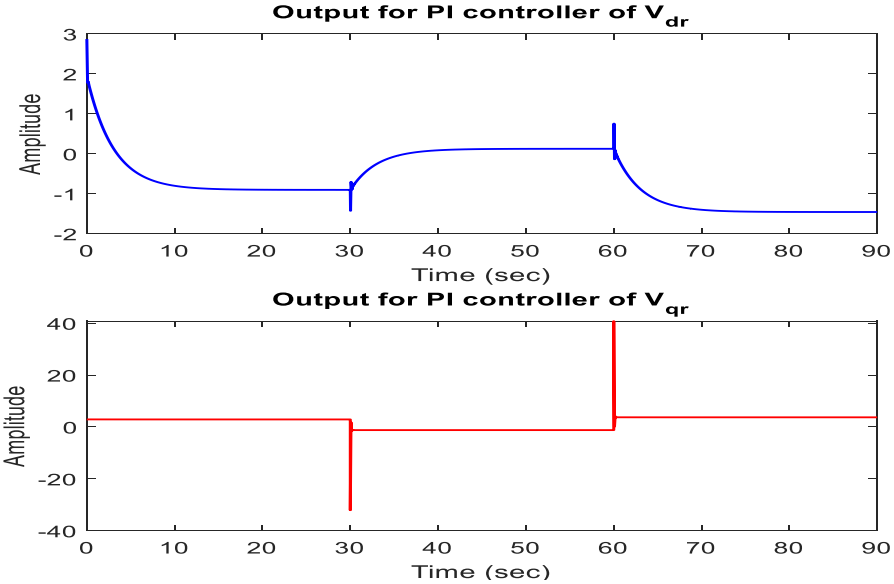

Fig. IV.9 Data output for PI Controller

By using this empirical data, the FLC can be designed in a more objective manner, relying on the observed relationships between input errors and control outputs.

- Design of input membership functions: The input membership functions are defined based on the error signals of rotor currents extracted from the PI-DSA controller. This

data-driven approach allows for more accurate and systematic definition of the fuzzy sets, without the need for subjective expert judgment. The input error is categorized into linguistic variables that describe the deviation in the system performance: Negative Large (NL), Negative Medium (NM), Negative Small (NS), Zero Equal (ZE), Positive Small (PS), Positive Medium (PM), and Positive Large (PL). These categories are derived from the input data of the PI-DSA controller and are illustrated in Figure IV.10, which shows how the membership functions are structured to reflect the actual input behavior observed from the PI-DSA.

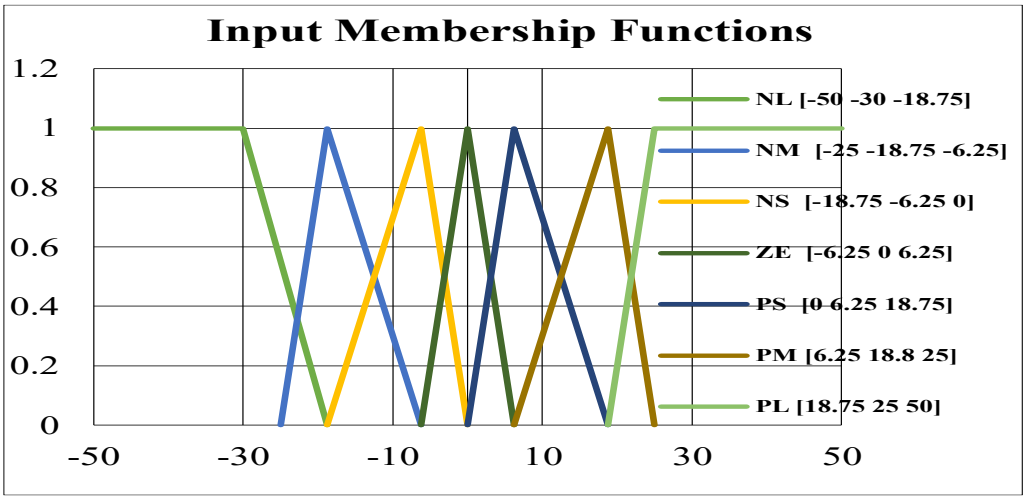

Fig. IV.10 Input membership functions.

- Design of output membership functions: Similarly, the output membership functions are defined using the control signals generated by the PI-DSA controller. By analyzing these control signals, appropriate fuzzy sets can be established to represent the range and distribution of the controller output. This data-driven approach eliminates the need for subjective tuning and ensures that the control actions generated by the FLC are consistent with the behavior observed from the PI-DSA controller. The output membership functions are categorized into the following linguistic terms: Negative Large (NL), Negative Medium (NM), Negative Small (NS), Zero Equal (ZE), Positive Small (PS), Positive Medium (PM), and Positive Large (PL). These categories are derived from the output data of the PI-DSA controller, and Figure IV.11 shows the output membership functions.

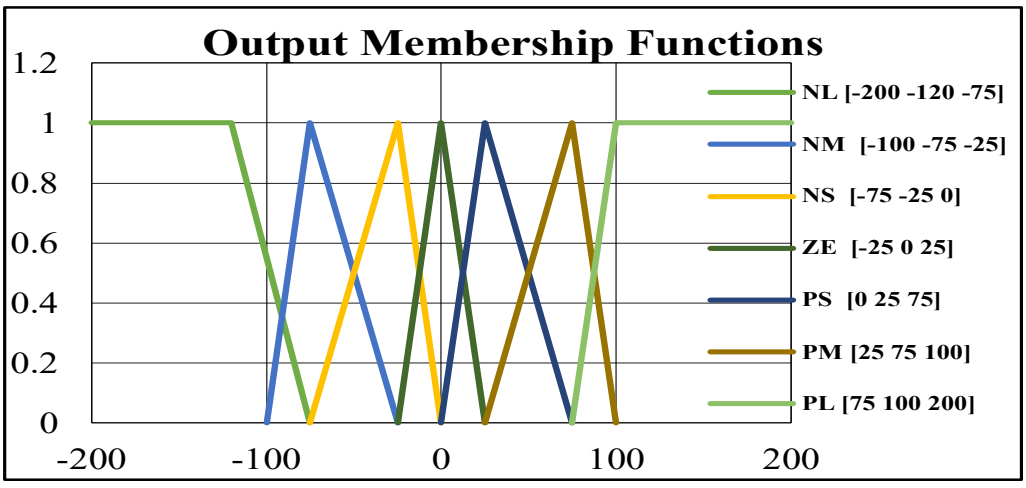

Fig. IV.11 Output membership functions.

- Fuzzy rule base
  The rule base of the FLC is constructed based on the input-output relationships observed in the PI-DSA controller's data. This allows the FLC to automate the process of rule generation, ensuring that the rules are aligned with the system's actual behavior under varying wind conditions. These rules are driven by the empirical data from the PI-DSA controller, ensuring that the FLC is tuned based on real performance rather than relying on expert knowledge. The complete set of rules is presented in Table. IV.1.

Tab. IV.1 Fuzzy rules.

Condition (Input) Output	**NL**	**NM**	**NS**	**ZE**	**PS**	**PM**	**PL**
NL	X	-	-	-	-	-	-
NM	-	X	-	-	-	-	-
NS	-	-	X	-	-	-	-
ZE	-	-	-	X	-	-	-
PS	-	-	-	-	X	-	-
PM	-	-	-	-	-	X	-
PL	-	-	-	-	-	-	X

- Fuzzification: The extracted error values are converted into fuzzy sets using the membership functions derived from the PI-DSA data. This step allows the FLC to interpret the error in a way that mimics human reasoning.
- Inference: The fuzzy inference engine applies the data-driven rules to the fuzzified input and determines the corresponding control actions in fuzzy terms. These rules are directly tied to the PI-DSA controller's observed behavior.
- Defuzzification: The fuzzy output is converted back into a crisp control signal using defuzzification techniques (such as the centroid method). This control signal is applied to the wind turbine system to correct its operation based on the FLC's decisions.
- Hybrid Fuzzy-Super Twisting Sliding Mode Control law: The Fuzzy-Super Twisting Sliding Mode Control (Fuzzy-STSMC) is developed to improve the robustness and precision of the control strategy by combining the adaptive nature of Fuzzy Logic with the robustness of the Super Twisting Sliding Mode Control (STSMC). While the STSMC effectively mitigates the chattering problem in standard SMC, using a sign function can still cause small residual oscillations. Replacing this sign function with a Fuzzy Logic Controller introduces smoother transitions, further reducing chattering while improving control precision.
  The sliding surface ($S(x)$) remains the same as in STSMC. Additionally, instead of applying a discontinuous sign function to drive the system toward the sliding surface, the control law is modified using fuzzy rules to provide a smooth, gradual transition. The fuzzy inference system interprets the error and its rate of change, and replaces the abrupt control action of the sign function with a smooth, nonlinear response. This reduces the chattering effect while maintaining the system's robustness. By doing so and from Eq. (IV-13), the control law for the Fuzzy-STSMC is:

$$u = \sigma L_r \dot{i}_{dqr\,ref}(t) + R_r I_{dqr}(t) - k_1 |S(x)|^{1/2}.Fuzzy(S(x)) - k_2 \int Fuzzy(S(x))\,dt \quad \text{(IV-14)}$$

This Hybrid Fuzzy-STSMC approach allows for better performance under variable conditions, maintaining the robustness of STSMC while minimizing the chattering effect through the use of fuzzy logic. This methodology integrates the strengths of both fuzzy control and sliding mode control, providing smoother, more precise control actions in highly dynamic systems like wind turbines.

The following section presents the simulation results, which will compare the performance of the Fuzzy-STSMC with both the classical STSMC and FLC. By evaluating the rotor current and power dynamics under varying wind conditions, the results will illustrate the effectiveness of the Fuzzy-STSMC in further reducing chattering while maintaining robust control.

IV.3.4. Simulation results

In this section, the performance of Super Twisting Sliding Mode Control (STSMC), Fuzzy Logic Control (FLC), and Hybrid Fuzzy-Super Twisting Sliding Mode Control (HFSTSMC) is evaluated and compared. The purpose of these comparisons is to assess the ability of these control strategies to ensure reference tracking and robustness under varying conditions. Specifically, the reference tracking is evaluated for rotor current and stator power, while robustness is tested under parameter variations.

The FLC used in these tests was designed in the previous section, and the STSMC remains the same as presented in the SMC section, but with adjusted gains to highlight differences when compared with HFSTSMC. The performance of each controller is measured in terms of precision, stability, response time, and oscillations, particularly in challenging scenarios with varying system parameters.

The following figures illustrate the behavior of the system under the influence of each control method.

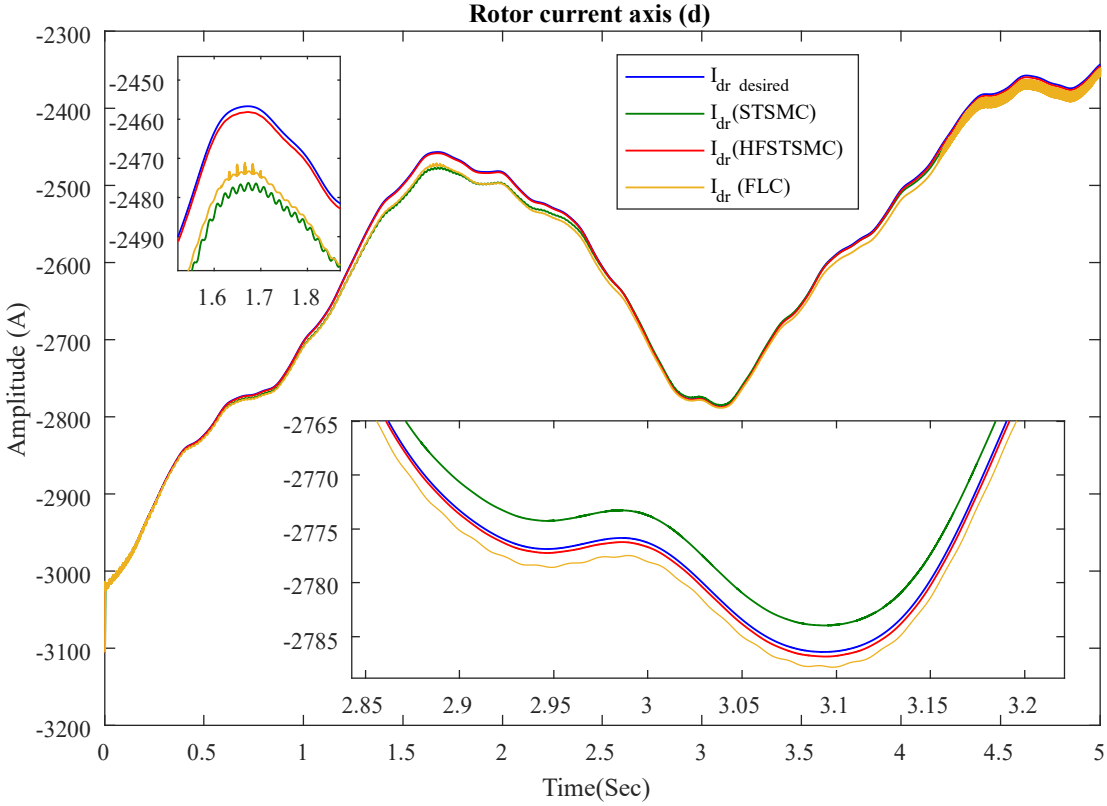

Fig. IV.12 Rotor current d-axis response.

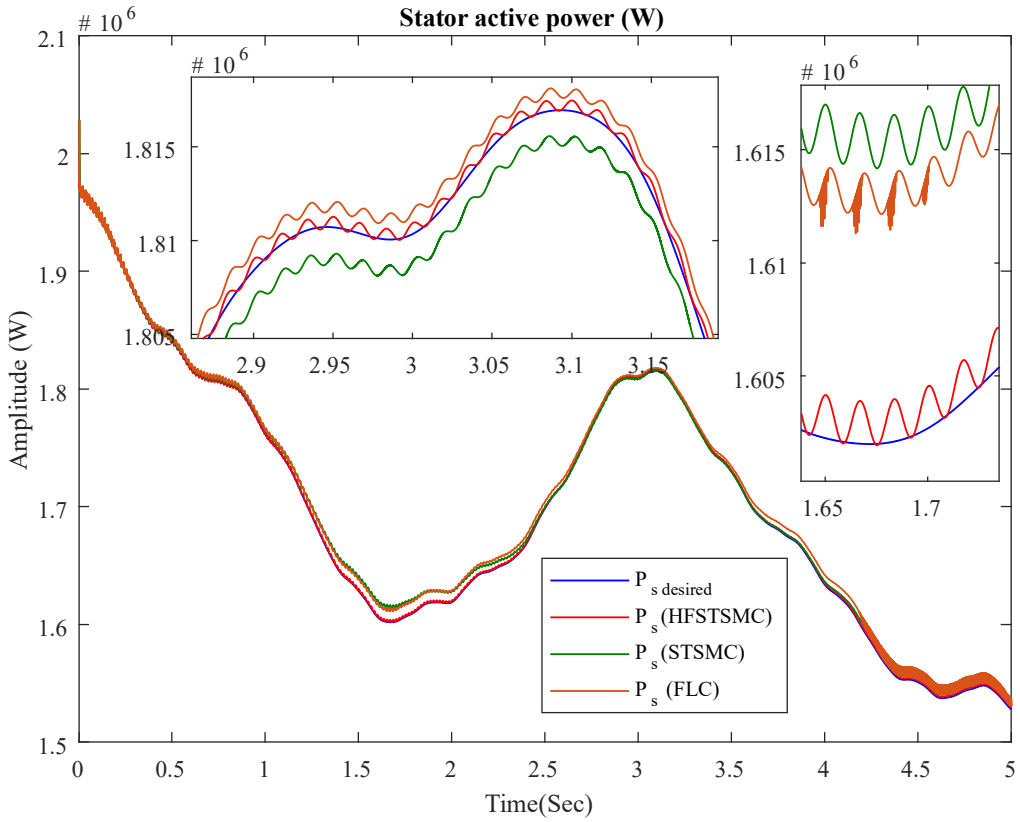

Fig. IV.13 Stator active power dynamics.

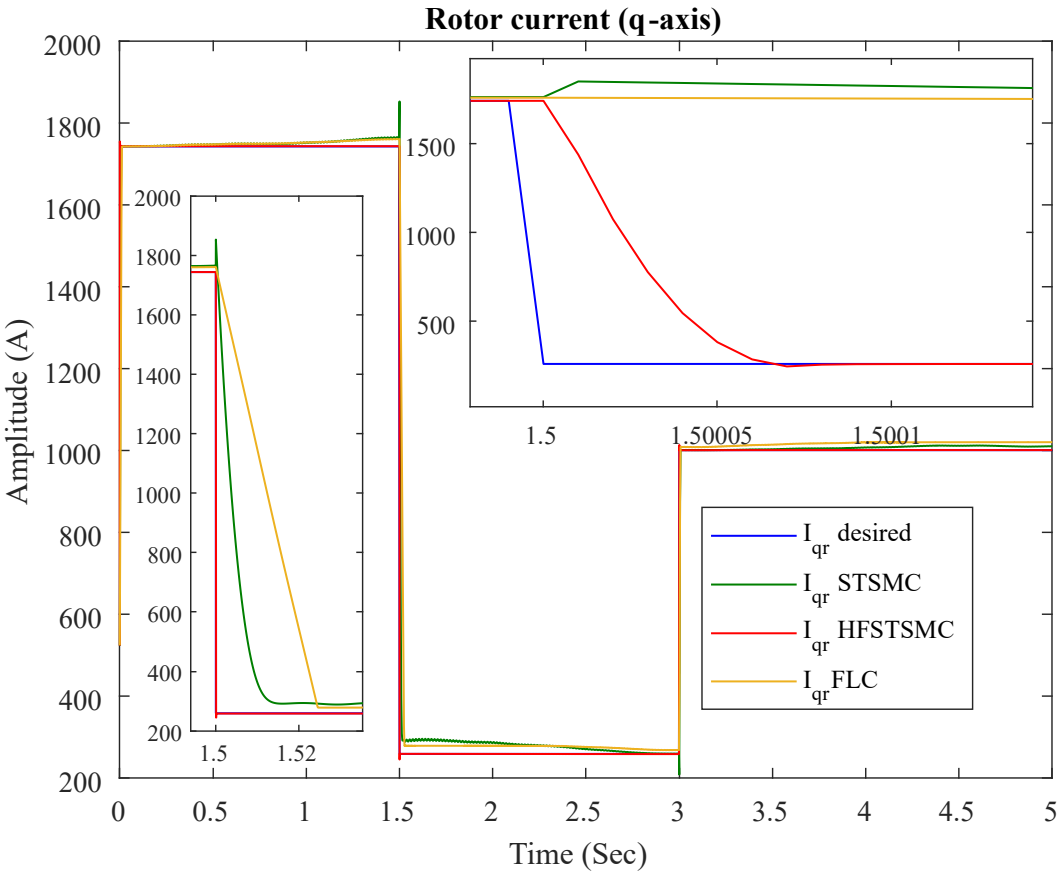

Fig. IV.14 Behavior of rotor current q-axis with a 100% variation in R_r, 60% in L_r, and 10% in L_m.

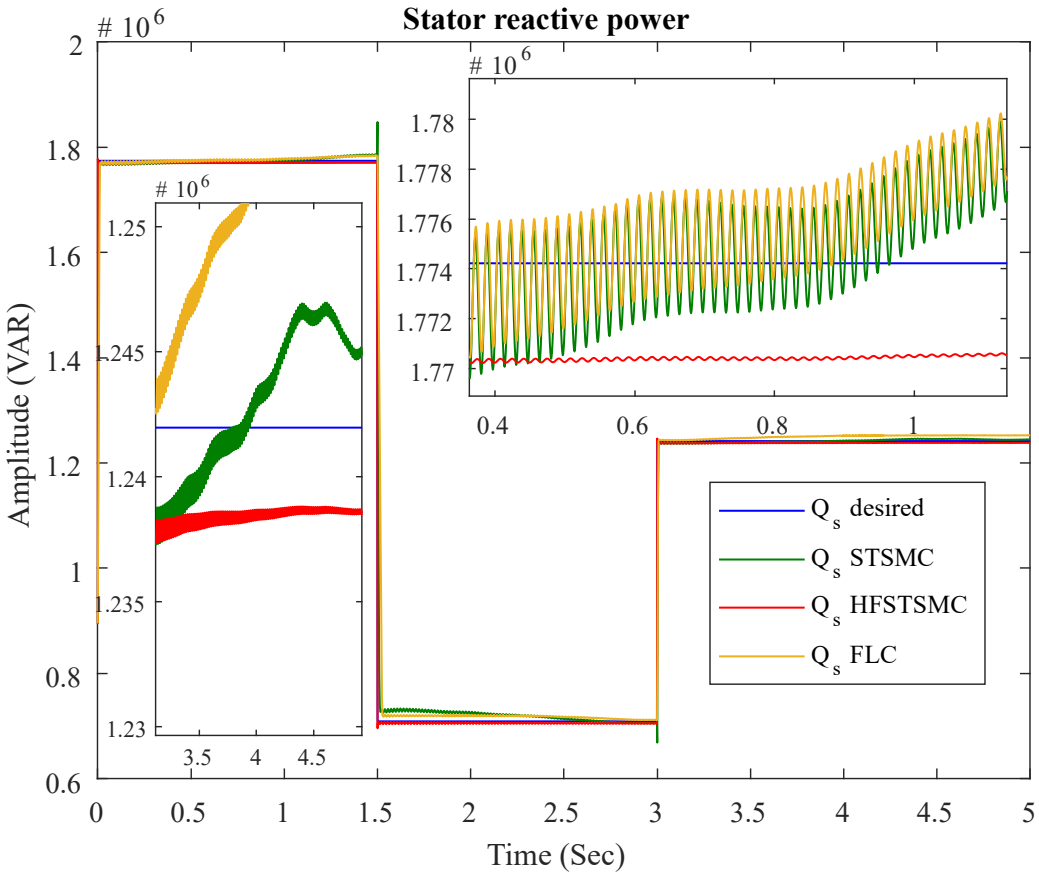

Fig. IV.15 Behavior of stator reactive power with a 100% variation in R_r, 60% in L_r, and 10% in L_m.

The reference tracking capability is tested through Figure IV.12 and Figure IV.13:

- Figure IV.12 shows that the FLC achieves system stabilization but with a slight error compared to the reference. The system controlled by FLC exhibits small oscillations, indicating that while the FLC is effective, it lacks the precision of STSMC and HFSTSMC.
- Figure IV.13 similarly highlights that both FLC and STSMC stabilize the system, but with some residual oscillations. The HFSTSMC outperforms both by providing an exceptional level of precision and stability, with no observable oscillations, making it the most accurate in tracking the desired reference signal.

In summary, for reference tracking, the FLC offers better performance than STSMC in terms of overall stability, but HFSTSMC eliminates oscillations completely and offers the most precise tracking of the reference signal.

To assess robustness, significant variations were introduced in system parameters ($R_r, L_r, and\ L_m$) and the corresponding system response was analyzed, as illustrated in Figure IV.14 and Figure IV.15:

- Figure IV.14 shows the rotor current response under parameter variations. While both FLC and STSMC demonstrate robustness, the STSMC has a small overshoot (response time of 0.01 seconds), whereas FLC exhibits a slower response (0.02 seconds). The HFSTSMC, however, shows an exceptional response time of 0.00005 seconds, with no overshoot, demonstrating superior robustness compared to both classical FLC and STSMC.

- Figure IV.15 confirms the robustness results, where STSMC is more precise than FLC but suffers from notable oscillations. The HFSTSMC not only eliminates these oscillations but also provides a more stable and precise response under these challenging conditions.

The Table. IV.2. summarizes the comparative performance of the different control strategies applied to the system. The evaluation is based on key dynamic performance indicators, including response time, overshoot, steady-state error, and robustness, to highlight the effectiveness of each control method.

Tab. IV.2 Comparative Performance Analysis of SMC, STSMC, FLC, and HFSTSMC Control Strategies.

Control Method	Response Time (s)	Overshoot (%)	Steady-State Error (W)	Robust
SMC	0.0037	0.005%	1000 (0.00056%)	Medium
STSMC	0.09	0.01%	400 (0.00024%)	High
FLC	0.0080	0.0085%	2000 (0.0011%)	Low
HFSTSMC	0.000052	0.0025%	280 (0.00015%)	Very High

From these results, the following conclusions can be drawn:

- FLC provides better stabilization than STSMC when tracking the reference signal, but both methods exhibit some level of oscillation and minor inaccuracies.
- STSMC proves to be more robust than FLC under significant parameter variations, but it suffers from slight overshoot and residual oscillations.
- The Hybrid Fuzzy-Super Twisting Sliding Mode Control (HFSTSMC) clearly outperforms both FLC and STSMC by combining their strengths—offering superior precision, faster response times, and excellent robustness without oscillations. This makes HFSTSMC the best approach for both reference tracking and robustness in the system.

IV.4. Artificial Neural Network

IV.4.1. Overview of ANN

Artificial Neural Networks (ANNs) are computational models inspired by the biological neural networks found in the human brain. They are designed to recognize patterns, learn from data, and make intelligent decisions or predictions based on learned experiences [108], [109]. ANNs have become a cornerstone in machine learning and artificial intelligence due to their ability to model complex relationships in data, making them highly suitable for applications involving nonlinear systems, such as wind turbine control [110].
The key features of ANNs:

- Structure: ANNs are composed of layers of interconnected nodes, called neurons (as presented in Figure IV.16). The typical structure includes
  - Input Layer: Receives input signals (features or data).
  - Hidden Layer: Processes inputs using weights and activation functions to learn relationships within the data. The number of hidden layers and neurons in each layer can vary depending on the complexity of the problem.
  - Output Layer: Produces the final prediction or control signal based on the processing performed in the hidden layers.
- Learning process: ANNs learn through a process called training, where the network adjusts the weights of the connections between neurons to minimize the difference

between the predicted output and the actual output (error). This process typically involves a backpropagation algorithm, which computes the gradient of the error and adjusts the weights iteratively using an optimization algorithm like gradient descent.

- Activation functions: Neurons apply activation functions to introduce nonlinearity, allowing the network to model complex relationships. Common activation functions include sigmoid, ReLU (Rectified Linear Unit), and tanh. These functions determine the output of each neuron based on its inputs.
- Training and generalization: The goal of ANN training is to minimize error while ensuring that the network can generalize to new, unseen data. Techniques such as cross-validation and regularization are used to prevent overfitting (where the network learns the training data too well but performs poorly on new data).

In the context of wind turbine control, ANNs can be employed to model the nonlinear behavior of the turbine and generate control signals for key variables, such as rotor speed, power output, and mechanical stresses. The adaptability and learning capabilities of ANNs make them well-suited for dynamic environments, where wind speed and operational conditions are constantly changing [23], [111].

Using an ANN-based controller allows the system to learn from past performance data and improve its control strategy over time. This approach is particularly effective when combined with optimization techniques or other advanced control strategies (such as sliding mode control or fuzzy logic), enabling more accurate and efficient control under varying conditions.

In the next sections, we will explore the methodology for applying ANNs to wind turbine control, including network design, training, and implementation, followed by simulation results that demonstrate the effectiveness of this approach.

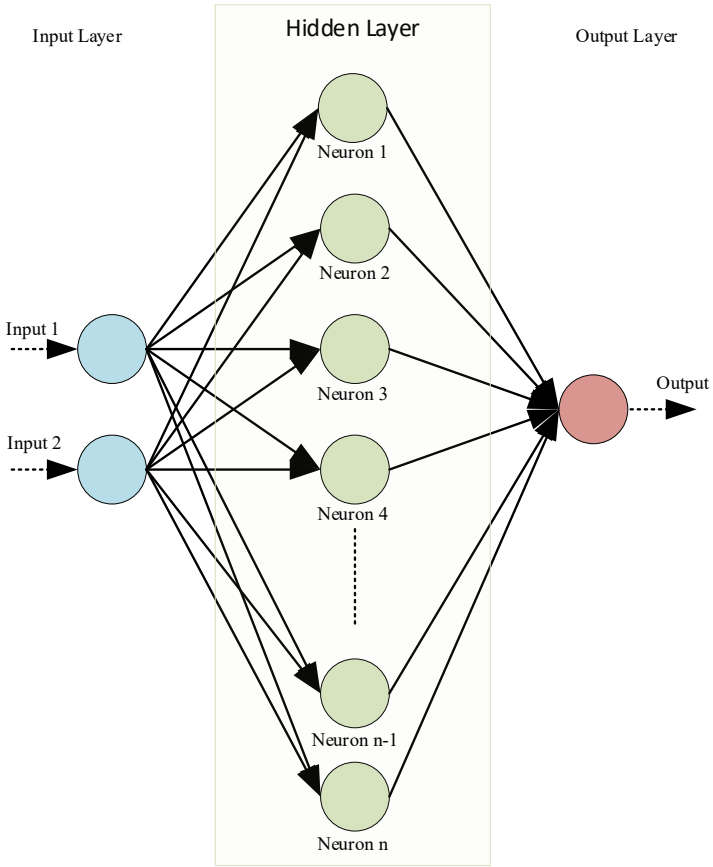

Fig. IV.16 ANN architecture featuring two inputs and a single output.

IV.4.2. Methodology

The implementation of an Artificial Neural Network (ANN) for wind turbine control is aimed at improving system performance by dynamically adjusting control parameters. This section outlines the methodology used to design and implement an ANN-based controller, which utilizes feedback from the control strategy's performance to learn and optimize control actions. The ANN controller is trained to manage the complex, nonlinear relationships in the wind turbine system, with a focus on minimizing the error between desired and actual system outputs.

- System modeling and data preparation: The first step in applying ANN to wind turbine control involves generating and preparing the necessary data. The system model is based on the wind turbine dynamics presented in Chapter II. Data is collected from simulations where the wind turbine is operated under varying wind speeds and power demand scenarios. Key variable, which is rotor currents is captured during the simulation to provide inputs for training the ANN.
- Input data: The ANN uses a dual-input approach, where the two inputs are the error signal (The difference between the desired control point (setpoint) and the actual system output), and desired control point (The target reference value for the system). This dual-input approach allows the ANN to learn how to adjust control signals based on both the current error and the control goal, ensuring that it adapts effectively to varying operating conditions.
- Neural network architecture design: The ANN used for wind turbine control is designed with the following architecture
    - Hidden layer: A single hidden layer with 100 neurons is employed to model the nonlinearities of the system. The number of neurons in the hidden layer is chosen to balance computational efficiency and the ability to capture complex dynamics.
    - Activation function: The hidden layer uses the “tansig” (hyperbolic tangent sigmoid) activation function, which is particularly effective for systems with nonlinear dynamics. This function maps input values into a range of [-1, 1], providing smooth control signal adjustments.
    - Output Layer: The output layer consists of a single neuron that provides the control adjustment based on the ANN’s learned interpretation of the system’s behavior.
- Training process: The training process involves using historical control data to train the ANN to learn from the control strategy's performance. The Levenberg-Marquardt training algorithm is used due to its effectiveness in optimizing neural networks for complex systems. The training process includes the following steps:
    - Training data: Historical data consisting of control inputs (error signal and desired control point) and the corresponding control outputs is used to train the ANN. This data enables the network to learn the appropriate control adjustments for a wide range of operating conditions.
    - Loss function: The Mean Squared Error (MSE) is used as the loss function, guiding the ANN to minimize the variance between its predicted control adjustments and the empirically derived optimal adjustments.
    - Training parameters: The network is trained with a learning rate of 0.06 and momentum of 0.075 to ensure stable and efficient learning. Training continues

until either the MSE goal of 10^{-16} is reached or a maximum of 10000 iterations is completed.

- Validation and testing: To ensure the ANN generalizes well to new operating conditions, the data is split into training, validation, and testing sets. The validation set is used to monitor the training process and prevent overfitting. During training, the performance of the network is evaluated on this unseen data, and the training process is stopped if performance begins to degrade on the validation set. After training, the ANN is tested on a separate test set to assess its real-world performance. This test set simulates new wind conditions and control challenges to validate the network's ability to optimize the wind turbine's operation.
- Implementation and control: Once the ANN is trained, it is integrated into the wind turbine control system. The ANN continuously receives the error signal and desired control point as inputs and generates a control signal that adjusts rotor current and stator power. This real-time control ensures that the system responds efficiently to varying wind speeds and power demands, providing adaptive and intelligent control.

The results of this methodology are presented and compared with conventional control strategies in the following section.

IV.4.3. Simulation results

In this section, we present the simulation results comparing the performance of the Artificial Neural Network (ANN) controller with the classical Proportional-Integral (PI) controller designed using the Direct Synthesis Approach (DSA), which was presented in the previous chapter. The goal of this comparison is to highlight the enhancements provided by the ANN controller, particularly in terms of stability, precision, and response characteristics.
The simulation tests are conducted under varying wind speed conditions, using the same system model and conditions as in Chapter II. The figures presented below illustrate the behavior of key control parameters such as rotor current (d-axis and q-axis) and stator power dynamics, providing insights into the performance differences between the ANN and PI-DSA controllers.

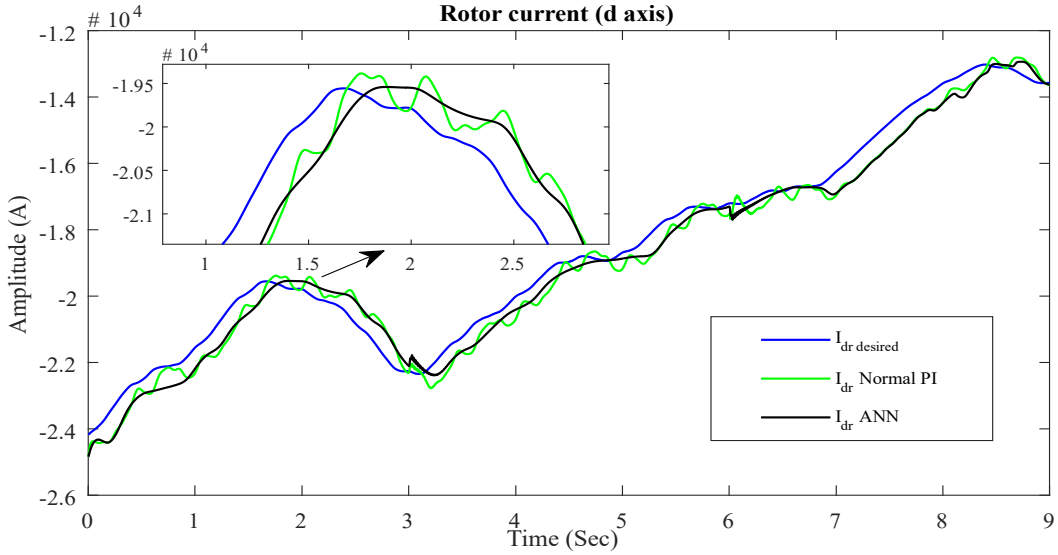

Fig. IV.17 Rotor current (d-axis) response.

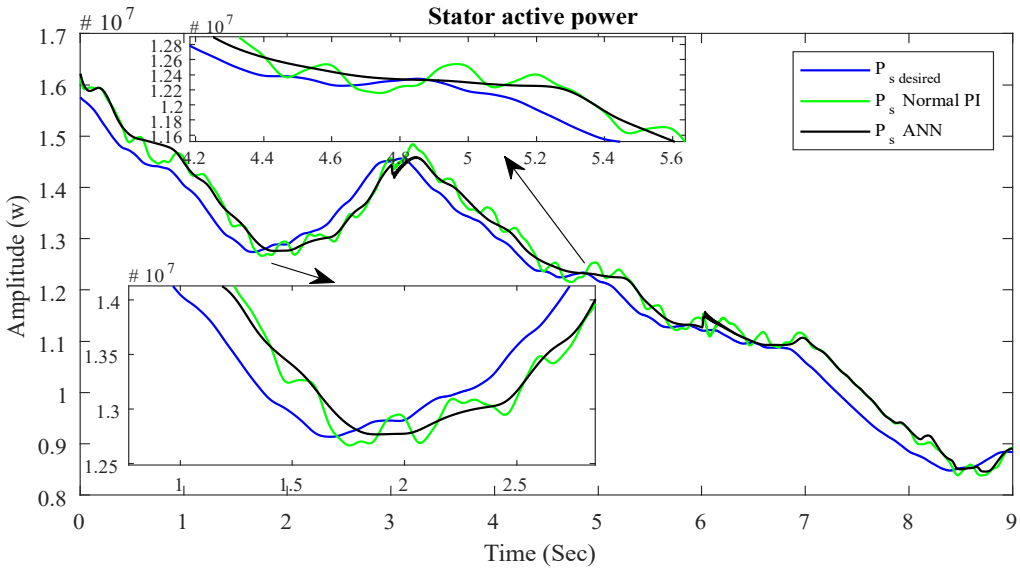

Fig. IV.18 Stator active power dynamics.

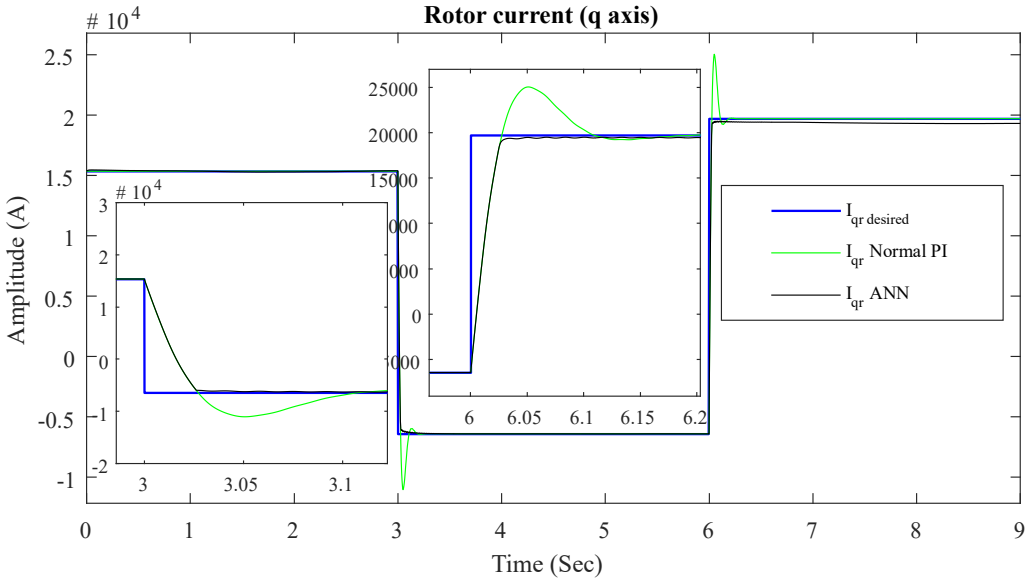

Fig. IV.19 Rotor current (q-axis) response.

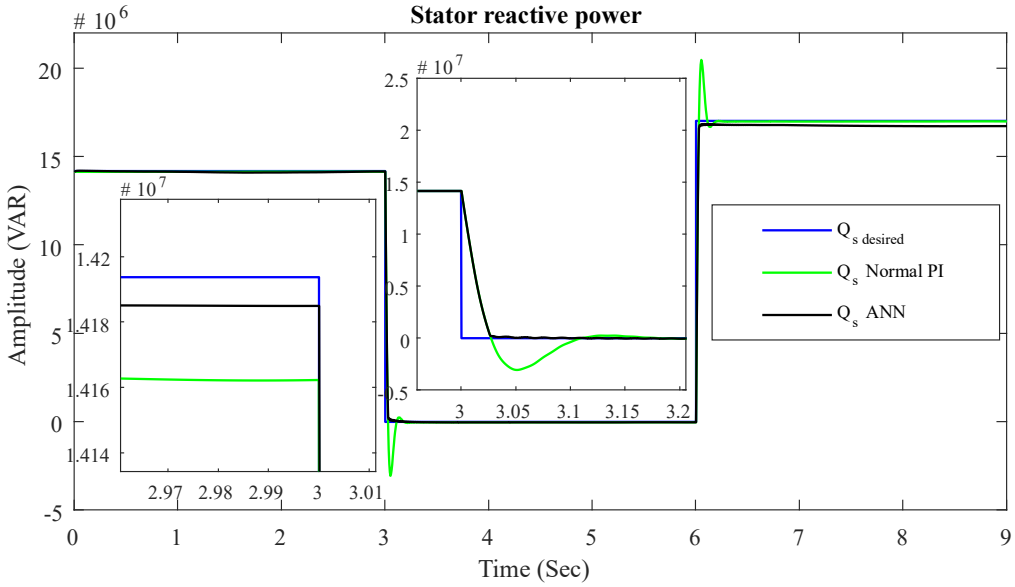

Fig. IV.20 Stator reactive power dynamics.

Figure IV.17 shows the rotor current response on the d-axis. From this figure, we observe that the ANN controller significantly improves the system's stability compared to the PI-DSA controller. The ANN controller eliminates the irregularities present in the PI-DSA response, providing a smoother and more stable current response.

Figure IV.18 presents the stator active power dynamics. Similar to the rotor current response, the ANN controller demonstrates improved stability and eliminates the fluctuations seen in the PI-DSA control. The ANN offers a more consistent and reliable power output, which is critical for maintaining efficient wind turbine operation.

Figure IV.19 illustrates the rotor current response on the q-axis. In this figure, we observe that the ANN and PI-DSA controllers have similar response times, but the ANN controller eliminates the overshoot present in the PI-DSA response. This enhancement is crucial as it reduces stress on the system and improves the overall control precision.

Figure IV.20 shows the stator reactive power dynamics. The results confirm that the ANN controller not only removes the overshoot seen in the PI-DSA controller but also offers a more precise control with less error. This improvement in precision leads to more efficient energy management and system performance under dynamic wind conditions.

The simulation results clearly demonstrate that the ANN controller provides several key enhancements over the classical PI-DSA controller. Specifically, the ANN controller:

- Fixes the irregularities in the PI-DSA response, resulting in smoother and more stable control of rotor current and stator power.
- Eliminates overshoot, which is particularly evident in the rotor current and stator reactive power responses, ensuring a more refined and precise control.
- Enhances precision, reducing the overall error in the system’s response, which leads to improved control accuracy and stability.

The Table. IV.3. presents a comparative evaluation of the PI and ANN controllers. The comparison is based on key time-domain performance indicators, including settling time, rise time, steady-state error, and overshoot, to assess the improvement achieved by the ANN-based control approach.

Tab. IV.3 Performance Comparison Between PI and ANN Controllers.

Control Method	Setling Time (s)	Rise Time (s)	Steady-State Error (W)	Overshoot (%)
PI	0.09	0.023	650 (0.0008%)	8.125%
ANN	0.025	0.023	450 (0.00035%)	0.0625%

Overall, the ANN controller effectively enhances the performance of the PI-DSA controller, providing more stable and precise control under varying wind conditions. These improvements make the ANN controller a superior choice for wind turbine control, especially in environments where dynamic and unpredictable changes in wind speed can challenge traditional control methods.

IV.5. Conclusion

In this chapter, we examined various intelligent control strategies applied to wind turbine systems, focusing on enhancing performance, stability, precision, and robustness in the face of nonlinearities and uncertainties associated with fluctuating wind conditions. The methodologies explored include Sliding Mode Control (SMC), Super Twisting Sliding Mode Control (STSMC), Fuzzy Logic Control (FLC), Artificial Neural Networks (ANN), and a hybrid approach combining FLC with STSMC (HFSTSMC).

Sliding Mode Control (SMC) demonstrated its effectiveness in handling system uncertainties, but it exhibited a significant drawback in the form of chattering, which can negatively impact mechanical components. The Super Twisting Sliding Mode Control (STSMC) was introduced as an enhancement to SMC, successfully mitigating the chattering effect and providing smoother control actions while maintaining robustness. However, STSMC still exhibited slight delays compared to the classical SMC, especially in terms of initial response times.

Fuzzy Logic Control (FLC) offered a more adaptable approach, as it can handle nonlinearities without requiring a precise mathematical model. By mimicking human reasoning through the use of fuzzy rules and membership functions, FLC provided smoother control actions. Nevertheless, FLC alone lacked the robustness needed to deal with highly dynamic and unpredictable wind conditions. In this study, the use of data-driven techniques helped to eliminate the need for expert knowledge in defining membership functions and fuzzy rules, making the FLC more accurate and reducing subjectivity in the control process.

The hybrid approach combining FLC with STSMC (HFSTSMC) presented significant improvements in control performance. By leveraging the strengths of both FLC and STSMC, the hybrid method provided exceptional precision and stability while further reducing chattering, achieving smoother control actions and faster convergence compared to either control method alone.

Artificial Neural Networks (ANNs) introduced a data-driven approach to control, allowing the system to learn from past performance and optimize control signals in real-time. The ANN improved stability and precision by minimizing overshoot and irregularities in the system's response. Through learning from historical data, the ANN adjusted control parameters effectively under varying wind conditions, providing a more adaptable control strategy.

In conclusion, the results of this chapter illustrate that each control strategy offers distinct advantages, depending on the specific requirements of stability, robustness, and precision. By comparing these methods, it is evident that combining advanced techniques, such as hybrid approaches, can provide enhanced system performance under dynamic and uncertain conditions. These intelligent control strategies are critical for optimizing wind turbine systems and ensuring efficient operation in complex, real-world environments.

Chapter V
Wind farm power management

V.1. Introduction

As the role of renewable energy sources continues to grow globally, wind power has emerged as a crucial contributor to electricity generation. A wind farm is a collection of wind turbines that work together to convert the kinetic energy of wind into electricity. The turbines are strategically placed to capture optimal wind conditions. The power generated by each turbine is combined and supplied to the electrical grid, contributing to a sustainable energy supply. However, managing the power generated by wind farms presents significant challenges, particularly in terms of maintaining a stable and reliable supply to the electrical grid. Wind speeds are inherently variable and unpredictable, leading to fluctuations in the amount of power produced by turbines. This variability makes power management in wind farms a critical factor in ensuring that the electricity grid receives a consistent supply of power to meet demand [112], [113].

Wind farm power management refers to the strategies and techniques used to control and optimize the power output from a group of wind turbines, ensuring that the generated electricity matches the demand of the grid. Given that wind speed is not constant, the output from wind turbines can fluctuate significantly over time, which poses a challenge for grid stability. Effective power management involves dynamically adjusting the operation of individual turbines to account for these fluctuations and maintain the desired power output at the grid connection point [114], [115].

In addition to managing the variability of wind speeds, power management also focuses on maximizing the efficiency of wind turbines and minimizing energy losses. This requires balancing the power generated by each turbine to avoid overproduction or underproduction, both of which can lead to inefficiencies or grid imbalances. In cases of excess wind energy, power may need to be curtailed, while in situations of low wind, turbines must be operated in a way that optimally captures available energy [116], [117].

One of the primary challenges in wind farm power management is the unpredictability of wind speeds. Since wind energy is dependent on natural weather patterns, it can be difficult to forecast and match the power generated by turbines with grid demand in real-time. This variability introduces complexity into the operation of wind farms, requiring sophisticated control algorithms and strategies to ensure that turbines deliver the right amount of power to the grid without destabilizing it.

Another key challenge is balancing the power output between different turbines within the wind farm. Each turbine may experience different wind speeds depending on its location, creating an imbalance in production that needs to be managed. Additionally, the mechanical and operational constraints of turbines, such as maximum power capacity and the need to protect turbines from overspeed or mechanical stress, further complicate power management [118], [119].

Grid requirements add another layer of complexity, as wind farms must adhere to grid codes and regulations that dictate how much power can be supplied and how quickly turbines should respond to changes in demand. Overproduction, for example, can lead to excess energy that the grid cannot absorb, while underproduction can cause supply shortages and destabilize the grid [120], [121].

In summary, the need for precise and efficient power management in wind farms is driven by the variability of wind, the need for balanced turbine operation, and the requirements of the electrical grid. The rest of this chapter will delve into a novel algorithm designed to address these challenges, ensuring optimal wind farm performance and grid stability through intelligent power management. This novel approach will also be compared with the classical PI controller method, highlighting the improvements in dynamic power distribution, efficiency, and the ability to handle fluctuating wind conditions. Through this comparison, we will demonstrate how the novel algorithm outperforms the traditional PI method in managing power across multiple turbines and stabilizing the grid, particularly under variable and unpredictable wind speeds.

V.2. Overview of the Novel Wind Farm Power Management Algorithm

The algorithm presented in this chapter offers an innovative solution for optimizing power output across a wind farm by dynamically managing the contribution of each turbine based on real-time wind conditions. The core idea is to distribute the power generation duties among turbines in a way that compensates for the variability in wind speeds, ensuring the grid receives a stable and reliable power supply. The algorithm begins by calculating a target stator power output for each turbine, based on the total power required by the grid. It then compares the actual power each turbine can generate with this target and adjusts their output accordingly.

Turbines that are unable to meet their target operate at full capacity, while those with surplus capacity contribute to covering the shortfall of underperforming turbines. This redistribution is proportional, meaning that turbines with more excess capacity provide a larger share of the required compensation. The algorithm adapts dynamically to real-time conditions, ensuring that the collective power output from the wind farm aligns with the grid's demands. This approach not only maximizes efficiency but also ensures that fluctuations in wind speed and turbine performance do not compromise grid stability, making it an effective tool for modern wind farm power management.
Figure V.1 illustrates the structure and flow of this wind farm power management system, where turbines communicate with the grid to ensure a stable power output, adapting to wind speed variability.

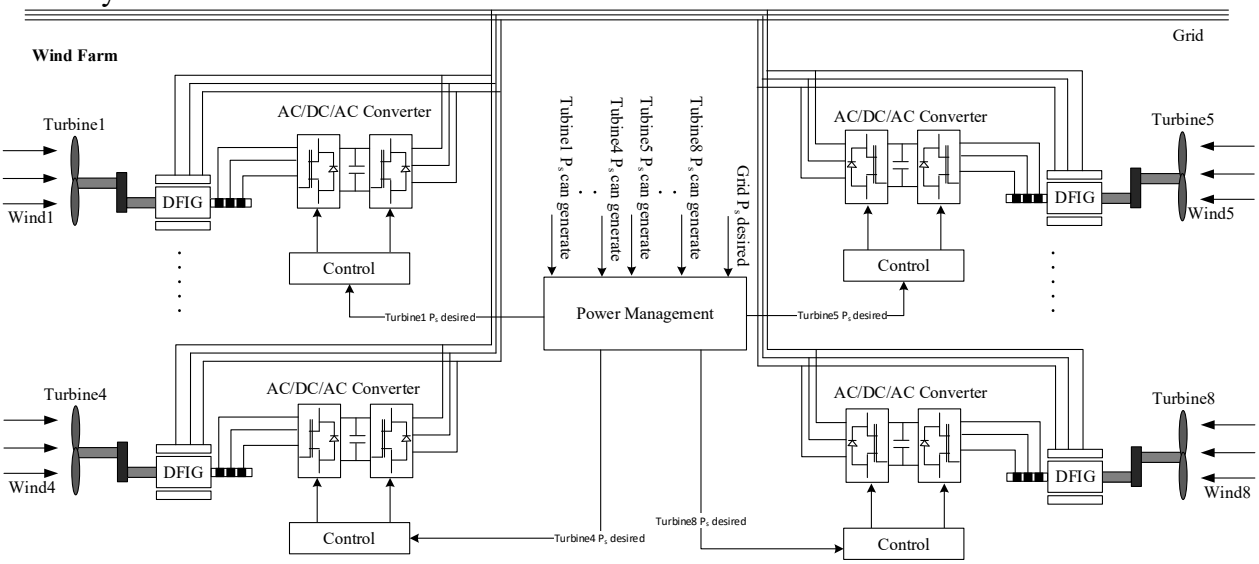

Fig. V.1 Wind farm system with power management.

V.3. Methodology

The following section outlines the methodology used to implement the proposed wind farm power management algorithm. It details the step-by-step process of collecting turbine power data, calculating target outputs, and dynamically redistributing power across turbines to ensure the grid's demands are met.

- Input collection: The algorithm starts by collecting essential real-time inputs from the wind farm system:
  - $P_{s,cangen}$: This is the power that each turbine can potentially generate based on current wind conditions. Each turbine has a unique maximum power output depending on the wind speed.
  - $P_{s,ref}$: The total stator power required by the grid. This is the overall power demand that the wind farm needs to supply.
  - n: The number of turbines in the wind farm.
- Calculate the target power output per turbine: The next step is to calculate the desired power output for each turbine by dividing the total grid-required power by the number of turbines:

$$P_{s,target} = P_{s,ref}/n \quad \text{(V-1)}$$

This gives a uniform target for each turbine to meet the grid's demand equally.

- Calculate the power generation ratio (Rapport): For each turbine, the algorithm calculates the ratio (referred to $ratio_i$) of the power it can generate ($P_{s,cangen\,i}$) to the target power.

$$ratio_i = {P_{s,cangen\,i}}/{P_{s,target}} \quad \text{(V-2)}$$

This ratio shows whether a turbine can meet or exceed its share of the required power ($ratio_i \geq 1$) or if it is underperforming $ratio_i \leq 1$.

- Handel underperforming turbines: For turbines with $ratio_i < 1$, meaning they cannot meet their target power output due to lower wind speeds, the algorithm:
  - Sets these turbines to operate at their maximum capacity:

$$P_{s,i} = P_{s,cangen\,i} \quad \text{(V-3)}$$

  - Calculates the cumulative deficit Sum_{under}, which is the total shortfall in power output from all underperforming turbines. This is computed as:

$$Sum_{under} = \sum(1 - ratio\_i) \quad \text{(V-4)}$$

    This variable will be important later when redistributing surplus power from better-performing turbines.
- Handle surplus turbines: For turbines with $ratio_i \geq 1$, meaning they are capable of generating more than the target power. The algorithm calculates the surplus generation capacity for these turbines by computing:

$$Sum_{over} = \sum(ratio_i - 1) \quad \text{(V-5)}$$

This variable stores the total excess power generation capability across the wind farm, which will be used to balance the overall power supply.

- Redistribute surplus power: The turbines with surplus capacity will be asked to compensate for the shortfall from underperforming turbines. The redistribution formula is

$$P_{s,i} = P_{s,target}(1 + Sum_{under}.(ratio_i - 1)/Sum_{over}) \quad \text{(V-6)}$$

This formula adjusts the power output of turbines that have surplus capacity in proportion to their available surplus, ensuring that they contribute more to compensate for turbines generating less than their target.

- Check for turbine capacity limits: A condition is introduced to ensure no turbine generates more than its maximum capacity. After calculating the redistributed power for turbines with surplus capacity, the algorithm checks if the new power output exceeds the turbine's maximum capacity:

$$P_{s,i} = \begin{cases} P_{s,target}(1 + Sum_{under}.(ratio_i - 1)/Sum_{over}), & P_{s,i} \leq P_{s,cangen\,i} \\ P_{s,cangen\,i}, & P_{s,i} > P_{s,cangen\,i} \end{cases} \quad \text{(V-7)}$$

- Real-time adjustment: The algorithm runs continuously, adjusting the power outputs of the turbines in real time as wind conditions change. This ensures that the wind farm can dynamically respond to fluctuating wind speeds and continue supplying stable power to the grid.

The steps of the algorithm are summarized in the flowchart presented in Figure V.2, which provides a clear visual representation of the dynamic redistribution process for power management across turbines.

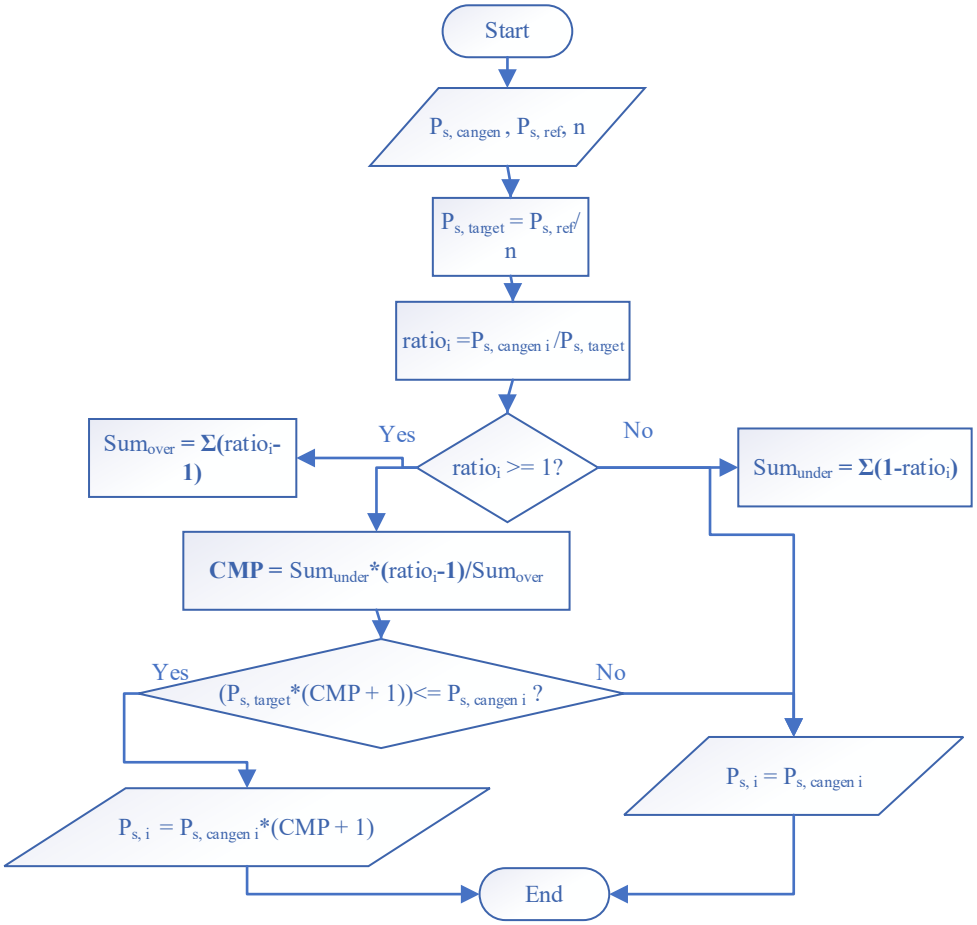

Fig. V.2 Flowchart of the novel wind farm power management algorithm.

Example:
Let's consider a wind farm with four turbines, each tasked with generating a total of 4 MW for the grid:

- Turbine 1 can generate 0.4 MW.
- Turbine 2 can generate 1.4 MW.
- Turbine 3 can generate 1.8 MW.
- Turbine 4 can generate 1 MW.

According to the algorithm: Turbine 1, unable to meet its target (1 MW), will generate its maximum power (0.4 MW), adding the difference to the Sum_{under}, Turbine 4 meets its target exactly (1 MW), Turbines 2 and 3, having surplus capacity, will adjust their power output to compensate for Turbine 1's shortfall. The surplus is distributed proportionally, with Turbine 3 providing a larger share due to its higher excess capacity.
This example demonstrates how the algorithm adapts to real-time conditions to ensure that the overall power generation matches the grid's demand, even when individual turbines underperform due to varying wind speeds.
By dynamically redistributing power based on real-time wind conditions, this algorithm optimizes the efficiency and reliability of wind farms, ensuring that the grid receives a stable and reliable power supply.

V.4. Simulation

In this section, we present the simulation setup for implementing the novel wind farm power management algorithm, developed in the previous sections. The simulation is designed using MATLAB/Simulink to accurately model the operational dynamics of an 8-turbine wind farm, with

each turbine modeled as per the detailed system analysis in Chapter II. The goal of the simulation is to demonstrate the methodology of the proposed algorithm, focusing on how it manages power distribution, adjusts turbine outputs in real-time, and maintains grid stability.
The simulation block diagrams reflect the core components of the power management strategy, including reference signal generation, dynamic redistribution of surplus power, and global power management. These models are integral to testing and validating the efficiency of the algorithm in handling fluctuating wind conditions across multiple turbines. The upcoming figures illustrate the detailed block models used in the simulation.
The Figure V.3 shows the modified model where the rotor current (d-axis) reference is generated by the power management algorithm, rather than being limited by each turbine's maximum generation, ensuring grid power demands are met dynamically.

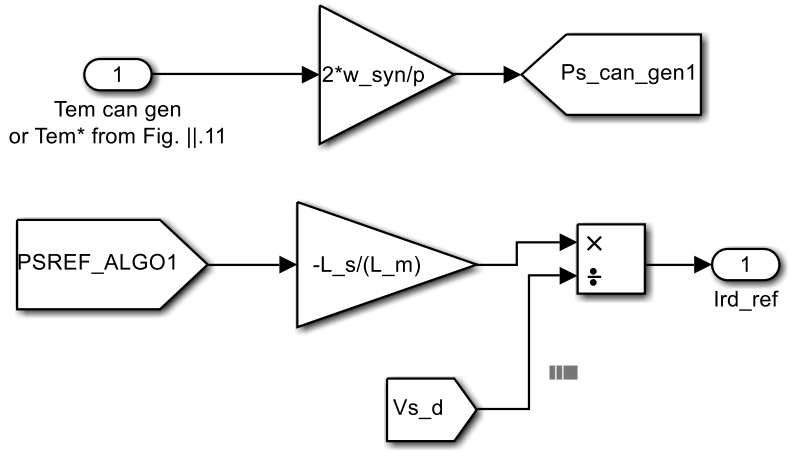

Fig. V.3 Model of the new reference signal generation i_{dr}^{*}.

The Figure V.4 demonstrates the process algorithm applied to a single turbine, adjusting its power output based on its capacity and the overall power management strategy.

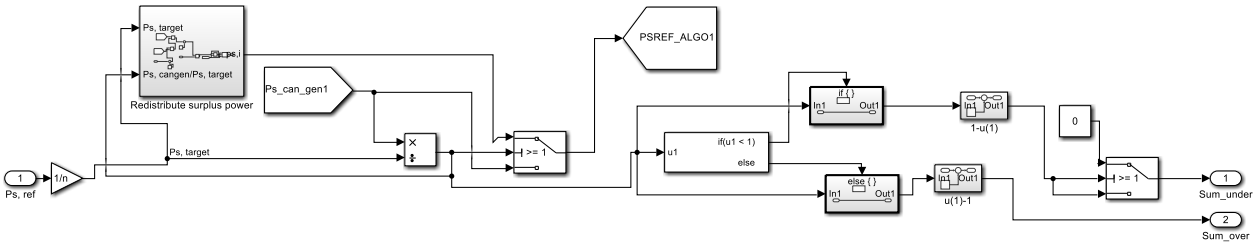

Fig. V.4 Simulink model of the process algorithm (For one turbine).

Additionally, Figure V.5 provides a schematic block representation of this process algorithm, highlighting the core steps in a simplified manner.

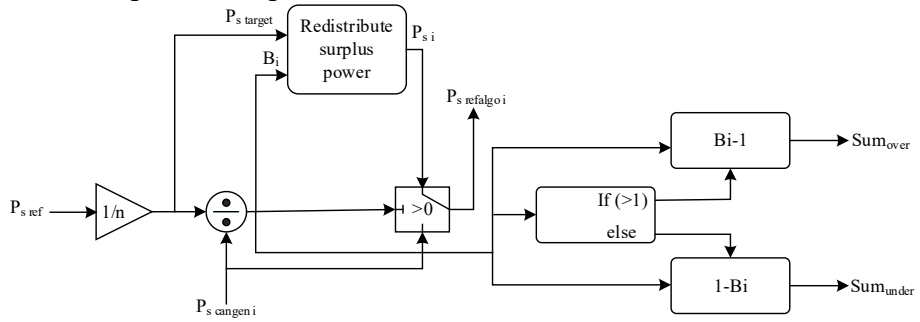

Fig. V.5 Bloc schema of the process algorithm (For one turbine).

The Figure V.6 illustrates how surplus power from overperforming turbines is redistributed to underperforming turbines, ensuring balanced power output across the wind farm.

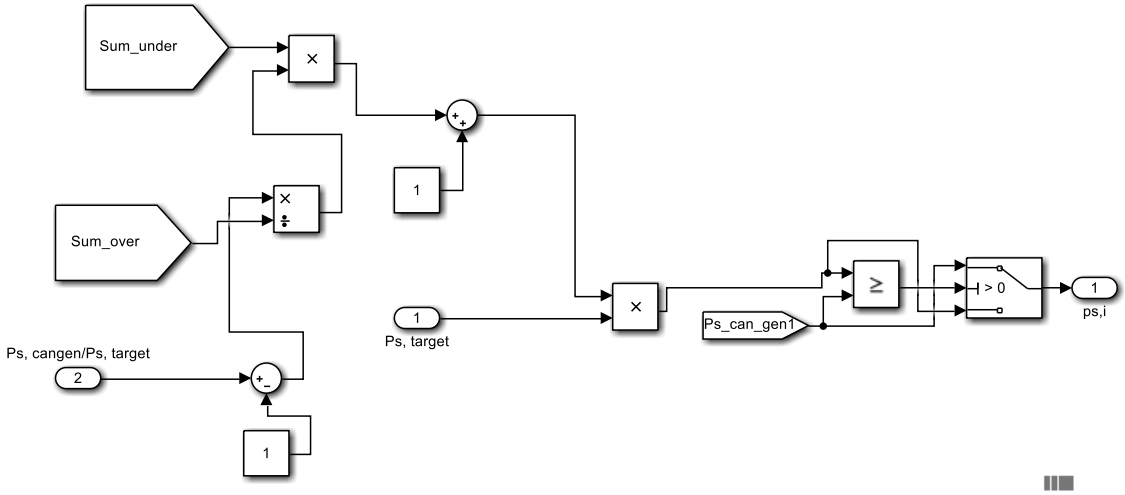

Fig. V.6 Simulink model of redistribute surplus power.

To further clarify the redistribution logic, Figure V.7 presents a schematic block diagram showing the process of power balancing across turbines.

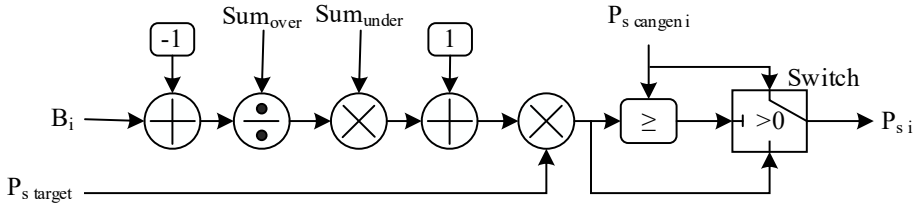

Fig. V.7 Bloc schema of redistribute surplus power.

The Figure V.8 shows the overall structure of the power management system, coordinating all turbines to dynamically meet the grid's power requirements while optimizing wind farm performance.

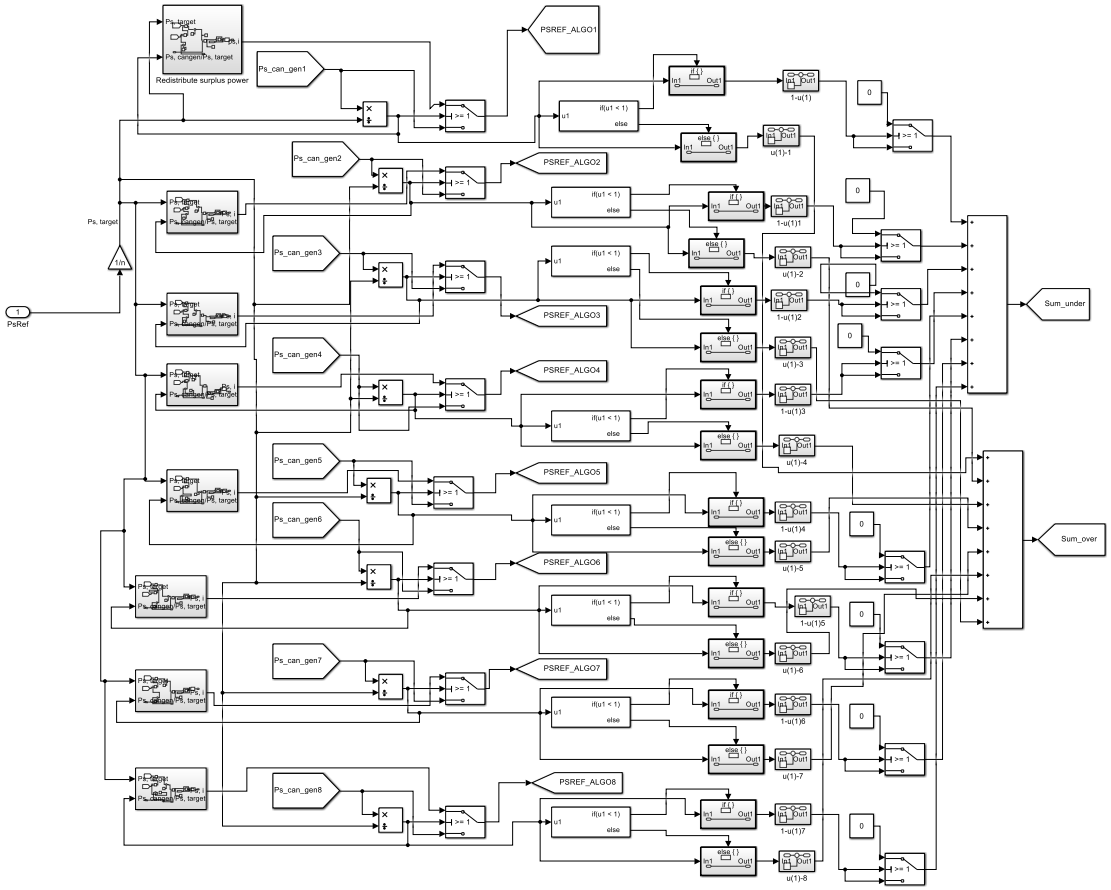

Fig. V.8 Simulink model of the global power management.

For a conceptual overview, Figure V.9 presents a schematic block diagram of the overall power management strategy.

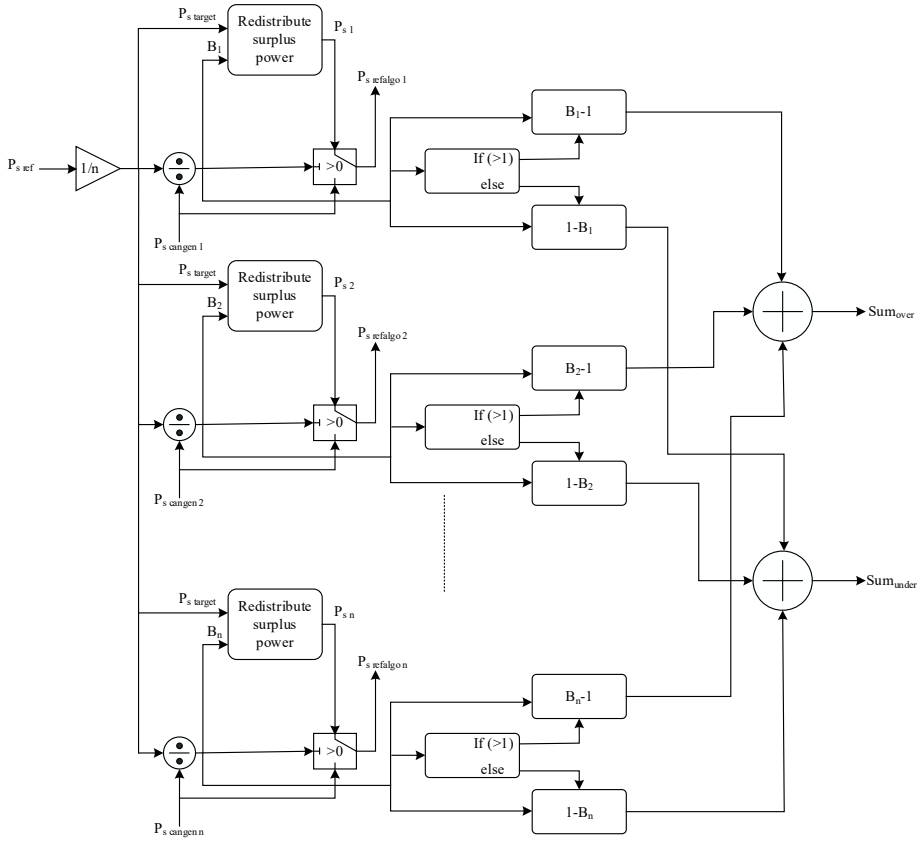

Fig. V.9 Bloc schema of the global power management.

In conclusion, the simulation section successfully demonstrates the implementation of the proposed wind farm power management algorithm using an eight-turbine system modeled in MATLAB/Simulink and block schema diagrams. Through the simulation models, we have illustrated how the novel algorithm dynamically adjusts the rotor current reference signals, redistributes surplus power, and manages the overall power output of the wind farm to maintain grid stability. The models provide a clear representation of the algorithm's real-time adaptability, ensuring efficient and reliable power generation across varying wind conditions.

With the simulation methodology established, we now turn to the results section, where the performance of the algorithm will be evaluated in comparison with traditional power management methods. This will highlight the effectiveness of the proposed approach in optimizing power distribution, enhancing grid stability, and maximizing turbine efficiency.

V.5. Simulation results

In this section, we present the simulation results obtained from the wind farm power management models discussed in the previous section. The simulation was conducted using an eight-turbine wind farm, with each turbine operating under different wind speed amplitudes to mimic real-world variability. The performance of the novel power management algorithm is compared against a classical PI controller, which attempts to minimize the error between the desired grid power and the actual total power output. In the classical PI approach, the output is divided equally among the turbines, setting the same power reference for each turbine. The desired grid power is set at 12MW.
The following figures illustrate the effectiveness of the proposed algorithm in dynamically adjusting turbine outputs based on real-time wind conditions, as well as its ability to balance power generation more efficiently than the classical PI controller. The results provide a comprehensive comparison in terms of grid stability, power redistribution, and overall system performance.

Figure V.10 presents the wind speed profiles applied to each of the eight turbines in the simulation. These profiles vary in amplitude to simulate real-world conditions, where each turbine experiences different wind speeds, affecting their power generation capabilities.

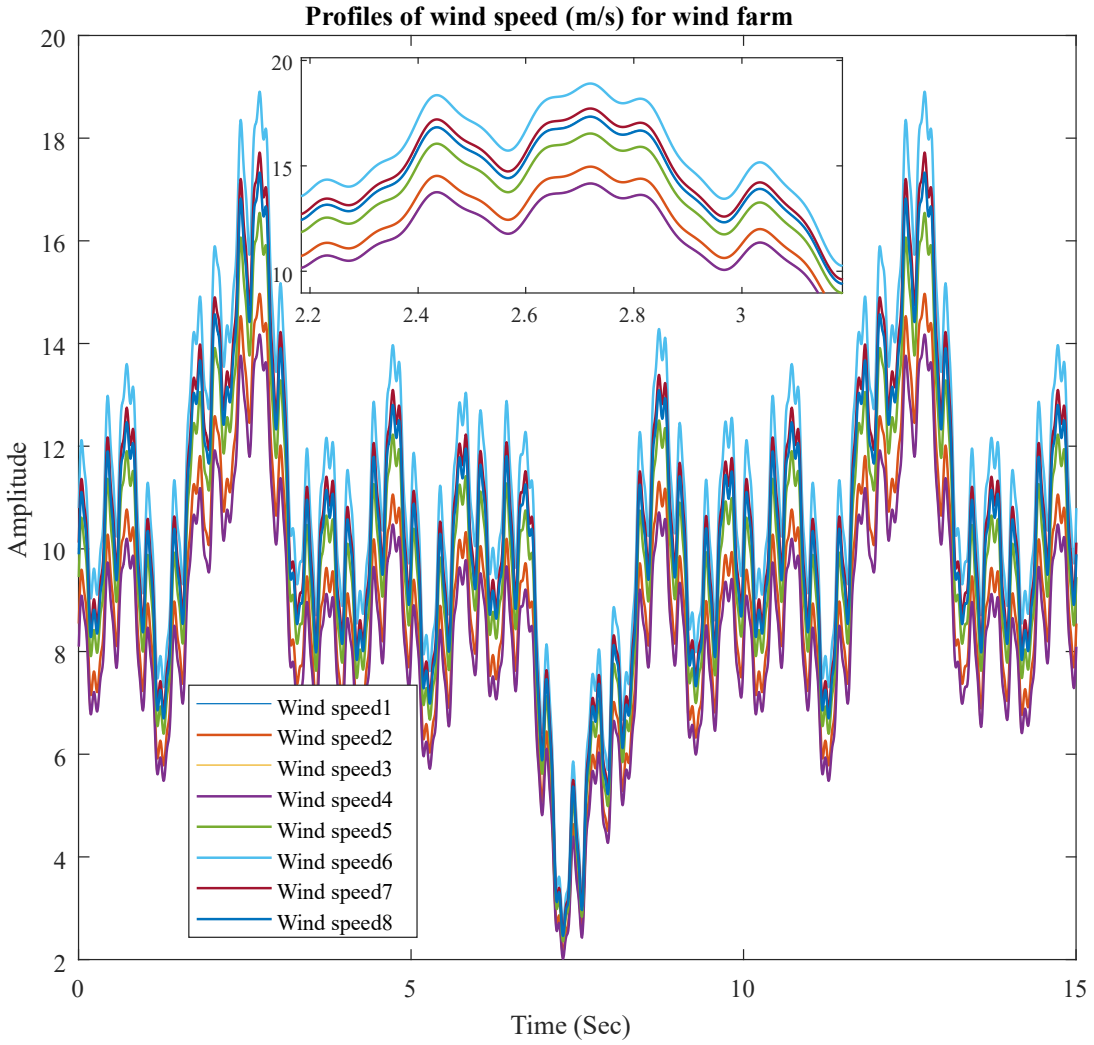

Fig. V.10 Wind speed profiles for each turbine in the simulation.

Figure V.11 presents the power distribution across the eight turbines, with each subplot representing one turbine's power behavior. The subplots show four key power variables for comparison:

- $P_s desired\ mean$ (desired power for each turbine "$P_{s,target}$").
- $P_{s,cangen}$ (the maximum power the turbine can generate).
- $P_s ref\ Algo$ (power reference from the novel algorithm "$P_{s,i}$").
- $P_s\ ref\ PI$ (power reference from the classical PI controller).

This figure illustrates how the novel algorithm manages power distribution across the turbines, especially when some turbines are underperforming, and highlights the differences between the novel approach and the traditional PI controller [120].

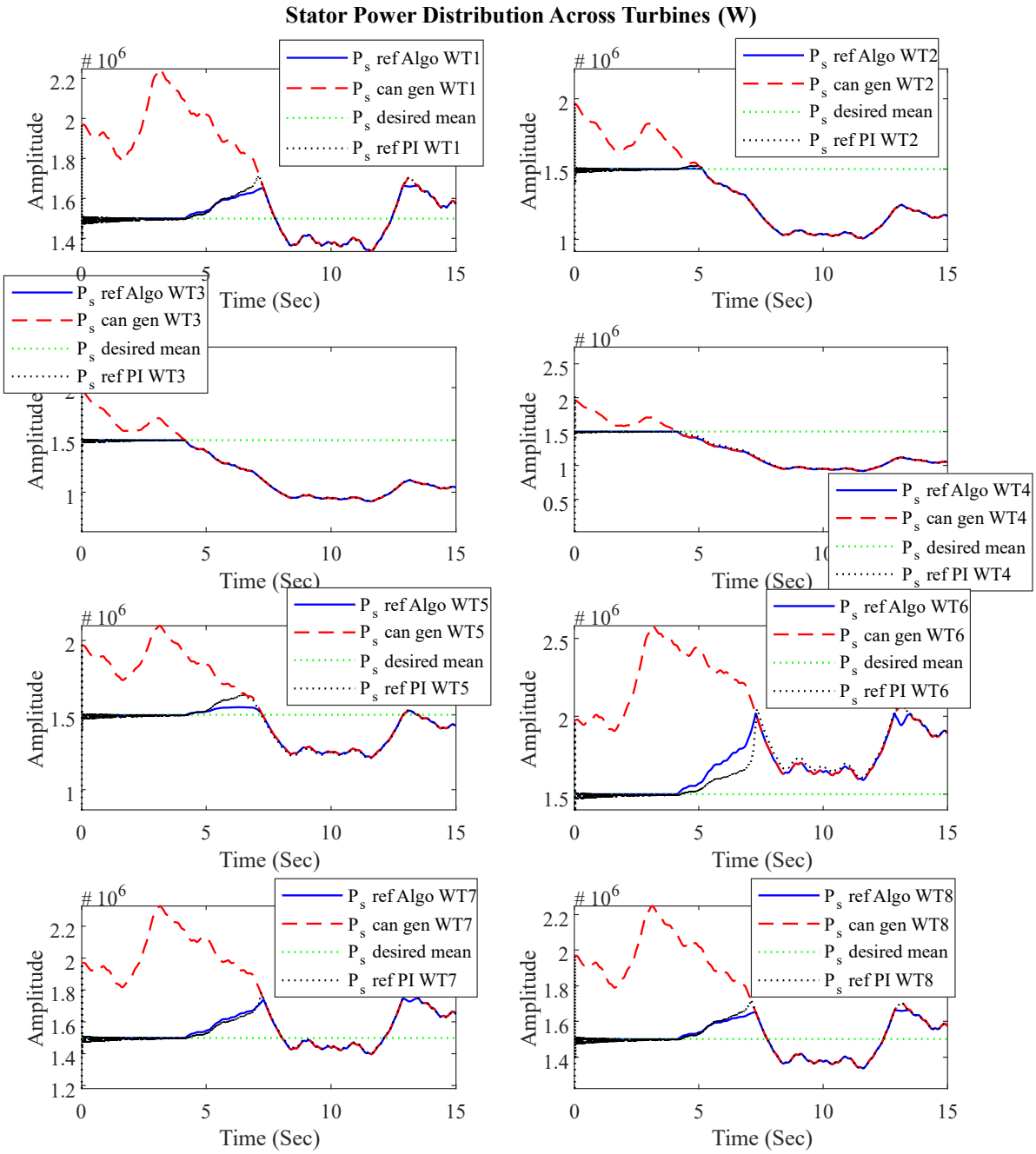

Fig. V.11 Power distribution comparison for each turbine using the novel algorithm and classical PI controller.

Figure V.12 presents the desired grid power of 12 MW alongside the total stator active power generated by the wind farm using the novel algorithm and the classical PI controller for comparison.

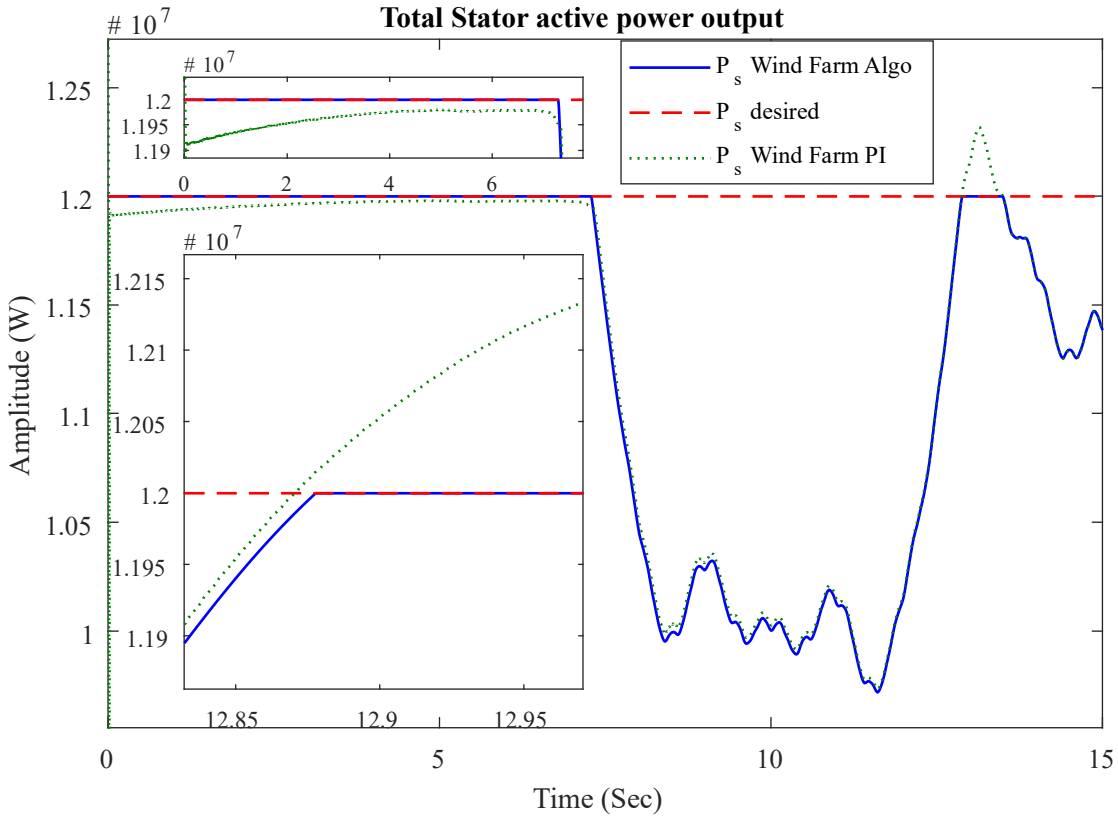

Fig. V.12 Total stator active power output of wind farm using the novel algorithm and PI controller.

The results presented in Figures V.11 and V.12 provide a comprehensive evaluation of the novel power management algorithm compared to the classical PI controller, highlighting its effectiveness, adaptability, and precision.

In Figure V.11, during the initial phase of the simulation, all turbines operate under favorable wind conditions, enabling an even power distribution of 1.5 MW per turbine (total 12 MW across 8 turbines). During this period, both the novel algorithm and the PI controller perform well, ensuring an equitable power allocation. However, the PI controller exhibits slight oscillations, indicating its inability to maintain perfectly steady control even under stable conditions.

As the simulation progresses, turbines 2, 3, and 4 experience reduced wind speeds, leading to underperformance. The novel algorithm dynamically adapts, redistributing power generation among the remaining turbines based on their available capacity, ensuring an optimal and realistic power distribution. In contrast, while the PI controller attempts compensation, it does so without considering individual turbine capacities, instead assigning identical power references to all turbines. Although the PI controller respects maximum turbine power limits, its uniform approach results in suboptimal performance compared to the novel algorithm.

At approximately 7.5 seconds, as depicted in Figure V.12, most turbines—except turbine 6—fail to reach their intended power levels due to widespread low wind speeds. The novel algorithm maximizes the output of all turbines based on their real-time capacity, ensuring the most effective use of available resources. Despite this, the total power output remains below 12 MW, reflecting the physical constraints imposed by insufficient wind speeds. In contrast, the PI controller exhibits significant steady-state errors and oscillations, reducing efficiency and stability. Furthermore, at 12.87 seconds, the PI controller overshoots, while the novel algorithm maintains a precise response with 0% overshoot, reinforcing its superior ability to dynamically adjust without instability.

Overall, the comparison highlights the advantages of the proposed algorithm in optimizing power distribution, respecting turbine operational limits, and maintaining stable grid power output under varying wind conditions. Although the PI controller provides compensation, its uniform

redistribution strategy and oscillatory behavior make it less effective for real-time wind farm power management. The novel algorithm's responsiveness, precision, and adaptability establish it as a more reliable and efficient solution for wind farm control.

To further assess the performance of the proposed algorithm, an additional scenario was simulated where Turbine 2 experiences a complete failure at 3.5 seconds. As shown in Figure V.13, at this precise moment, Turbine 2 stops generating power, which introduces a sudden loss in the total output. In response, the power management algorithm rapidly redistributes the power generation load among the remaining turbines. Each operational turbine compensates for the loss by increasing its output proportionally, ensuring that the grid's power demand remains met without causing instability in the system.

The overall impact of Turbine 2's failure on the wind farm's power generation is illustrated in Figure V.14. Initially, the remaining turbines successfully adjust their power output to offset the loss and maintain the target generation level. However, at approximately 8.55 seconds, the turbines reach their maximum operational capacity, at which point the wind farm is no longer able to sustain the 10 MW power target. This limitation reflects the physical constraints of the turbines and wind conditions, emphasizing the importance of redundancy in power generation.

Despite these constraints, the algorithm demonstrates its effectiveness in maximizing available resources, ensuring that each turbine contributes as much power as possible under the given circumstances. This capability highlights its adaptability in maintaining optimal performance even under unforeseen failures, making it a robust solution for real-world wind farm operations.

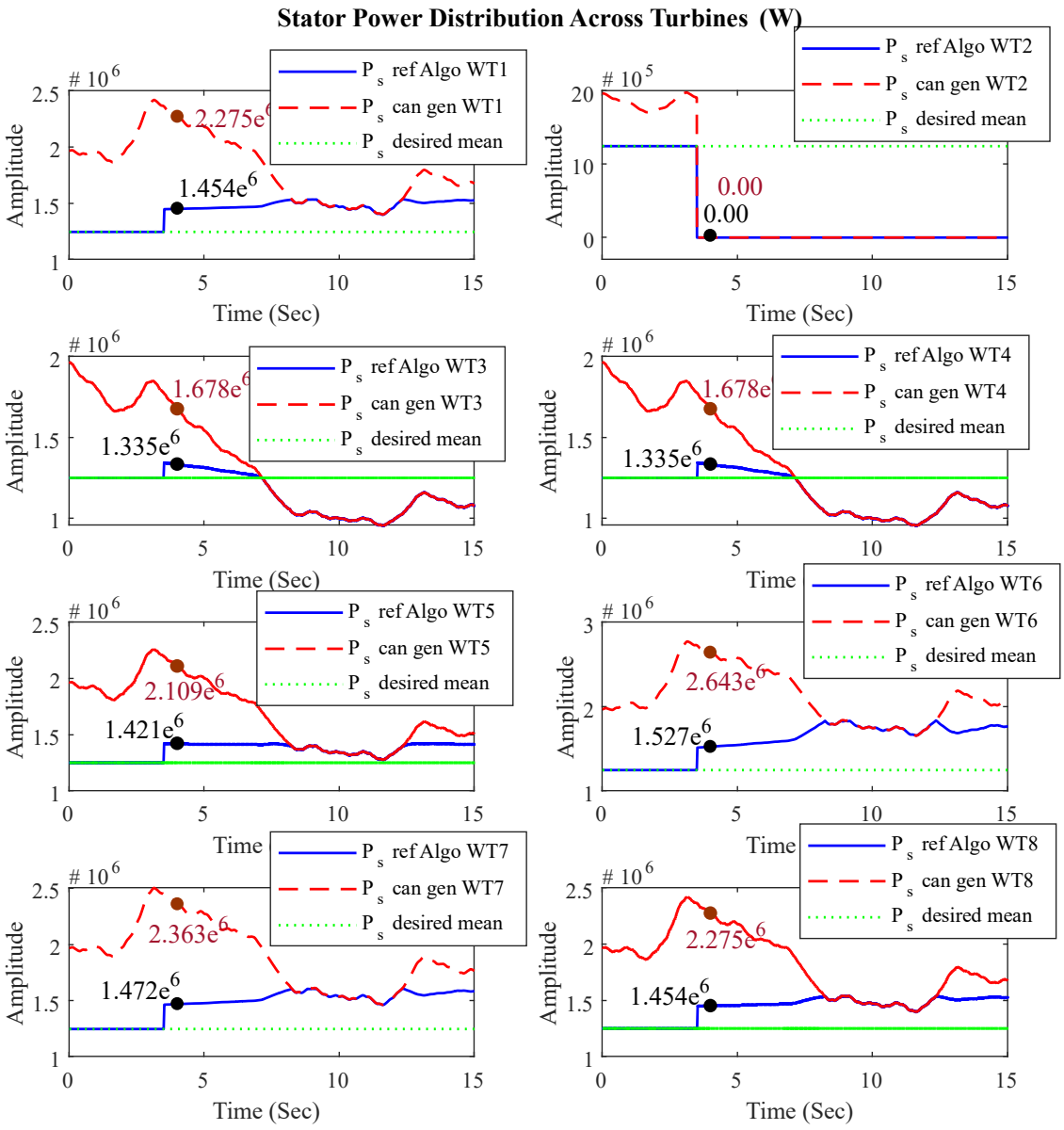

Fig. V.13 Power distribution for each turbine using the novel algorithm after Turbine 2 break-down.

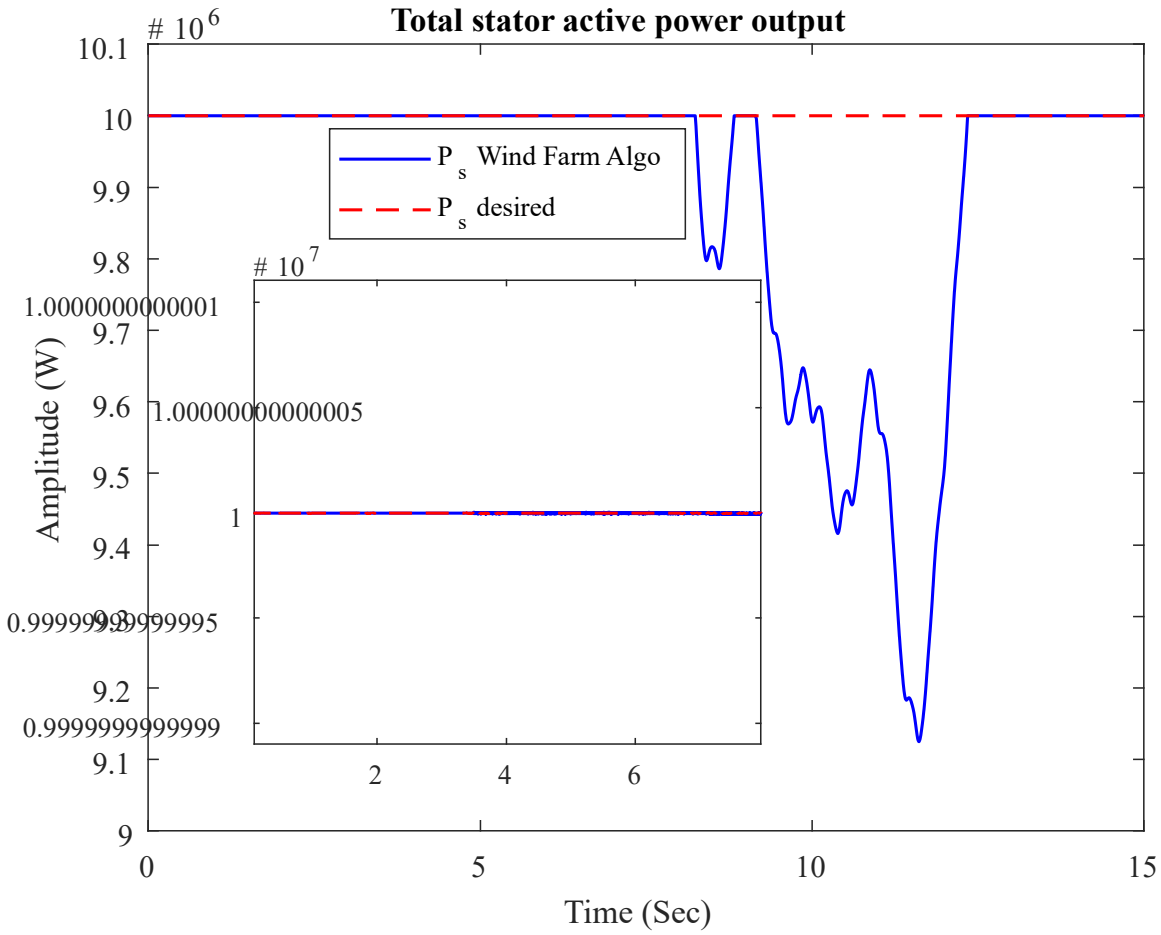

Fig. V.14 Total wind farm power following Turbine 2 break-down.

The simulation results confirm the superior performance of the novel power management algorithm in effectively distributing power, adapting to real-time wind variations, and handling turbine failures. Compared to the classical PI controller, the proposed algorithm exhibits greater responsiveness, enhanced stability, and more efficient resource allocation.

In the standard operating scenario, where turbines experience varying wind speeds, the algorithm dynamically adjusts power references based on each turbine's real-time capacity, ensuring an optimized power distribution. Unlike the PI controller, which assigns identical power references without considering individual turbine capabilities, the novel approach maximizes available output while preventing overloading or unrealistic power demands.

When subjected to turbine failure conditions, as shown in Figures V.13 and V.14, the algorithm swiftly redistributes power generation tasks, allowing the remaining turbines to compensate for the lost capacity. This real-time adaptability maintains grid stability until the system reaches its physical limits, demonstrating its robustness under unexpected failures. In contrast, the PI controller exhibits steady-state errors, oscillations, and overshoot, leading to instability and inefficiencies in power management.

Overall, the proposed algorithm proves to be a more practical and reliable solution for wind farm power management, ensuring grid stability, optimized power utilization, and seamless adaptation to changing wind conditions and turbine availability. These advantages establish it as a superior alternative to conventional PI-based control strategies for modern wind energy systems.

Application example of the proposed algorithm

To evaluate the performance of the developed wind farm power management algorithm, a case study is considered, corresponding to the scenario depicted in Figure V.13 at a specific moment

in time, at 4.0 seconds. The wind farm comprises eight turbines, with a required grid power output of $P_{sref} = 10MW$. The ideal power contribution per turbine is determined as follows:

$$P_{s\,target} = \frac{P_{sref}}{n} = \frac{10}{8} = 1.25MW$$

At this instant, the available power generation capacities of the individual turbines ($P_{s\,cangen}$) are represented by the brown key points in Figure V.13, with the following values:

- Turbine1: $P_{s\,cangen\,1} = 2.275MW$.
- Turbine2: $P_{s\,cangen\,2} = 0.00MW$.
- Turbine3: $P_{s\,cangen\,3} = 1.678MW$.
- Turbine4: $P_{s\,cangen\,4} = 1.678MW$.
- Turbine5: $P_{s\,cangen\,5} = 2.109MW$.
- Turbine6: $P_{s\,cangen\,6} = 2.643MW$.
- Turbine7: $P_{s\,cangen\,7} = 2.363MW$.
- Turbine8: $P_{s\,cangen\,8} = 2.275MW$.

To assess the disparity between each turbine's available generation and the target power output, the ratio B_i is computed as:

$$B_1 = \frac{2.275}{1.25} = 1.82 \qquad B_2 = \frac{0.00}{1.25} = 0.00$$
$$B_3 = \frac{1.678}{1.25} = 1.3424 \quad B_4 = \frac{1.678}{1.25} = 1.3424$$
$$B_5 = \frac{2.109}{1.25} = 1.6872 \quad B_6 = \frac{2.643}{1.25} = 2.1144$$
$$B_7 = \frac{2.363}{1.25} = 1.8904 \qquad B_8 = \frac{2.275}{1.25} = 1.82$$

Classification of turbines: Underperforming and Surplus

- Underperforming turbines ($B_i \leq 1$): only Turbine 2 with $B_2 = 0.00$.
- Surplus turbines ($B_i > 1$): All remaining turbines.

The overall shortfall and surplus are determined as:

$$Sum_{under} = 1, Sum_{over} = 5.0168$$

Applying the developed algorithm, the revised power references for each turbine ($P_{s\,refalgo}$) are computed using Eq. (V-7). The final power assignments, depicted as black key points in Figure V.13, are:

$$P_{s\,refalgo\,1} = 1.454MW \quad P_{s\,refalgo\,2} = 0.00MW$$
$$P_{s\,refalgo\,3} = 1.335MW \quad P_{s\,refalgo\,4} = 1.335MW$$
$$P_{s\,refalgo\,5} = 1.421MW \quad P_{s\,refalgo\,7} = 1.527MW$$
$$P_{s\,refalgo\,7} = 1.472MW \quad P_{s\,refalgo\,8} = 1.454MW$$

The total allocated power sums up to:

$$P_{s\,refalgo\,1} + \cdots + P_{s\,refalgo\,7} + P_{s\,refalgo\,8} = 10MW$$

which precisely meets the required grid power of $P_{s\,ref} = 10MW$. This confirms that the algorithm effectively redistributes power across the turbines while ensuring compliance with their generation limits.

The calculated values of $P_{s\,refalgo}$ align with the black key points in Figure V.13, further validating the accuracy and effectiveness of the algorithm in this scenario.

V.6. Conclusion

In this chapter, a novel wind farm power management algorithm was introduced and rigorously evaluated through simulations. The primary focus was to address the challenges of

fluctuating wind conditions, turbine underperformance, and grid stability by dynamically redistributing power across multiple turbines. The methodology and simulation models of the proposed algorithm were presented in detail, providing a step-by-step explanation of how turbine outputs are managed in real-time.

The novel algorithm successfully demonstrated its ability to adapt to real-time wind variations, ensuring that the grid receives a stable power supply. Compared with the traditional PI controller, the novel algorithm showed significant improvements in handling underperforming turbines and redistributing surplus power proportionally among turbines with higher capacities. This dynamic adaptability ensures that turbine power generation remains within operational limits while efficiently meeting grid demands. The results also revealed that the novel algorithm effectively eliminates issues such as excessive oscillations and unrealistic power references generated by the PI controller, thereby ensuring more stable and reliable wind farm performance.

In conclusion, the proposed wind farm power management algorithm proves to be a practical and highly efficient solution for managing variable wind conditions, providing better overall stability, and enhancing grid reliability. This method represents a significant advancement in optimizing wind energy production and sets the foundation for future developments in intelligent wind farm control systems.

Chapter VI

Conclusion & future work

VI.1. Conclusion

This thesis has presented a comprehensive exploration of control and management strategies for DFIG-based wind turbines, advancing the integration of AI-based methods to address limitations in conventional approaches.

Chapter I introduced the research problem, objectives, and scope of the study, providing a foundation by reviewing relevant literature on renewable energy systems, control strategies, and wind farm power management techniques. This chapter set the stage for a detailed analysis of control methods and AI-driven enhancements across wind turbine systems.

Chapter II laid the theoretical groundwork by delving into wind turbine modeling and control techniques. It covered essential aspects of aerodynamic modeling and DFIG dynamics, establishing a foundation for the development of robust control methodologies. This background was instrumental in understanding the specific dynamics and requirements of wind turbine control, supporting the subsequent exploration of more advanced techniques.

Chapter III focused on classical PI control using the Direct Synthesis Approach, enhanced by optimization techniques. Results indicated significant improvements in control performance with optimized PI controllers, with Particle Swarm Optimization (PSO) delivering the most effective results. However, challenges emerged in rotor power stability, particularly oscillations and variations under certain operating conditions, prompting the need for more advanced control techniques.

Chapter IV introduced advanced control strategies, starting with Sliding Mode Control (SMC) and its enhancement through Super Twisting SMC to address the issue of chattering. Following this, fuzzy logic control was implemented and further developed into a hybrid Fuzzy-Super Twisting Sliding Mode Control, which yielded the best results among all tested strategies. Additionally, Artificial Neural Networks (ANN) were applied to improve classical PI (DSA), demonstrating satisfactory results by eliminating overshoot present in the DSA.

Chapter V expanded the research to wind farm power management using a novel algorithm developed to distribute power proportionally across turbines. This algorithm was benchmarked against the traditional PI controller, showing exceptional responsiveness, precision, and proportional power distribution in scenarios with underperforming turbines. The results highlight the algorithm's ability to achieve grid stability and enhance power allocation efficiency.

Through these explorations, this thesis has demonstrated the feasibility and advantages of combining AI with classical control methods to improve DFIG-based wind turbine and wind farm performance. Each chapter contributes to a deeper understanding of how AI-driven methods can be tailored to address specific challenges in renewable energy systems, setting the stage for further developments in the field.

VI.2. Future work

Building on the findings of this thesis, several future research directions are proposed to further enhance the effectiveness and adaptability of control and management strategies for wind energy systems:

- **Optimized PI control:** Future research could integrate rotor power into the PI optimization process to improve control signal stability, potentially minimizing the variations observed in rotor power.
- **Fuzzy logic enhancements:** Fuzzy logic control can be refined using intelligent methods like Adaptive Neuro-Fuzzy Inference Systems (ANFIS) or other optimization techniques to automatically determine membership functions and rules, enhancing the adaptability and performance of the fuzzy logic controller.

- **ANN application:** The ANN-based controller could be further enhanced by training on optimized data, such as that from the optimized PI or Hybrid Fuzzy-SMC controllers, to leverage the performance strengths of these methods.
- **Super twisting sliding mode control optimization:** The gains K_1, K_2 of the ST-SMC could be optimized using advanced techniques to further minimize chattering and enhance overall system robustness.
- **Wind farm power management algorithm:** The novel power management algorithm could be implemented in a prototype model for practical testing, with additional development to incorporate AI learning (such as ANN training) based on performance data to improve adaptability and intelligence in real-world scenarios.

These future directions offer a pathway for refining AI-driven control and management systems in renewable energy, fostering a more resilient, efficient, and intelligent approach to wind energy generation.

References

[1] Joyce Lee and Feng Zhao, "Global Wind Energy Report," 2024. [Online]. Available: www.gwec.net

[2] Joyce Lee and Feng Zhao, "Global Wind Energy Report," 2022.

[3] Z. Zhang, A. Kusiak, and Z. Song, "Scheduling electric power production at a wind farm," *Eur J Oper Res*, vol. 224, no. 1, pp. 227–238, Jan. 2013, doi: 10.1016/j.ejor.2012.07.043.

[4] S. Siniscalchi Minna, "Advanced wind farm control strategies for enhancing grid support," UNIVERSITAT POLIT`ECNICA DE CATALUNYA, 2019.

[5] B. R. Karthikeya and R. J. Schutt, "Overview of wind park control strategies," *IEEE Trans Sustain Energy*, vol. 5, no. 2, pp. 416–422, Apr. 2014, doi: 10.1109/TSTE.2013.2285392.

[6] A. Feddaoui, L. Farah, A. Benretem, M. A. Djehaf, Z. Bouguerra, and Y. Djeriri, "Enhancing power control in doubly fed induction generator based wind turbines: a performance comparison of fuzzy logic and sliding mode control methods," *The Scientific Bulletin of Electrical Engineering Faculty*, vol. 23, no. 2, pp. 42–50, 2023, doi: 10.2478/sbeef-2023-0018.

[7] A. Feddaoui, L. Farah, A. Benretem, M. A. Djehaf, and L. Kadabenchiha, "COMPARATIVE STUDY BETWEEN SLIDING MODE CONTROL (SMC) & PI CONTROLLER FOR DFIG-BASED WIND TURBINE," in *10th INTERNATIONAL ZEUGMA CONFERENCE ON SCIENTIFIC RESEARCH*, Gaziantep, Türkiye, Jun. 2023.

[8] R. Dembri *et al.*, "SSO optimized FOFPID regulator design for performance enhancement of doubly fed induction generator based wind turbine system," *Sci Rep*, vol. 14, no. 1, p. 28305, 2024, doi: 10.1038/s41598-024-76457-z.

[9] M. R. Velpula and H. P. S. Kona, "An emotional control approach to grid-connected DFIG based wind turbine," *Int J Dyn Control*, vol. 12, no. 8, pp. 3048–3063, Aug. 2023, doi: 10.1007/s40435-023-01379-z.

[10] B. Jyoti Saharia, H. Brahma, and N. Sarmah, "A review of algorithms for control and optimization for energy management of hybrid renewable energy systems," *Journal of Renewable and Sustainable Energy*, vol. 10, no. 5, Sep. 2018, doi: 10.1063/1.5032146.

[11] H. Delavari and A. Veisi, "A new robust nonlinear controller for fractional model of wind turbine based DFIG with a novel disturbance observer," *Energy Systems*, vol. 15, no. 2, pp. 827–861, 2024, doi: 10.1007/s12667-023-00566-3.

[12] Y. Qiao and D. Guo, "Event-Triggered Robust Optimized Scheme with Impulse Control for DFIG Based Wind Turbine," *Journal of Electrical Engineering & Technology*, vol. 18, no. 5, pp. 3695–3708, 2023, doi: 10.1007/s42835-023-01462-7.

[13] K. Boureguig, S. Soued, F. Ouagueni, and A. Chahmi, "Optimal Metaheuristic-Based Feedback Linearization Control of DFIG Wind Turbine System," *Journal of Electrical Engineering & Technology*, 2023, doi: 10.1007/s42835-023-01386-2.

[14] D. Bhatia, "Performance Comparison of SMC, LQR and PD control for Spacecraft High Accuracy Pointing (Teilvorhaben TU Braunschweig)," 2021, doi: 10.13140/RG.2.2.20358.50247.

[15] Youcef Djeriri, "Commande directe du couple et des puissances d'une MADA associée à un système éolien par les techniques de l'intelligence artificielle.," 2015.

[16] ABDELKADER ACHAR, "Stratégies de commandes robustes pour la gestion des puissances d'une ferme éolienne associée à des convertisseurs multiniveaux.," Djillali Liabes University of Sidi Bel Abbes, 2023.

[17] P. Xu, "EE5705 Electric Drives in Sustainable Energy Systems Course Project 3," 2016.

[18] H. Gasmi, H. Benbouhenni, I. Colak, T. Tafticht, and N. Bizon, "Using the proportional dual integral strategy to improve the characteristics of the indirect field-oriented control of DFIG-

based wind turbine systems," *e-Prime - Advances in Electrical Engineering, Electronics and Energy*, vol. 9, p. 100749, Sep. 2024, doi: 10.1016/j.prime.2024.100749.
[19] Z. OMAÇ and İ. ERDEM, "Rotor Field-Oriented Control of Doubly Fed Induction Generator in Wind Energy Conversion System," *Gazi University Journal of Science*, vol. 36, no. 3, pp. 1217–1229, Sep. 2023, doi: 10.35378/gujs.987303.
[20] Y. Sahri *et al.*, "Effectiveness analysis of twelve sectors of DTC based on a newly modified switching table implemented on a wind turbine DFIG system under variable wind velocity," *Ain Shams Engineering Journal*, vol. 14, no. 11, p. 102221, Nov. 2023, doi: 10.1016/j.asej.2023.102221.
[21] A. A. Ansari and G. Dyanamina, "Comparative Analysis of Controlling Methods for Doubly Fed Induction Generator Based Wind Energy System," 2022, pp. 493–507. doi: 10.1007/978-981-16-9239-0_37.
[22] K. F. Sayeh, S. Tamalouzt, D. Ziane, Y. Sahri, B. Deffaf, and S. Lalouni Belaid, "Control of a Wind Turbine based on DFIG by Improved Direct Torque Control using Fuzzy Logic," *Journal of Renewable Energies*, May 2024, doi: 10.54966/jreen.v1i1.1173.
[23] I. YAICHI, A. SEMMAH, and P. WIRA, "CONTROL OF DOUBLY FED INDUCTION GENERATOR USING ARTIFICIAL NEURAL NETWORK CONTROLLER," *REVUE ROUMAINE DES SCIENCES TECHNIQUES — SÉRIE ÉLECTROTECHNIQUE ET ÉNERGÉTIQUE*, vol. 68, no. 1, pp. 46–51, Apr. 2023, doi: 10.59277/RRST-EE.2023.68.1.8.
[24] H. Chojaa *et al.*, "A Novel DPC Approach for DFIG-Based Variable Speed Wind Power Systems Using DSpace," *IEEE Access*, vol. 11, pp. 9493–9510, 2023, doi: 10.1109/ACCESS.2023.3237511.
[25] I. Hamdan, M. M.M. Youssef, and O. Noureldeen, "A Review of Intelligent Control Systems for Grid Tie Doubly Fed Induction Generator Based Wind Farm," *SVU-International Journal of Engineering Sciences and Applications*, vol. 4, no. 2, pp. 269–278, Dec. 2023, doi: 10.21608/svusrc.2023.215683.1132.
[26] M. A. Karami, S. M. Shariatmadar, M. E. Nazari, and J. Rahmani-Fard, "High-order sliding mode control of rotor-side converter in doubly-fed wind power generation system," *Scientia Iranica*, vol. 0, no. 0, pp. 0–0, Dec. 2023, doi: 10.24200/sci.2023.62927.8111.
[27] Y. Sahri *et al.*, "New intelligent direct power control of DFIG-based wind conversion system by using machine learning under variations of all operating and compensation modes," *Energy Reports*, vol. 7, pp. 6394–6412, Nov. 2021, doi: 10.1016/j.egyr.2021.09.075.
[28] S. Siniscalchi-Minna, F. D. Bianchi, M. De-Prada-Gil, and C. Ocampo-Martinez, "A wind farm control strategy for power reserve maximization," *Renew Energy*, vol. 131, pp. 37–44, Feb. 2019, doi: 10.1016/j.renene.2018.06.112.
[29] B. Zhang, P. Hou, W. Hu, M. Soltani, C. Chen, and Z. Chen, "A Reactive Power Dispatch Strategy with Loss Minimization for a DFIG-Based Wind Farm," *IEEE Trans Sustain Energy*, vol. 7, no. 3, pp. 914–923, Jul. 2016, doi: 10.1109/TSTE.2015.2509647.
[30] N. Gionfra, G. Sandou, H. Siguerdidjane, D. Faille, and P. Loevenbruck, "Wind farm distributed PSO-based control for constrained power generation maximization," *Renew Energy*, vol. 133, pp. 103–117, Apr. 2019, doi: 10.1016/j.renene.2018.09.084.
[31] S. Siniscalchi-Minna, M. De-Prada-Gil, F. D. Bianchi, C. Ocampo-Martinez, and B. De Schutter, "A multi-objective predictive control strategy for enhancing primary frequency support with wind farms," *J Phys Conf Ser*, vol. 1037, p. 032034, Jun. 2018, doi: 10.1088/1742-6596/1037/3/032034.
[32] P. Hou, W. Hu, B. Zhang, M. Soltani, C. Chen, and Z. Chen, "Optimised power dispatch strategy for offshore wind farms," *IET Renewable Power Generation*, vol. 10, no. 3, pp. 399–409, Mar. 2016, doi: 10.1049/iet-rpg.2015.0176.
[33] M. Kim, M. Jang, and S. Park, "A Data-Driven Model Predictive Control for Wind Farm Power Maximization," *IEEE Access*, vol. 12, pp. 90670–90683, 2024, doi: 10.1109/ACCESS.2024.3420872.
[34] G. Bai, Y. Feng, S. Huang, and P. Wang, "Distributed coordinated control method with multiple objectives optimization algorithm for wind farms," *IET Renewable Power Generation*, vol. 17, no. 5, pp. 1068–1077, Apr. 2023, doi: 10.1049/rpg2.12660.

[35] G. Bo, D. Man, Z. Meng, Z. Hongtao, and H. Hu, “A Wind Farm Power Maximization Method Based on Multi-Strategy Improved Sparrow Search Algorithm,” *J Sol Energy Eng*, vol. 146, no. 3, Jun. 2024, doi: 10.1115/1.4064189.
[36] J. J. Yang, M. Yang, M. X. Wang, P. J. Du, and Y. X. Yu, “A deep reinforcement learning method for managing wind farm uncertainties through energy storage system control and external reserve purchasing,” *International Journal of Electrical Power & Energy Systems*, vol. 119, p. 105928, Jul. 2020, doi: 10.1016/j.ijepes.2020.105928.
[37] V. H. Bui, T. T. Nguyen, and H. M. Kim, “Distributed operation of wind farm for maximizing output power: A multi-agent deep reinforcement learning approach,” *IEEE Access*, vol. 8, pp. 173136–173146, 2020, doi: 10.1109/ACCESS.2020.3022890.
[38] K. Petrichenko, T. C. Farrell, T. Thorsch Krader, and A. Tsakiris, “Energy Efficiency,” 2016.
[39] F. D. Bianchi, R. J. Mantz, and H. De Battista, *Wind Turbine Control Systems*. London: Springer London, 2007. doi: 10.1007/1-84628-493-7.
[40] Q. Wu and Y. Sun, *Modeling and Modern Control of Wind Power*. Wiley, 2018. doi: 10.1002/9781119236382.
[41] M. M. M. Ali, A.-R. Youssef, G. Abdel-Gaber, and A. S. Ali, “Adaptive Fuzzy-PID Based Pitch Angle Control of Wind Turbine,” in *2018 Twentieth International Middle East Power Systems Conference (MEPCON)*, IEEE, Dec. 2018, pp. 1110–1114. doi: 10.1109/MEPCON.2018.8635229.
[42] L. Fan, R. Kavasseri, Z. L. Miao, and C. Zhu, “Modeling of DFIG-Based Wind Farms for SSR Analysis,” *IEEE Transactions on Power Delivery*, vol. 25, no. 4, pp. 2073–2082, Oct. 2010, doi: 10.1109/TPWRD.2010.2050912.
[43] E. Youssef, A. Sharaf, A. Amin, and A. El Samhey, “Wind Energy FACTS Applications and Stabilization Schemes,” in *Advances in Renewable Energies and Power Technologies*, Elsevier, 2018, pp. 431–460. doi: 10.1016/B978-0-12-812959-3.00014-9.
[44] D. S. L. Simonetti, A. E. A. Amorim, and F. D. C. Oliveira, “Doubly Fed Induction Generator in Wind Energy Conversion Systems,” in *Advances in Renewable Energies and Power Technologies*, Elsevier, 2018, pp. 461–490. doi: 10.1016/B978-0-12-812959-3.00015-0.
[45] N. Mohan, *Advanced Electric Drives*. Wiley, 2014. doi: 10.1002/9781118910962.
[46] N. MOHAN, *Electric Machines and Drives A First Course*. Wiley, 2012.
[47] M. Hansen, *Aerodynamics of Wind Turbines*. Routledge, 2015. doi: 10.4324/9781315769981.
[48] S. Sven, *Aerodynamics of Wind Turbines: A Physical Basis for Analysis and Design*. Wiley, 2019.
[49] D. A. Spera, *Wind Turbine Technology: Fundamental Concepts in Wind Turbine Engineering, Second Edition*. ASME Press, 2009. doi: 10.1115/1.802601.
[50] T. Burton, N. Jenkins, D. Sharpe, and E. Bossanyi, *Wind Energy Handbook*. Wiley, 2011. doi: 10.1002/9781119992714.
[51] J. F. Manwell, J. G. McGowan, and A. L. Rogers, *Wind Energy Explained*. Wiley, 2009. doi: 10.1002/9781119994367.
[52] A. Rauh and W. Seelert, “The Betz optimum efficiency for windmills,” *Appl Energy*, vol. 17, no. 1, pp. 15–23, Jan. 1984, doi: 10.1016/0306-2619(84)90037-0.
[53] S. Muller, M. Deicke, and R. W. De Doncker, “Doubly fed induction generator systems for wind turbines,” *IEEE Industry Applications Magazine*, vol. 8, no. 3, pp. 26–33, 2002, doi: 10.1109/2943.999610.
[54] J. G. Slootweg and W. L. Kling, “Modelling and Analysing Impacts of Wind Power on Transient Stability of Power Systems,” *Wind Engineering*, vol. 26, no. 1, pp. 3–20, Jan. 2002, doi: 10.1260/030952402320775254.
[55] J. Ekanayake, “Control of DFIG wind turbines,” *Power Engineer*, vol. 17, no. 1, p. 28, 2003, doi: 10.1049/pe:20030107.
[56] R. Pena, J. C. Clare, and G. M. Asher, “Doubly fed induction generator using back-to-back PWM converters and its application to variable-speed wind-energy generation,” *IEE Proceedings - Electric Power Applications*, vol. 143, no. 3, p. 231, 1996, doi: 10.1049/ip-epa:19960288.
[57] F. Blaabjerg and Z. Chen, *Power Electronics for Modern Wind Turbines*. Cham: Springer International Publishing, 2006. doi: 10.1007/978-3-031-02494-8.

[58] A. Thomas, *Wind Power in Power Systems*, 2nd ed. Wiley, 2012.
[59] K. J. Åström and T. Hägglund, *Advanced PID Control*. ISA - The Instrumentation, Systems and Automation Society, 2006.
[60] I. D. Díaz-Rodríguez, S. Han, and S. P. Bhattacharyya, *Analytical Design of PID Controllers*. Cham: Springer International Publishing, 2019. doi: 10.1007/978-3-030-18228-1.
[61] O. P. Bharti, R. K. Saket, and S. K. Nagar, "Design of PI controller for doubly fed induction generator using static output feedback," in *2015 39th National Systems Conference (NSC)*, IEEE, Dec. 2015, pp. 1–6. doi: 10.1109/NATSYS.2015.7489128.
[62] G. Ellis, "Four Types of Controllers," in *Control System Design Guide*, Elsevier, 2012, pp. 97–119. doi: 10.1016/B978-0-12-385920-4.00006-0.
[63] K. S. Kula, "Tuning a PI/PID Controller with Direct Synthesis to Obtain a Non-Oscillatory Response of Time-Delayed Systems," *Applied Sciences*, vol. 14, no. 13, p. 5468, Jun. 2024, doi: 10.3390/app14135468.
[64] A. Abraham, N. Nedjah, and L. de M. Mourelle, "Evolutionary Computation: from Genetic Algorithms to Genetic Programming," 2006, pp. 1–20. doi: 10.1007/3-540-32498-4_1.
[65] D. Marco and S. Thomas, *Ant Colony Optimization*. Massachusetts Institute of Technology, 2004.
[66] J. Kennedy and R. Eberhart, "Particle swarm optimization," in *Proceedings of ICNN'95 - International Conference on Neural Networks*, IEEE, 1995, pp. 1942–1948. doi: 10.1109/ICNN.1995.488968.
[67] S. Mirjalili, S. M. Mirjalili, and A. Lewis, "Grey Wolf Optimizer," *Advances in Engineering Software*, vol. 69, pp. 46–61, Mar. 2014, doi: 10.1016/j.advengsoft.2013.12.007.
[68] R. Yerolla, P. Suhailam, and C. S. Besta, "A new analytical method for designing centralised PI controllers for unstable systems using a direct synthesis approach," *Int J Syst Sci*, vol. 55, no. 14, pp. 2857–2873, Oct. 2024, doi: 10.1080/00207721.2024.2363541.
[69] S. Nagammai, S. Latha, and S. Balamurugan, "Experimental Validation of Direct Synthesis-Based PI/PID Controller Applied to First and Second Order Variable Area Tank Process," 2024, pp. 65–76. doi: 10.1007/978-981-99-6855-8_6.
[70] M. Li, M. Xin, Z. Zhao, J. Wang, and X. Hu, "Smith-Predictor-Based Design of Analytical PI-PD Control for Series Cascade Processes with Time Delay," *Electronics (Basel)*, vol. 12, no. 19, p. 4089, Sep. 2023, doi: 10.3390/electronics12194089.
[71] C. S. Jung, H. K. Song, and J. C. Hyun, "A new direct-synthesis tuning method for pi-controllers," *Can J Chem Eng*, vol. 77, no. 1, pp. 180–185, Feb. 1999, doi: 10.1002/cjce.5450770129.
[72] J.-C. Jeng, "A model-free direct synthesis method for PI/PID controller design based on disturbance rejection," *Chemometrics and Intelligent Laboratory Systems*, vol. 147, pp. 14–29, Oct. 2015, doi: 10.1016/j.chemolab.2015.08.004.
[73] Sukanta Nayak, *Fundamentals of Optimization Techniques with Algorithms*. Elsevier, 2020. doi: 10.1016/C2019-1-02539-9.
[74] M. Cavazzuti, *Optimization Methods*. Berlin, Heidelberg: Springer Berlin Heidelberg, 2013. doi: 10.1007/978-3-642-31187-1.
[75] S. Butenko, P. M. Pardalos, and V. Shylo, *Optimization Methods and Applications*, vol. 130. Cham: Springer International Publishing, 2017. doi: 10.1007/978-3-319-68640-0.
[76] O. Laila, S. Asmaa, Saber M. Saleh, and Mohamed Kourany, "Meta-heuristic Optimization for Wind Turbine Control: Evaluating Performance with PI and Fractional PI Controllers for Maximum Power Extraction," *Journal of Electrical Systems*, vol. 20, no. 3, 2024.
[77] W. JAIKHANG, "Optimization of PI Controller Using Ant Colony Algorithm for Wind Turbine System," *PRZEGLĄD ELEKTROTECHNICZNY*, vol. 1, no. 10, pp. 66–70, Oct. 2024, doi: 10.15199/48.2024.10.11.
[78] M. Mirzaei, C. Tibaldi, and M. H. Hansen, "PI controller design of a wind turbine: evaluation of the pole-placement method and tuning using constrained optimization," *J Phys Conf Ser*, vol. 753, p. 052026, Sep. 2016, doi: 10.1088/1742-6596/753/5/052026.
[79] V. Rotkin, "Optimization Methods for Wind Turbines," Jan. 03, 2024. doi: 10.20944/preprints202401.0035.v1.

[80] H. Tian, Z. Tang, H. Ouyang, R. Wang, F. Wang, and S. Duan, "Optimization and control strategy for wind turbine aerodynamic performance under uncertainties," *Journal of Renewable and Sustainable Energy*, vol. 16, no. 1, Jan. 2024, doi: 10.1063/5.0167442.

[81] A. Tawhid, T. Teotia, and H. Elmiligi, "Machine learning for optimizing healthcare resources," in *Machine Learning, Big Data, and IoT for Medical Informatics*, Elsevier, 2021, pp. 215–239. doi: 10.1016/B978-0-12-821777-1.00020-3.

[82] S. Katoch, S. S. Chauhan, and V. Kumar, "A review on genetic algorithm: past, present, and future," *Multimed Tools Appl*, vol. 80, no. 5, pp. 8091–8126, Feb. 2021, doi: 10.1007/s11042-020-10139-6.

[83] T. Tezer, R. Yaman, and G. Yaman, "Evaluation of approaches used for optimization of stand-alone hybrid renewable energy systems," *Renewable and Sustainable Energy Reviews*, vol. 73, pp. 840–853, Jun. 2017, doi: 10.1016/j.rser.2017.01.118.

[84] M. Guediri, N. Ikhlef, H. Bouchekhou, A. Guediri, and A. Guediri, "Optimization by Genetic Algorithm of a Wind Energy System applied to a Dual-feed Generator," *Engineering, Technology & Applied Science Research*, vol. 14, no. 5, pp. 16890–16896, Oct. 2024, doi: 10.48084/etasr.8122.

[85] A. Guediri, A. Guediri, and S. Touil, "Optimization Using a Genetic Algorithm Based on DFIG Power Supply for the Electrical Grid," *International Journal of Engineering*, vol. 35, no. 1, Jan. 2022, doi: 10.5829/ije.2022.35.01A.11.

[86] G. Park, K.-N. Hong, and H. Yoon, "Vision-Based Structural FE Model Updating Using Genetic Algorithm," *Applied Sciences*, vol. 11, no. 4, p. 1622, Feb. 2021, doi: 10.3390/app11041622.

[87] Y. Bekakra and D. Ben Attous, "Optimal tuning of PI controller using PSO optimization for indirect power control for DFIG based wind turbine with MPPT," *International Journal of System Assurance Engineering and Management*, vol. 5, no. 3, pp. 219–229, Sep. 2014, doi: 10.1007/s13198-013-0150-0.

[88] O. El Qouarti, A. Essadki, H. Laghridat, and T. Nasser, "Power Control of DFIG based WECS using SOSMC and PSO algorithm," in *2022 2nd International Conference on Innovative Research in Applied Science, Engineering and Technology (IRASET)*, IEEE, Mar. 2022, pp. 1–6. doi: 10.1109/IRASET52964.2022.9738382.

[89] A. Iqbal, D. Ying, A. Saleem, M. A. Hayat, and M. Mateen, "Proposed particle swarm optimization technique for the wind turbine control system," *Measurement and Control*, vol. 53, no. 5–6, pp. 1022–1030, May 2020, doi: 10.1177/0020294020902785.

[90] Y. Al-Smadi, M. Eshtay, A. Al-Qerem, S. Nashwan, O. Ouda, and A. A. Abd El-Aziz, "Reliable prediction of software defects using Shapley interpretable machine learning models," *Egyptian Informatics Journal*, vol. 24, no. 3, p. 100386, Sep. 2023, doi: 10.1016/j.eij.2023.05.011.

[91] J. Giri, N. K. Mishra, A. Patra, and M. K. Shukla, "Control Strategies of DFIG Technology-based Variable-Speed Wind Turbines-A Review," *IOP Conf Ser Earth Environ Sci*, vol. 1285, no. 1, p. 012007, Jan. 2024, doi: 10.1088/1755-1315/1285/1/012007.

[92] J.-J. E. SLOTINE, "Sliding controller design for non-linear systems," *Int J Control*, vol. 40, no. 2, pp. 421–434, Aug. 1984, doi: 10.1080/00207178408933284.

[93] Z. R. Wani *et al.*, "A Critical Review on Control Strategies for Structural Vibration Control," *Annu Rev Control*, vol. 54, pp. 103–124, 2022, doi: 10.1016/j.arcontrol.2022.09.002.

[94] A. Feddaoui, D. M. Abdeldjalil, B. Bilal, D. K. Youcef Islam, and D. Youcef, "Sliding Mode Control For Underactuated Nonlinear Mechanical Systems," in *2024 3rd International Conference on Advanced Electrical Engineering (ICAEE)*, IEEE, Nov. 2024, pp. 1–6. doi: 10.1109/ICAEE61760.2024.10783171.

[95] Z. Bouguerra, "Comparative study between PI, FLC, SMC and Fuzzy sliding mode controllers of DFIG wind turbine," *Journal of Renewable Energies*, vol. 26, no. 2, Dec. 2023, doi: 10.54966/jreen.v26i2.1146.

[96] Yang Li, Jianhua Zhang, and Qiong Wu, "Basic Concepts," in *Adaptive Sliding Mode Neural Network Control for Nonlinear Systems*, Elsevier, 2019, pp. 1–16. doi: 10.1016/B978-0-12-815372-7.00001-X.

[97] H. Bahlouli, A. Mansouri, and M. Bouhamida, "Super-Twisting Control for a Doubly Fed Induction Generator (DFIG)-Based Wind Turbine Using a Nonlinear Observer," *Journal of*

Operation and Automation in Power Engineering, vol. 13, no. 1, pp. 1–19, 2025, doi: 10.22098/joape.2023.11663.1873.
[98] H. Bekouche and A. Chaker, "Advanced control scheme of doubly fed induction generator for wind turbine using second sliding mode control," *International Journal of Electrical and Computer Engineering*, vol. 14, no. 3, pp. 2562–2570, Jun. 2024, doi: 10.11591/ijece.v14i3.pp2562-2570.
[99] A. KERBOUA and M. ABID, "Hybrid fuzzy sliding mode control of a doubly-fed induction generator speed in wind turbines," *Journal of Power Technologies*, vol. 95, no. 2, 2015.
[100] H. AHMED and A. RAJORIYA, "A hybrid of sliding mode control and fuzzy logic control using a fuzzy supervisory switched system for DC motor speed control," *TURKISH JOURNAL OF ELECTRICAL ENGINEERING & COMPUTER SCIENCES*, vol. 25, pp. 1993–2004, 2017, doi: 10.3906/elk-1511-213.
[101] R. E. Bellman and Lotfi A.Zadeh, "Decision-making in a fuzzy environment," *NASA CONTRACTOR REPORT*, May 1970.
[102] Lotfi A.Zadeh, "Fuzzy logic," *Computer (Long Beach Calif)*, 1988.
[103] Lotfi A.Zadeh, "Fuzzy sets," *Information and control*, vol. 8, 1965.
[104] E. Bounadja, A. B. Djilali, W. M. Kacemi, A. Yahdou, H. Benbouhenni, and I. Colak, "Enhancing performance and power quality in a wind energy conversion system based on permanent magnet synchronous generator through improved 3rd-order super-twisting control," *Energy Reports*, vol. 13, pp. 3204–3224, Jun. 2025, doi: 10.1016/j.egyr.2025.02.052.
[105] T. Wang, S. Sun, and Q. Chen, "Non-singular terminal super-twitsing control of servo systems with backlash," *Sci Rep*, vol. 15, no. 1, p. 5329, Feb. 2025, doi: 10.1038/s41598-025-88795-7.
[106] A. F. Sheikh and S. K. Starrett, "Comparison of input signal choices for a fuzzy logic-based power system stabilizer," in *2015 North American Power Symposium (NAPS)*, IEEE, Oct. 2015, pp. 1–6. doi: 10.1109/NAPS.2015.7335158.
[107] J.A. Laghari, "How To Implement Fuzzy Logic Control in MATLAB/SIMULINK," 2021.
[108] Teuvo KOHONEN, Kai MÄKISARA, Olli SIMULA, and Jari KANGAS, *Artificial Neural Networks*. Elsevier, 1991. doi: 10.1016/C2009-0-12894-5.
[109] S. Walczak and N. Cerpa, "Artificial Neural Networks," in *Encyclopedia of Physical Science and Technology*, Elsevier, 2003, pp. 631–645. doi: 10.1016/B0-12-227410-5/00837-1.
[110] I. N. da Silva, D. Hernane Spatti, R. Andrade Flauzino, L. H. B. Liboni, and S. F. dos Reis Alves, *Artificial Neural Networks*. Cham: Springer International Publishing, 2017. doi: 10.1007/978-3-319-43162-8.
[111] S. Labdai, N. Bounar, A. Boulkroune, B. Hemici, and L. Nezli, "Artificial neural network-based adaptive control for a DFIG-based WECS," *ISA Trans*, vol. 128, pp. 171–180, Sep. 2022, doi: 10.1016/j.isatra.2021.11.045.
[112] J. Meyers *et al.*, "Wind farm flow control: prospects and challenges," *Wind Energy Science*, vol. 7, no. 6, pp. 2271–2306, Nov. 2022, doi: 10.5194/wes-7-2271-2022.
[113] I. E. Sundarapandi Edward and R. Ponpandi, "Challenges, strategies and opportunities for wind farm incorporated power systems: a review with bibliographic coupling analysis," *Environmental Science and Pollution Research*, vol. 30, no. 5, pp. 11332–11356, Dec. 2022, doi: 10.1007/s11356-022-24658-2.
[114] V. van de Scheur and S. Boersma, "A Distributed Model Predictive Wind Farm Controller for Active Power Control," Jul. 2020.
[115] C. J. Bay, J. Annoni, T. Taylor, L. Pao, and K. Johnson, "Active Power Control for Wind Farms Using Distributed Model Predictive Control and Nearest Neighbor Communication," in *2018 Annual American Control Conference (ACC)*, IEEE, Jun. 2018, pp. 682–687. doi: 10.23919/ACC.2018.8431764.
[116] M. Atallah *et al.*, "Supervisory control of reactive power in wind farms with doubly fed induction generator-based wind turbines for voltage regulation and power losses reduction," *Electric Power Systems Research*, vol. 228, p. 110059, Mar. 2024, doi: 10.1016/j.epsr.2023.110059.
[117] B. Desalegn and B. Tamrat, "Overview of the PI (2DoF) algorithm in wind power system optimization and control," *Front Energy Res*, vol. 12, Aug. 2024, doi: 10.3389/fenrg.2024.1435455.

[118] S. Tamaro and C. L. Bottasso, “A New Wind Farm Active Power Control Strategy to Boost Tracking Margins in High-demand Scenarios,” in *2023 American Control Conference (ACC)*, IEEE, May 2023, pp. 192–197. doi: 10.23919/ACC55779.2023.10156275.
[119] Y. Zhang, X. Chen, S. Gong, and J. Chen, “Collective large-scale wind farm multivariate power output control based on hierarchical communication multi-agent proximal policy optimization,” *Renew Energy*, vol. 219, p. 119479, Dec. 2023, doi: 10.1016/j.renene.2023.119479.
[120] T. Ghennam, B. Francois, and E. M. Berkouk, “Local supervisory algorithm for reactive power dispatching of a wind farm.”
[121] H. Benbouhenni *et al.*, “Experimental analysis of genetic algorithm-enhanced PI controller for power optimization in multi-rotor variable-speed wind turbine systems,” *Sci Rep*, vol. 15, no. 1, p. 1407, Jan. 2025, doi: 10.1038/s41598-024-81281-6.